The University Of Sheffield.

Implanted Antennas for Biomedical Applications

By

Saeed M. Alamri

Thesis submitted for the degree of PhD

To the
Department of Electronic and Electrical Engineering
Faculty of Engineering
The University of Sheffield

December 2016

To my mother soul, my father and my lovely and great family

Abstract

Body-Centric Wireless Communication (BCWC) is a central topic in the development of healthcare and biomedical technologies. Increasing healthcare quality, in addition to the continuous miniaturisation of sensors and the advancement in wearable electronics, embedded software, digital signal processing and biomedical technologies, has led to a new era of biomedical devices and increases possibility of continuous monitoring, diagnostic and/or treatment of many diseases. However, the major difference between BCWC, particularly implantable devices, and conventional wireless systems is the radio channel over which the communication takes place. The human body is a hostile environment from a radio propagation perspective. This environment is a highly lossy and has a high effect on the antenna elements, the radio channel parameters and, hence a dramatic drop in the implanted antenna performance. Therefore, this thesis focuses on how to improve the gain of implanted antennas.

In order to improve the gain and performance of implanted antennas, this thesis uses a combination of experimental and electromagnetic numerical investigations. Extensive simulation and experimental investigations are carried out to study the effects of various external elements on the performance improvement of implanted antennas. This thesis shows the design, characterisation, simulation and measurements of four different antennas to work at ISM band and seventeen different scenarios for body wireless communication. A 3- layer (skin, fat and muscle) and a

liquid homogenise phantom were used for human body modelling in both simulation and measurements.

The results shows that a length of printed line and a grid can be used on top of the human skin in order enhance the performance of the implanted antennas. Moreover, a ring and a hemispherical lens can be used externally in order to enhance the performance of the implanted antenna. This approach yields a significant improvement in the antenna gain and reduces the specific absorption rate (SAR) in most cases and the obtained gain varies between 2 dB and 8 dB.

Such external elements could be manufactured in a sticking plaster form and applied to the skin giving much improved implant communication performance and significantly reduced battery power consumption. Implications of the results and future research directions are also presented.

List of Publications

Alamri, Saeed, Richard Langley, and Ahmed AlAmoudi. "Gain Enhancement of Implanted Antennas Using Lens and Parasitic Ring." *Electronics Letters*, 2016.

Alamri, Saeed, Richard J. Langley, and Ahmed O. AlAmoudi. "Gain Enhancement of Implanted Antenna for Medical Applications." In *Electromagnetics in Advanced Applications (ICEAA), 2015*.

Alamri, Saeed, Richard J. Langley, and Ahmed O. AlAmoudi. "Novel Compact Dual-Band Implanted Antenna." In *Antennas and Propagation Conference (LAPC), 2014 Loughborough*, pp. 333-335. IEEE, 2014.

Alamri, Saeed, Richard J. Langley, and Ahmed O. AlAmoudi. "Compact Dual-Band Implanted Antenna for Wireless Communication" - *2014 8th European Conference on Antennas and Propagation (EuCAP),* , 7-11 April 2014.

Alamri, Saeed, Richard J. Langley, and Ahmed O. AlAmoudi. "Improved performance of 2.45 GHz implanted patch antenna for wireless communication." In *Antennas and Propagation Conference (LAPC), 2013 Loughborough*, pp. 27-30. IEEE, 2013.

Zhu, Shaozhen, Alamri, Saeed, O. AlAmoudj, and R. J. Langley. "Implanted antenna efficiency improvement." *2013 7th European Conference on Antennas and Propagation (EuCAP).*

AlAmoudi, Ahmed O., Saeed Almari, Shuyuan Zhu, and Richard J. Langley. "Improved performance of 2.45 GHz implanted antenna for wireless communication." In *Applied Electromagnetics (APACE), 2012 IEEE Asia-Pacific Conference on*, pp. 308-312. IEEE, 2012.

Table of Contents

Acknowledgments

I am grateful to acknowledge and give special thanks to my first supervisor, Prof. Richard Langley for his support, guidance and supervision throughout my PhD project. Special thanks and acknowledgement are also due to my second supervisor, Dr. Ahmed Alamoudi for his supervision and generous help. It has been my great pleasure and honour to be under their supervision and to work with them.

Many thanks to Dr Qiang Bai and Dr. Zhu, Shaozhen for their valuable help during my first year. I wish to thank the technical staff in the fabrication lab for their help and fabrication of the antennas. I would like to acknowledge and thank all of the department and university staff for their assistance throughout my PhD work.

Special thanks to Saudi Ministry of Education, Royal Embassy of Saudi Arabia, Saudi Cultural Bureau in London and Albaha University for the valuable support and help.

I would like to give a special thank to my fellow colleagues and friends, who I will never forget moments with them during my PhD journey. Special thanks to Dr. Salim Abukharis, Dr. Yasir Alharbi and Dr. Salman Salman for their help and support.

I will never forget my mother, even she has passed away, her remembrance has always inspired me. I am deeply grateful to acknowledge my father and my brothers for their support and encouragement.

Finally, I am very thankful to my wife, Norah, for her love, support and encouragement and to my lovely children, Mohammed, Lama Abdullah and Omar.

List of Figures

List of Tables

List of Symbols and Abbreviation

3D	Three Dimensions
α	Attenuation constant
σ	Conductivity
ρ	Mass density
μ	Micro
μW	Microwatt
μ	Permeability
Ω	Ohm
λ, λ_o	Wavelength
ε	Permittivity
Γ	Reflection coefficient
η	Intrinsic impedance
ANSI	American National Standards Institute
BAN	Body Area Network
BCWC	Body-Centric Wireless Communication
BSN	Body Sensor Network
c	The light speed
cm	Centimetre
COPD	Chronic Obstructive Pulmonary Disease
CST	Computer Simulation Technology

CVDs	Cardiovascular diseases
dB	Decibels
EH	Energy Harvesting
ERC	European Radio communications Committee
e_p	Polarization mismatch factor
EIRP	Effective Isotropic Radiated Power
ERP	Effective Radiated Power or Equivalent Radiated Power
EM	Electromagnetic
F	Frequency
FCC	Federal Communication Commission
FIT	Finite integration technique
FSS	Frequency Selective Surface
g	Gram
GHz	Giga Hertz
GI	Gastrointestinal
IIMD	Implantable and Ingestible Medical Devices
ISM band	Industrial, Scientific and Medical band (2.4 - 2.5 GHz)
ITU-R	International Communication Union Recommendations
kg	Kilogram
m	metre
MHz	Mega Hertz
mm	Millimetre
MMW	Millimetre waves

mV	Millivolte
MedRadio	Medical Radio Communication Band (401 - 406 MHz) for medical telemetry applications
MICS	Medical Implant Communication Service (402 - 405 MHz)
mW	Milliwatt
MWO	Microwave Office
NF	Noise figure
PCB	Printed Circuit Board
P_f	Loss in the free-space
Pin	Input power
PIFA	Planar Inverted F Antenna
Pmax	Maximum power
Pout	Output power
RF	Radio Frequency
S	The random scatter
SAR	Specific Absorption Rate
SNR	Signal to Noise Ratio
ULP	Ultra Low Power
VNA	Vector Network Analyzer
LAN/WAN	Local area network (LAN) and Wide area network (WAN)
WPAN	Wireless Personal Area Networks

Chapter 1

Introduction

Research in body sensors networks (BSN) for wireless communications (or Body-Centric Wireless Communication (BCWC)) is a relatively new topic with little work worldwide compared to mobile communications. Research in implanted devices - as one of BSN topics - for wireless medical applications has been growing rapidly over the past decade. In order to provide vital information such as glucose level, blood pressure, etc, the implantable devices are embedded into the body. This information can be transmitted from implantable devices to external equipment outside the body through a wireless communication link. Examples of electronic implants include heart pacemakers, cochlear implants and intraocular implanted antennas for retinal prosthesis application [1-4]. Implantable devices increase the healthcare quality as it reduces the risk of some diseases complications, for example, by continuous monitoring of some disease developments. Moreover, it reduces healthcare cost, as for example patients can be continuously monitored without being admitted to the hospital [5-9]. Figure 1.1 shows examples of implanted devices for continues monitoring.

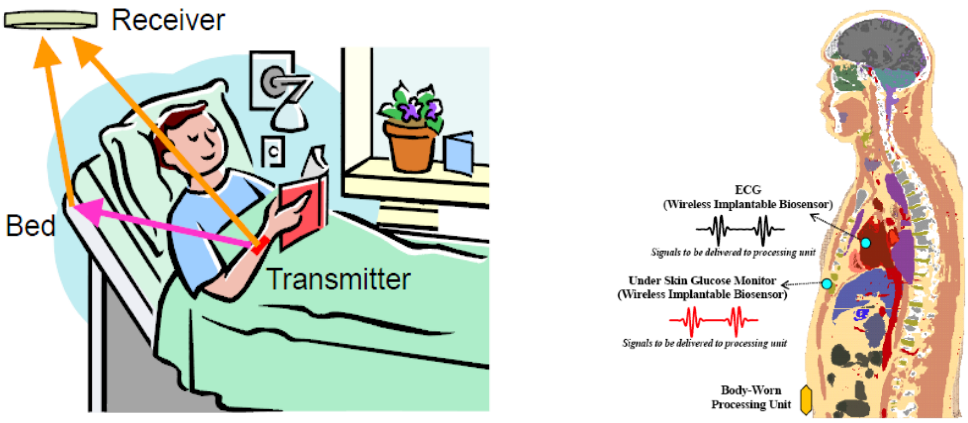

Figure 1.1: Body sensor network systems [9, 10]

The main applications of implanted devices are either therapeutic - such as hyperthermia treatment - or diagnostic to detect and transmit data. Medical and biomedical researchers show the importance of the continuous monitoring for many diseases such as heart rate, blood oxygenation levels in Chronic Obstructive Pulmonary Disease (COPD), blood sugar level for diabetes patient, blood pressure and patient's daily activity [5-8, 11]. These vital information can be obtained using sensors which can be implanted under the skin as a type of implanted device.

Recently, some other diseases can be diagnosed by another type of implantable system; capsule endoscopy which is a procedure used to observe digestive disorders [12, 13]. Symptoms such as chronic abdominal pain, unexplained weight loss or Gastroenterology (GI) bleeding are digestive disorders. Many diseases could cause these symptoms such as inflammatory bowel, Crohn's disease or ulcerative colitis, celiac disease, benign and cancerous tumours, or any other digestive disorders [12, 13]. Capsule endoscopy can be used to take photographic images for diagnosing the disease or digestive system disorders such as stomach and the small bowel. In a

similar or close to vitamin capsule size, capsule endoscopy consists of batteries, a light source, camera, transmitter and antenna as shown in Figure 1.2.

Figure 1.2: Capsule endoscopy [14]

1.1 Research Motivation:

Implantable devices are playing a vital role toward increasing the quality of healthcare diagnose and treatment and medical research. Such applications have motivated research on implanted antennas as an important part of the implantable wireless devices. These areas of research are still immature and have significant potential, due to the many challenges that need to be overcome particularly antennas which are surrounded by highly lossy media. And hence the human body reduces the radiation efficiency of the radiating element due to electromagnetic absorption in the body tissues [15]. The highly lossy medium causes radiation pattern distortion and

affects antennas behaviour and specifications. Therefore, the performance of implanted antennas is still one of the most challenging parts for implanted systems. This area of research motivates us to focus on increasing the performance of implanted antennas using different performance improvement techniques.

1.2 Objectives

This work focuses on how to increase the implanted antennas performance using external elements such as a grid structure, printed lines and lens. In order to enhance the capsule antenna performance, a technique to distribute the current around the capsule antenna will be used. These antennas will be modelled using CST software and will be fabricated and tested in the laboratory. A three layer human body model (skin, fat and muscle) will be used for subcutaneous implanted antennas and a liquid body phantom will be used for the capsule. These objectives are converted into the following measurable tasks:

- Enhancing the performance of the subcutaneous implanted antenna.
- Designing an efficient, miniaturized and high performance dual-band implanted antenna and improving its performance using external elements.
- Designing an efficient, high gain, omni-directional implanted antenna for medical capsule systems. The antenna should - also - allow maximum possible space for other parts of the capsule system.
- Developing a liquid phantom in order to perform the measurements of the capsule antenna.

1.3 Novelty and originality

This thesis proposes design of different efficient miniaturised implanted antennas to achieve reliable medical implant communication. Different technologies and designs are investigated in order to improve the antenna gain. The areas of novelty are listed below:

1- A probe implanted antenna was designed to be implanted under the skin for biomedical wireless communication.

2- A microstrip patch implanted antenna was designed to be implanted under the skin for biomedical wireless communication.

3- An external parasitic grid structure was used for the first time to improve the implantable antennas performance and both, probe and microstrip gain were improved by a minimum of 3 dB.

4- A parasitic resonator was used for the first time to improve the implantable antennas performance and both, probe and microstrip antennas gain were improved by a minimum of 3 dB.

5- Both external parasitic elements, grid structure and parasitic resonators, were used together for further performance improvement and the gain was improved by a minimum of 6 dB for both probe and microstrip antenna designes.

6- An external hemispherical lens was used to improve the performance of the implantable antennas and the microstrip antenna gain was improved by 6 dB.

7- An external parasitic ring was used for the first time to improve the performance of the implantable antennas and the microstrip antenna gain was improved by 2 dB.

8- A combination of external; hemispherical lens and parasitic ring were used together for further performance improvement the implantable microstrip antenna gain was improved by 7.5 dB.

9- A new efficient, miniaturised and high performance dual-band implantable antenna for biomedical applications was designed to be implanted under the skin. The size achieved is 1/25 of the wavelength.

10- External hemispherical lens and a parasitic ring were used separately and together to improve the performance of the dual-band implantable antenna. The gain was improved by up to 7 dB.

11- A new miniaturised flexible omni-directional implantable antenna for capsule endoscopy was designed and the size achieved is 10 x 16 x 10 mm^3 at 403 MHz.

12- The performance of this capsule antenna was improved and the minimum gain improved by almost 15 dB by distributing the current around the capsule

13- A formula to produce a liquid phantom for homogenous human body developed and used.

1.4 Thesis Outline

This thesis is organised in seven chapters. Following this introductory chapter, the rest of the thesis is organised as follows:

Chapter 2 gives a brief introduction of implantable systems and antennas for biomedical applications. Requirements and challenges of implantable antennas, frequency allocation, current regulations and standards are also addressed. The latest research on implantable antennas and State-of-the-art of performance and improvements are reviewed. In addition, human body modelling techniques are discussed.

Chapter 3 presents the design and characterisation of 2.45 GHz implanted probe and microstrip patch antennas for wireless communication. In addition, performance improvement of these two antennas using different external techniques is proposed. This includes external grid structure, parasitic printed line.

Chapter 4 proposes the improvement of a 2.45 GHz implanted microstrip patch antenna for wireless communication using hemispherical lens. Another scenario of improvement using hemispherical lens combined with parasitic ring for gain enhancement is presented.

Chapter 5 addresses the design and realisation of a novel compact dual band antenna for ISM implantable biotelemetry application to be operating at 915 MHz and 2.45 GHz. In addition, performance improvement of this antenna using mix scenarios of hemispherical lens and parasitic ring is presented.

Chapter 6 illustrates the design, analysis and measurements of a novel compact flexible implantable antenna for capsule systems to be operating at 403 MHz. In addition, performance improvement of this antenna is presented. The antenna is higher gain and omni-directional. Moreover, a formula to produce a liquid phantom for homogenous human body is presented and tested.

Chapter 7 Summarises the main contributions and findings of the study and concludes this thesis researches. Moreover, suggestions and areas of potential future research are given.

1.5 References

[1] R. D. Beach, R. W. Conlan, M. C. Godwin, and F. Moussy, "Towards a miniature implantable in vivo telemetry monitoring system dynamically configurable as a potentiostat or galvanostat for two-and three-electrode biosensors," *Instrumentation and Measurement, IEEE Transactions on,* vol. 54, pp. 61-72, 2005.

[2] T. Karacolak, A. Z. Hood, and E. Topsakal, "Design of a dual-band implantable antenna and development of skin mimicking gels for continuous glucose monitoring," *Microwave Theory and Techniques, IEEE Transactions on,* vol. 56, pp. 1001-1008, 2008.

[3] L. Thuc, "Human implanted spiral antenna for a 2.45 GHz wireless temperature and pressure SAW sensor system," in *2008 IEEE Antennas and Propagation Society International Symposium*, 2008, pp. 1-4.

[4] K. Gosalia, M. S. Humayun, and G. Lazzi, "Impedance matching and implementation of planar space-filling dipoles as intraocular implanted antennas in a retinal prosthesis," *Antennas and Propagation, IEEE Transactions on,* vol. 53, pp. 2365-2373, 2005.

[5] D. Andre and D. L. Wolf, "Recent advances in free-living physical activity monitoring: a review," *Journal of diabetes science and technology,* vol. 1, pp. 760-767, 2007.

[6] F. Braunschweig, P. T. Mortensen, D. Gras, W. Reiser, T. Lawo, H. Mansour*, et al.*, "Monitoring of physical activity and heart rate variability in patients with chronic heart failure using cardiac resynchronization devices," *The American journal of cardiology,* vol. 95, pp. 1104-1107, 2005.

[7] M. Gerritsen, J. Jansen, and J. Lutterman, "Performance of subcutaneously implanted glucose sensors for continuous monitoring," *The Netherlands journal of medicine,* vol. 54, pp. 167-179, 1999.

[8] P. Kupelian, T. Willoughby, A. Mahadevan, T. Djemil, G. Weinstein, S. Jani*, et al.*, "Multi-institutional clinical experience with the Calypso System in localization and continuous, real-time monitoring of the prostate gland during external radiotherapy," *International Journal of Radiation Oncology* Biology* Physics,* vol. 67, pp. 1088-1098, 2007.

[9] *Body-Centric Wireless Communications*. Available: http://antennas.eecs.qmul.ac.uk/research/body-centric-wireless-commnication-and-networks/

[10] P. S. Hall and Y. Hao, "Antennas and propagation for body centric communications," in *Antennas and Propagation, 2006. EuCAP 2006. First European Conference on*, 2006, pp. 1-7.

[11] M. Marzegalli, M. Landolina, M. Lunati, G. B. Perego, A. Pappone, G. Guenzati*, et al.*, "Design of the evolution of management strategies of heart failure patients with implantable defibrillators (EVOLVO) study to assess the ability of remote monitoring to treat and triage patients more effectively," *Trials,* vol. 10, p. 42, 2009.

[12] R. Sidhu, D. Sanders, A. Morris, and M. McAlindon, "Guidelines on small bowel enteroscopy and capsule endoscopy in adults," *Gut,* vol. 57, pp. 125-136, 2008.

[13] *Small Bowel Capsule Endoscopy – A Backgrounder*. Available: http://www.olympusamerica.com/presspass/press_pass_cut/documents/EndoCapsuleBackgrounder.pdf

[14] *Capsule Endoscopy*. Available: http://alliancetech.com.vn/modules.php?name=Product&op=viewcat2&catid=252&newlang=english

[15] A. K. Skrivervik, "Implantable antennas: The challenge of efficiency," in *Antennas and Propagation (EuCAP), 2013 7th European Conference on*, 2013, pp. 3627-3631.

Chapter 2

Antennas in Lossy media: Background and Literature Review

2.1 Introduction:

This chapter extensively details the state of the art research on implantable antennas and ways to improve their performance. In addition, designs of implanted antennas, challenges and human body modelling for body wireless communication are presented with a special focus on its performance. The implantable antenna performance is characterized by antenna gain, bandwidth, SAR and size.

The rest of this chapter is divided into five sections: Section 2.2 briefly introduces the importance of the BSN/BCWC technology with a special focus on the implanted devices in the context of biomedical applications. Section 2.3 discusses the effects of the human body tissues on the implanted antennas performance. Section 2.5 proposes implanted antennas requirements and challenges with an extra focus on the challenge of performance. Section 2.6 presents a detailed discussion on the state of the art of implantable antennas design and performance and the recent growth in this area. The state of the art of human body modelling techniques is presented in section 2.7 and finally, a summary of this chapter is drawn in section 2.8.

2.2 Implantable Devices and Medical Applications

Diseases of the heart and circulatory system (cardiovascular disease or CVD) are the main cause of death in the UK accounting for almost one in three of all deaths [1]. Heart related disease particularly cardiovascular is the leading cause of death with 46% in Saudi Arabia [2] and 47% in Europe [3]. Globally, an estimated 17.5 million people died from cardiovascular diseases (CVDs) in 2012, representing 31% of all deaths worldwide [4, 5]. Most heart disease associated with the incidental instead of continuing irregularity such as transient waves in blood pressure, paroxysmal arrhythmias or disease caused by myocardial ischemia [6]. Thus, these incidents cannot be detected or analysed by the medical team specialist. However, if these incidents are accurately and instantly predicted, health care and the quality of life will be improved. Therefore, Body Sensor Network (BSN) is an important technology to prohibit heart disease, to detect any abnormality or to be used for patients long term monitoring [7].

2.2.1 Body Sensor Network (BSN)

Body Sensor Network (BSN), Body Area Network (BAN) or Body-Centric Wireless Communication (BCWC) is formally defined by IEEE 802.15 as, "*a communication standard optimized for low power devices and operation on, in or around the human body (but not limited to humans) to serve a variety of applications including medical, consumer electronics, personal entertainment and other*" [8]. Communications in body sensors networks can be off-body, within on-body networks (on-body) or

communications to a medical implant (in-body). They can be either wearable devices around the body or implantable devices inside the body [9]. These are all emerging technologies that have a wide range of applications such as, healthcare and biomedical applications, entertainment, surveillance, emergency, sports and military [10].

2.2.2 Biomedical applications of Implantable antennas

Implanted wireless sensors have been investigated for medical applications and interest in them has been rapidly increasing over the past years. Biomedical applications for such technologies focus on early detection of disease especially chronic conditions [11]. Long term monitoring of patient activities under normal physiological conditions has a great impact on the quality of life where patients can engage in normal daily life activities, instead of stay home or hospital [12]. Implantable devices increase the healthcare quality as it reduces the risk of some diseases complications, for example, by continuous monitoring of some disease developments [13-16]. Moreover, it reduces healthcare cost, as for example patients can be continuously monitored without being admitted to the hospital [13-17]. Therefore, the most important advantage is the monitoring of patients in their normal daily activities. Thus, the traditional clinical monitoring would be replaced by continuous and remote monitoring [18]. This will have a significant impact on the quality of life, improve the accuracy of diagnostic and reduce health care costs [19].

Examples of electronic implants include heart pacemakers, cochlear implants and intraocular implants for retinal prosthesis application [20-22]. Implants can be used for monitoring the healing of soft tissue trauma and to allow early stage diagnosis of

infection [23]. The main applications of implanted devices are either therapeutic, such as hyperthermia, or diagnostic to detect and transmit data. These implantable devices are embedded into the body in order to provide vital information such as glucose level, blood pressure, etc. This information can be transmitted from implantable devices to external equipment outside the body through a wireless communication link [22, 24-26]. Therefore, research on implanted antennas for transmission and reception of power in these implanted devices is extremely important. Implantable antennas have been growing rapidly over the past few years with the potential for producing efficient medical treatments and improving the quality of healthcare.

2.3 The Effect of the Human Body on the Implanted Antenna Performance

Although implantable devices are important for the healthcare applications they encounter considerable challenges to design it. Implanted devices have benefited from recent advanced microelectronics and sensor technology while challenges still remain with antenna. Design and performance of the implanted antennas is significantly affected by the lossy medium of human body as most of human body tissues have a high relative permittivity and high conductivity. For example, the conductivity and relative permittivity of muscle is 0.79 S/m and 57.1, respectively at 403 MHz [27]. The human body is also frequency dependent. For example, the conductivity and relative permittivity of the skin is 0.69 S/m and 46.7, respectively at 403 MHz while they are 1.48 S/m and 37.95 , respectively at 2.45 GHz [27, 28].

The main influence of the high conductivity and permittivity is the significant increase of the attenuation loss. This attenuation can be calculated inside the body human tissues using the following equation [29]:

$$L_\alpha = 20\, log_{10}\,(e^{-\alpha l}) \qquad (2\text{-}1)$$

Where α (Np/m) is the attenuation constant, L_α (dB) is the attenuation loss, l (m) is the distance in the tissue. The attenuation constant can be calculated using equation [29]:

$$\alpha = \omega\sqrt{\mu\varepsilon}\left[\frac{1}{2}\sqrt{1+\left(\frac{\sigma}{\omega\varepsilon}\right)^2}-1\right]^{1/2} \qquad (2\text{-}2)$$

Where ω (rad/m) is the angular frequency, μ is the tissue permeability (H/m), ε (F/m) is the permittivity and σ is the tissue conductivity (S/m). The tissue permittivity ε can be calculated as:

$$\varepsilon = \varepsilon_o\, \varepsilon_r \qquad (2\text{-}3)$$

Where ε_o is the free space permittivity and ε_r is the relative permittivity. It should be mentioned that the human body tissues are non-magnetic and, therefore, the human body tissues permeability μ (H/m) is equal to free space permeability μo [29].

There are additional losses in the human body due to reflections between the tissues at the boundary during the signal travel. These losses can be calculated using Equations (2-4) to (2-6) [29, 30] where incidence in Equation (2-5) is assumed to be normal:

$$L_r = -20\, log_{10}\,(\Gamma) \tag{2-4}$$

$$\Gamma = \frac{\eta_2 - \eta_1}{\eta_2 + \eta_1} \tag{2-5}$$

$$\eta = \sqrt{\frac{j\omega\mu}{\sigma + j\omega\varepsilon}} \tag{2-6}$$

Where η (Ω) is the intrinsic impedance and Γ is the reflection coefficient at the boundary between tissues.

The received power at the receiver device can be calculated using the following equation [31, 32]:

$$P_{RX} = P_{TX} + G_{TX} + G_{RX} - Loss \quad (2\text{-}7)$$

where P_{RX} (dBm) is the received power, P_{TX} (dBm) transmitted power, G_{TX} (dB) is the transmitter antenna gain, G_{RX} (dB) is the receiver antenna gain and *Loss* (dBm) is the total loss which can be calculated using the following equation [31, 32]:

$$Loss = P_L + e_P - ML_{TX} - ML_{TX} \quad (2\text{-}8)$$

Where P_L (dB) is the path loss, e_p (dB) is the polarization mismatch factor, ML_{TX} (dB) is the transmitter impedance mismatch loss, ML_{RX} (dB) is the receiver impedance mismatch loss.

The path loss P_L can be calculated using the following equation [32]:

$$P_L = 10n\, log\left(\frac{d}{d_o}\right) + 10\, log_{10}\left(\frac{4\pi d_o}{\lambda_o}\right)^2 + S \quad (2\text{-}9)$$

where n is the path loss component, where; n =1.5 for line-of-sight indoor propagation, while n= 3 for none-line-of-sight indoor propagation and n= 2 for free space propagation. d is the Tx-Rx distance, λ_o is the free-space wavelength and S is the random scatter [31, 32].

For loss in the free-space propagation, *n*= 2 and equation (2-9) can be simplified to the Friis equation as following:

$$P_f = 20\, log_{10}\left(\frac{4\,\pi\, d}{\lambda_o}\right) \qquad (2\text{-}10)$$

It is clear that the antennas in the human body suffered from attenuation and the challenges of low gain. Moreover, since these antennas are implanted in the human body, there are further challenges and limitations as illustrated in the next section.

2.4 System and Path Loss Consideration

As mentioned in Chapter 1, implantable devices should collect important information from the patient and send it to hospital records through a hotspot. Figure 2.1 shows an example of a hospital admittance room with four patients. In this example, assuming that all patients have implanted subcutaneous antennas, patients in bed (1) and bed (2) have the largest distance to the receiver with about 5 meters. In order to examine the availability of the communication between the implanted antenna and receiver, path loss is calculated. Most of specifications and assumptions of the receiver are taken from International Communication Union (ITU-R) report [33].

Table 2.1 lists the parameters used for the analysis of the path loss calculations. Using Equation (2-10), the path loss in the free space at 2.45 GHz with 5 m distance is -54.2 dB. By adding the free space loss, Effective Radiated Power (ERP) and excess loss, as suggested by IUR, the power at the receiver is -102.7 dBm. This value is below the Receiver noise floor (- 101 dBm) and therefore, the system power should be improved.

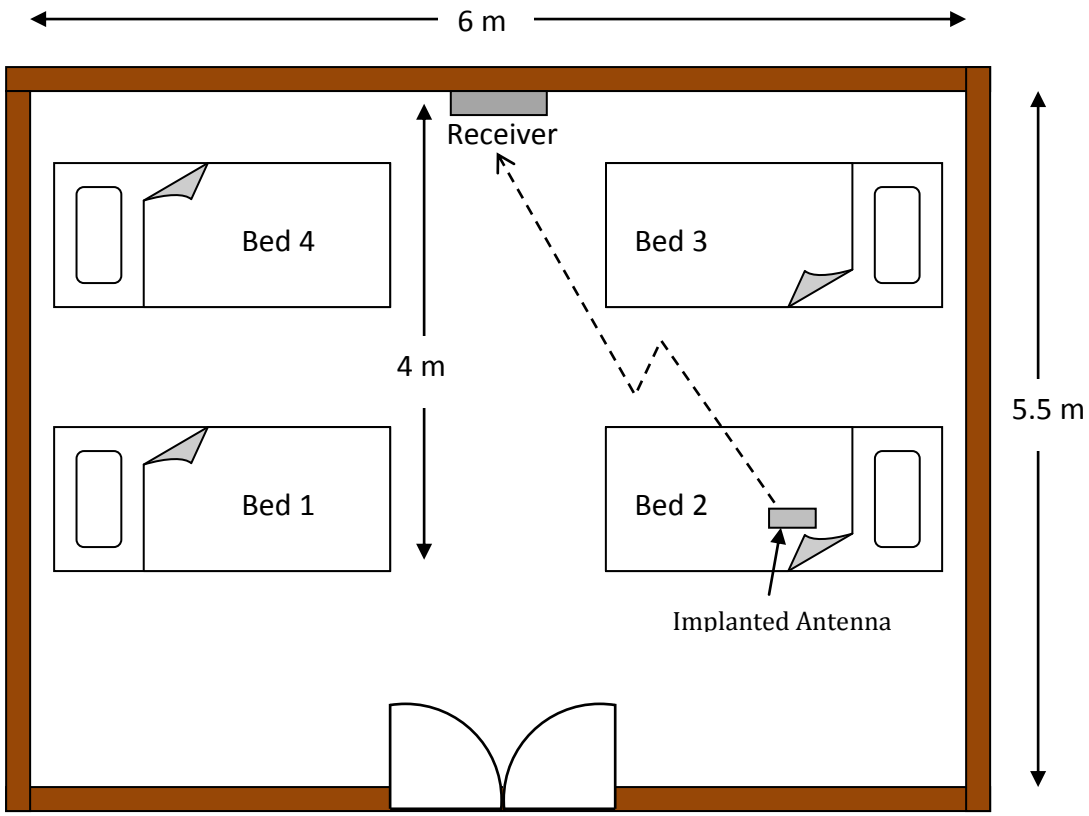

Figure 2.1: Hospital admittance room

Table 2.1: The parameters used for the analysis of path loss (adapted from [33])

Parameter	value
Frequency	2.45 MHz
Receiver noise floor	–101 dBm
Receive antenna gain	2 dBi
Free space loss at 5 metres	-54.2 dB
Excess loss (polarization, etc.)	15 dB
Transmit antenna gain	–31.5 dBi
Power into antenna	–2 dBm
ERP	–33.5 dBm (at body surface)

2.5 Requirements, Standards and Challenges of Implantable Antennas

Due the electromagnetic properties of the human body, implantable systems face more challenges and difficulties in designing antennas than conventional wireless communication systems. Unlike free space, human body tissues are lossy and have large relative permittivity. Therefore, the antenna requires the compliance with many conditions, standards and requirements such as: size, radiation performance, frequency of operation and SAR.

2.5.1 Antenna size:

Implantable antennas have to be physically small enough to be compatible and inserted inside the human body and, thus, researchers apply extra effort to reduce the implanted antenna size. However, antenna electrical size directly affects the electromagnetic performance where the reduction of antenna size reduces the antenna performance [34-36]. Therefore, a new technique to maintain a combination of low profile antenna design and a reasonable performance is required for implantable antennas.

2.5.2 Radiation performance

Due to the high path loss, the implanted antenna should have gain as high as possible in the desired direction to guarantee communication between the antenna and the external devices. In the case of capsule endoscopy antennas, omni-directional radiation is required in order to cover all direction during fluctuation of the capsule endoscopy device. However, implanted antenna radiation has to comply with SAR requirements and emitted power regulations.

2.5.3 Specific Absorption Rate (SAR)

As described in section 2.3, the one of the main effects of the human body on the implanted antennas is the high attenuation of the radiated power. This power attenuation in the lossy surrounding media generates heat in the human body tissues which could be hazardous to health. Therefore, for safety reason, in-body radiation is restricted to certain level. Thus, the Specific Absorption Rate (SAR) has been introduced to measure the Electromagnetic (EM) Energy absorbed by biological

tissues mass when exposed to radiating devices. SAR can be defined using the following equation [37]:

$$SAR = \frac{P_L}{\rho} = \frac{\sigma\,|E|^2}{\rho} \qquad (2\text{-}11)$$

Where E (V/m) is the electric field and ρ (kg/m^3) is the mass density.

SAR can be defined in many terms such as (Mass averaged SAR) for each point SAR, a cube with a defined mass (1 g or 10 g) is found. Then, the power loss density is integrated over this cube and then the integrated power loss is divided by the cube mass [38].

The FCC and ERC define that the maximum limits for SAR averaged over 1 g and 10 g of tissue mass by 1.6 and 2 W/kg respectively [39, 40]. The maximum EIRP, according to European Telecommunications Standards Institute (ETSI) [41], is -10 dBW (100 mW) where EIRP is the Effective Isotropic Radiated Power. Therefore, the antenna radiation has to comply with SAR requirements and emitted power regulations (EIRP).

2.5.4 Frequency of operation

Medical electronic devices can be classified into two categories depending on the protocol and standards that these devices use. The first category is Wireless Medical Telemetry Services (WMTS) for wearable devices. The second category is Medical

Implant Communications Service (MICS) which was allocated by the European Telecommunications Standards Institute (ETSI) for implantable devices. The frequency band allocation for MICS is 402 MHz to 405 MHz [41].

The Industrial, Scientific, and Medical (ISM) bands (433.1-434.8 MHz, 868-868.6 MHz, 902.8-928 MHz, and 2400-2500 MHz) are also suggested for implantable medical device biotelemetry in some countries, especially for subcutaneous application [42, 43].

For deeper implanted antennas inside the human body, such as capsule endoscopy, implanted antennas operate at the medical implant communications service (MICS) frequency band (402–405 MHz) which is regulated by the European Radio communications Committee (ERC) [44] and the Federal Communication Commission (FCC) [45] for ultra low power active medical implants. This is because the MICS band has relatively low power loss inside human body. In recent studies of the total loss between transmitter and receiver antennas, it was founded that the minimum total loss is achieved when the MICS frequency band is used [46-48].

2.6 State of the Art Implantable Antennas Design and Challenges

A large number of implanted antennas have been presented the literature. However, they can be classified into two categories; the first one is subcutaneous implanted antennas or antennas to be placed in a fixed area of the body, and the second category is implantable antennas that move through the body such as capsule endoscopy

systems. In this section, antennas are reviewed in term of bandwidth, gain and size. In addition, capsules antennas minimum gain and radiation pattern directionality are reviewed and compared.

2.6.1 Antennas Size

In the literature, different techniques have been used thoroughly to reduce implantable antenna size. Designing antennas to operate at high frequency bands, such as 5.8 GHz or higher, is one of the techniques to presents applicable size antennas to be implanted inside human body [49-51]. The other technique to overcome the size problem is to design a conducting microstrip antenna with meandered, folded or spiralled surface along the substrate either in one layer or multi layers [52-55]. Further miniaturisation can be realised by employing substrate with a high dielectric constant and, thus, a large number of researches presented antennas with high permittivity substrate to reduce the implanted antenna size [24, 56-59]. An example of this technique is shown in Figure 2.2 [52]. Table 2.2 shows a comparison between design parameters of [60] and [52] which both resonates at MICS band. Although both are operating at the same frequency, the antenna size in [52] has 63% smaller area compared to the same antenna design presented in [60] due to the higher-dielectric-constant material used in [52]. However, a high dielectric constant substrate is susceptible to surface wave excitation, which degrades the radiation pattern of the antenna [61]. Figure 2.3 shows examples of implanted antennas with miniaturisation techniques.

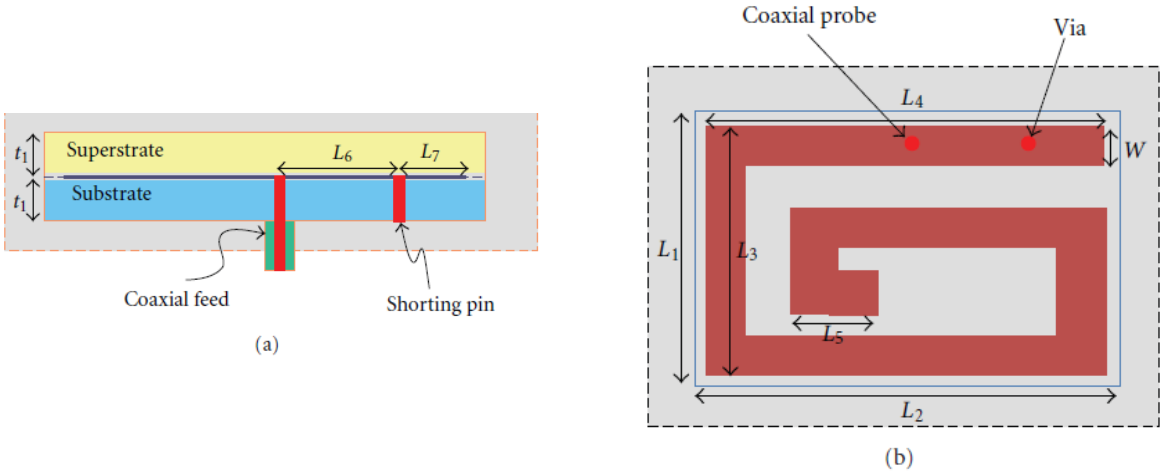

Figure 2.2: Geometry of embedded spiral-shaped microstrip implantable antenna, (a) side view, (b) top view.

Table 2.2: Comparison between design parameters of [60] and [52] which both resonates at MICS band

Parameter	Design in [60]	Design in [52]
L1	19.6	11.9
L2	29.6	18.2
L3	16.8	11
L4	26.6	17.4
L5	13	3.6
L6	7.7	4.9
L7	4.9	3.4
t1	3	1.9
t2	3	1.9
W	2.8	1.8
Total area reduction		62.67%

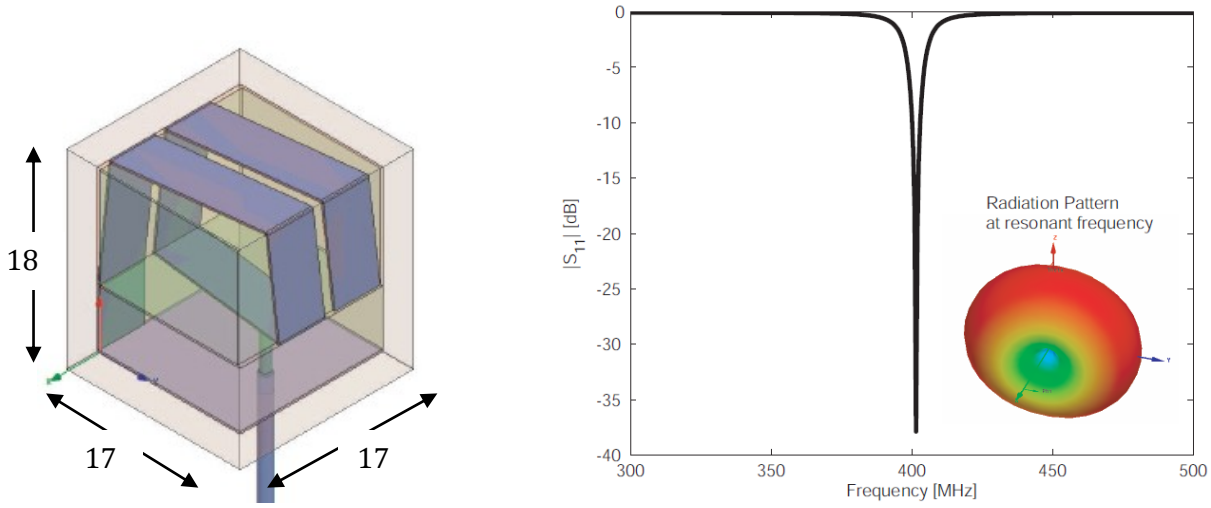

(a) (b)

Figure 2.3: 3D-spiral small antenna design (a) the proposed design and (b) simulated S11 and radiation pattern [54]

A dual-band capsule multilayer conformal antenna to operate at the MedRadio and 2.45 GHz is proposed in [62] and the proposed design is shown in Figure 2.4. The Measured S11 is compared to the simulated one as presented in Figure 2.5 (a) and the far-field pattern is compared for the homogeneous cylindrical body phantom and at the intra-muscular location (Duke 1) as shown in Figure 2.5 (b). The implant size is large (5 mm in radius and 30 mm in length) and the antenna bandwidth for this antenna very narrow (< 20 MHz) around the MedRadio band.

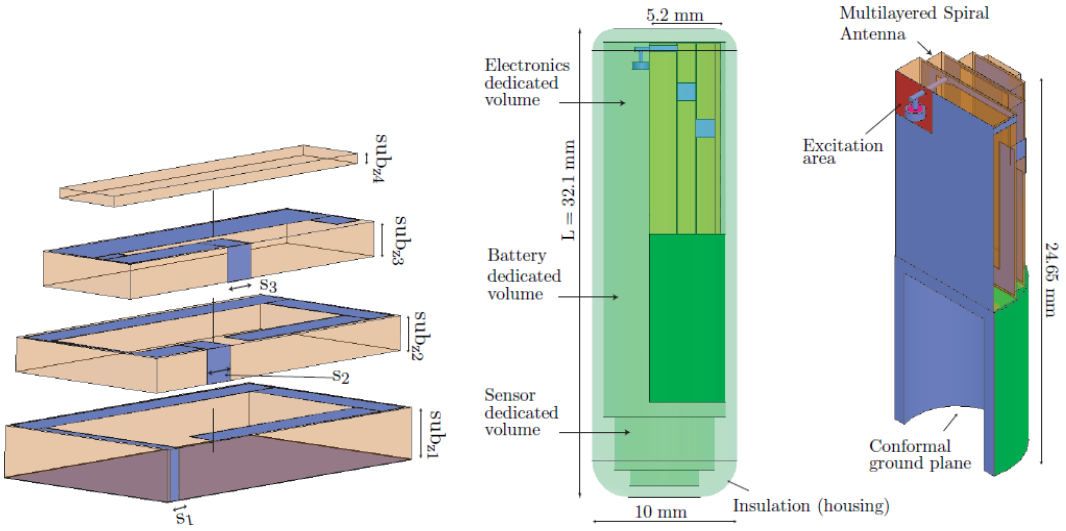

Figure 2.4: Capsule multilayer conformal antenna [62] proposed design for the homogeneous cylindrical body phantom and at the intra-muscular location (Duke 1)

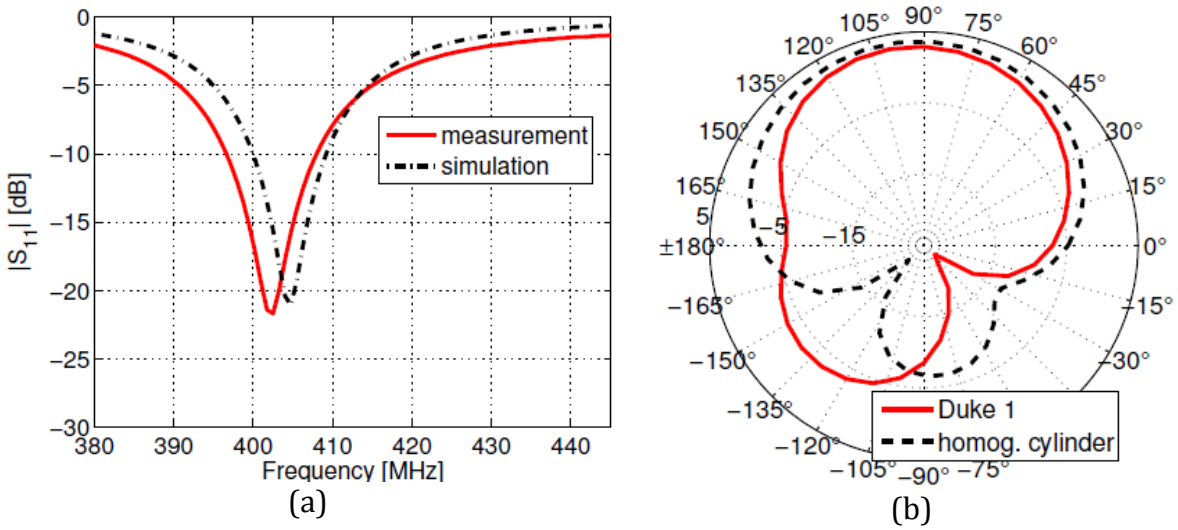

Figure 2.5: Capsule multilayer conformal antenna [62] (a) Measured vs. Simulated S11 and (b) Simulated radiation patterns in [dBi] in the homogeneous cylindrical body phantom and at the intra-muscular location (Duke 1)

A dual band of 402- 405 MHz (MICS) and 2.45 GHz (ISM) implanted antenna was presented in [24] as shown in Figure 2.6. This antenna obtained 20% and 35.3% simulated and measured -10 dB bandwidth at the MICS band. However, it had only 4.2% and 7.1% bandwidth simulated and measured at ISM region. This bandwidth is narrowband and the antenna may not resonate at the expected frequency when a realistic body model is used.

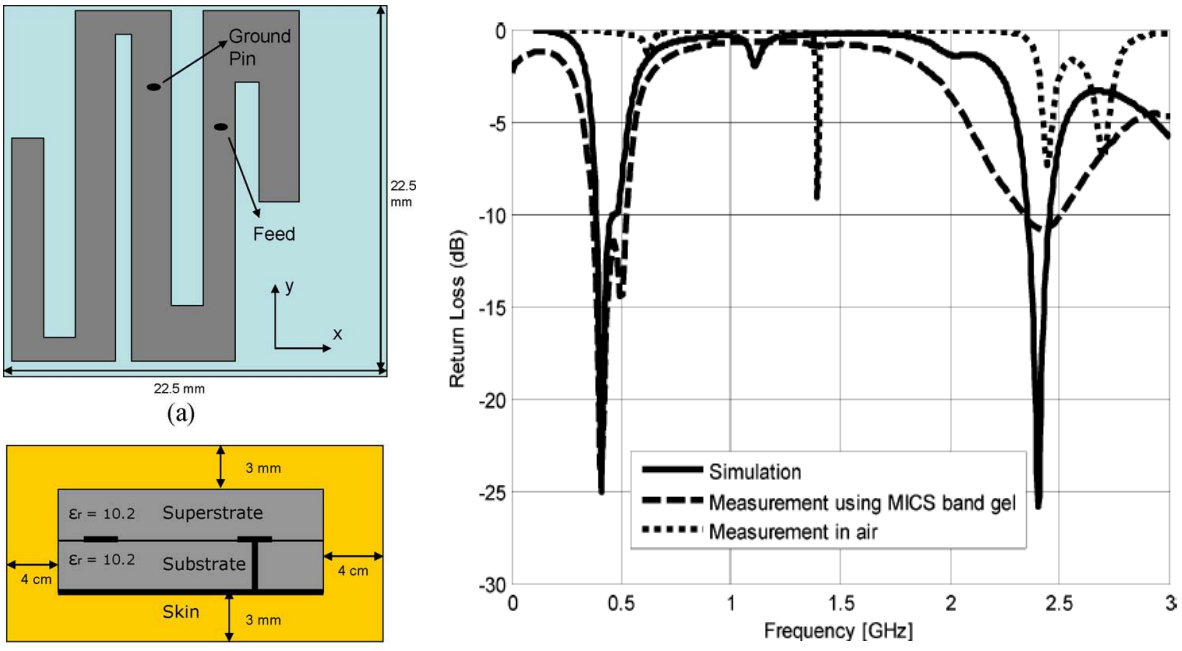

(a) (b)

Figure 2.6: Dual-band meandered implanted antenna design of [24] (a) the proposed design and (b) simulated vs. measured S11

Table 2.3: Performance comparison of implanted antennas reported in the literature

Antenna	Bands (MHz)	Dielectric Material Permittivity	Dimensions (mm)	Max. Gain (dBi)	Min. Gain (dBi) (*for capsule antennas*)
Meandered PIFA [24]	402-405 & 2450	10.2	22.5x22.5x2.5	-24.9 @ MICS & -11 @ ISM	NA
[60]	402-405		29.6x19.6	-35	NA
[52]	402-405	10.2	18.2x11.9	No data	NA
conformal meandered dipole antenna [63]	700 MHz	2.2	12.25 x 9.6	– 29	- 55 *
Flexible microstrip patch [64]	403 MHz	3.4	15 x 7	- 33	-65
Loop antenna [65]	403 MHz	-	9 x 10	-28.4	-48 *
Planner antenna [66]	403 MHz	4.4	20 x 10	Normalised to 0	- 16 dB from highest gain
Multilayer spiral antenna [62]	402.8 MHz	4.4	24.5x 9 X5.2	-30.2	-55
Flexible meandered inverted-F Antenna [67]	1.4 GHz	2.2	15 x 9	- 25.2	-56

* The number is estimated from the colours chart of the presented antenna

2.7 Human Body Modelling

The human body is, complex, having a large number of systems with different electromagnetic characteristics for every part of the body. The human body's permittivity vary from 70 to 0 overlapping tissues [27, 68] as detailed in Appendix A. During implanted antenna design process, human body modelling carries out two times: during numerical simulation and during measurements investigations.

Numerical simulation involves evaluating the fundamental field quantities from the Maxwell's curl equations using numerical methods to describe propagation of electromagnetic waves and their interactions with a material [69]. There are many different methods which can be used to solve three dimensional electromagnetic problems. These methods can be classified into integral equation and differential equation methods. Method of moments, Finite element method, Finite difference time domain method and Transmission line matrix method are the most commonly used numerical techniques.

2.7.1 Numerical Phantoms

Numerical body phantom can be a single component with single electromagnetic characteristics (homogeneous) or multilayer, multi-component represents the variety of the human body's electromagnetic characteristics (inhomogeneous). In numerical investigation, implanted antennas can be inserted inside numerical inhomogeneous lossy media that simulate biological tissues, however, inhomogeneous models are expensive. Homogeneous lossy media can be used in case of some applications such as capsule endoscopy. Values of electromagnetic properties of the biological tissues can

be entered using the simulation software. Tissues numerical modelling can be either a single layer or multilayer depend on the simplicity of the modelling. An example of a single layer tissue model is shown in Figure 2.7 (a) [31] and multilayer tissue model example in Figure 2.7 (b) [70]. Numerical human body modelling can be carried out using numerical techniques such as Finite-Element (FE) Method and Finite-Difference Time-Domain (FDTD) Method. These techniques are built in some simulation software such as Ansoft HFSS [52, 71, 72] and CST design studio respectively [31, 70, 73].

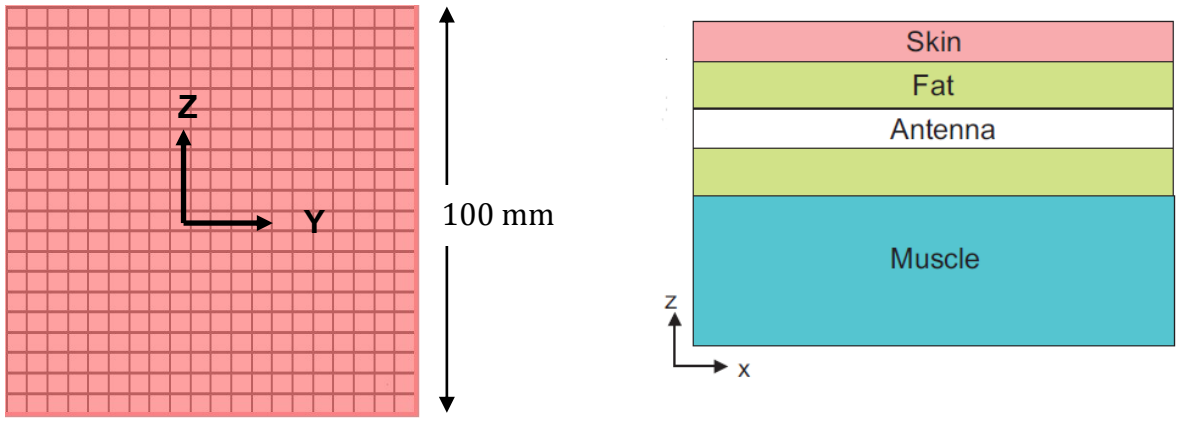

(a) (b)

Figure 2.7: (a) Example of single layer model of simulated human tissue (adapted from [31]) and (b) multilayer model [70]

2.7.2 Measurements modelling

For measurements investigations, human body modelling can be carries out using either animals-tissues or phantoms.

2.7.2.1 Modelling using animals-tissues

Measurements using animal tissues are a useful way to mimic the human body tissues where they have frequency-dependency characteristics. It provides a suitable environment when the measurements are conducting for dual or multi-band implanted antennas. Measurements using animal tissue can be carried out either by inserting the antenna inside tissue samples, or by implanting the antenna inside a live model animal by surgical operation (in-vivo).

In [74], a pig front leg was minced to measure a dual band implanted patch antenna. A rat skin with dimensions of 50 mm × 50 mm × 5 mm was also used to test a dual band patch antenna [75]. Minced pork meat is used to measure an implantable antenna in [76] and a dual-band antenna was tested in vivo using rats as model animals in [77].

Two types of antennas, namely a balanced dipole antenna and a balanced loop antenna are used in the measurement. Two boxes are filled with minced pork lean meat to be used for the measurements in [78]. It is founded that pork meat has close electromagnetic characteristics to the human body [79]. Figure 2.8 shows example of measurements using animal tissues.

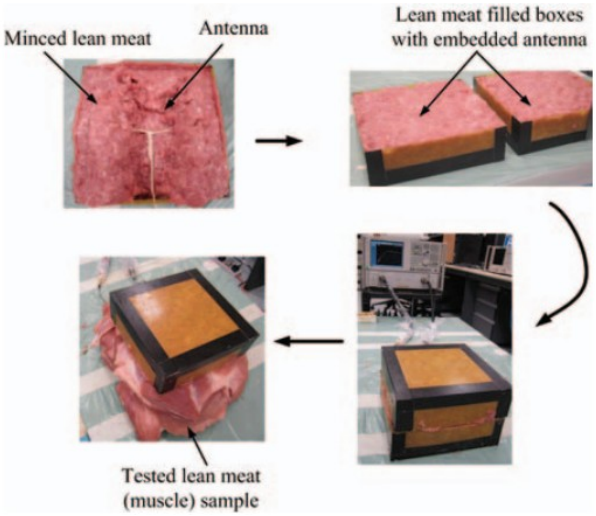

(a) Minced pork meat model [78]

(b) In Vivo Verification of Implantable Antennas Using Rats as Model Animals [77]

Figure 2.8: Example of measurements using animal tissues

2.7.2.2 Physical Phantoms

In order to experimentally investigate the interaction between the human body tissue and the electromagnetic fields, phantoms are used to simulate the biological tissues of human body. For this purpose, phantoms have been used extensively in medical and engineering research. Examples of using phantoms include the effects of electromagnetic radiation on health, X-ray, magnetic resonance imaging (MRI) scan and implantable system design.

Many different phantoms have been proposed to model the human body tissues [24, 68, 80, 81]. However, they can all be classified into three categories based on their state: liquid, semisolid, or solid phantoms and each type has advantages and disadvantages [82, 83]. The main features of solid phantoms are the stability of the

electromagnetic properties and the possibility of covering wide range frequencies. However, solid phantoms are expensive and not easy to fabricate. One of the main features for the semisolid phantoms is the flexibility of reshaping. However, it has a problem of limited control for the electromagnetic prosperities over a wide frequency range. For the liquid phantoms, there are many drawbacks such as the need of a shell to contain the liquid, limited range of frequencies and difficulty of handling the container. However, although liquid phantoms have these disadvantages, they still have the important advantage of being easy to fabricate by mixing different components.

2.8 Summary:

In this chapter, a general background of BSN and implantable antennas for biomedical applications, current regulations and standards are presented. In addition, designs of implanted antennas, effects of lossy media on the antenna performance, challenges and human body modelling for body wireless communication are discussed. Current researches progresses toward high performance implantable antennas are also reviewed and summarized.

Studies show that the human body reduces the radiation efficiency of implantable antennas due to electromagnetic absorption in body tissues. The highly lossy media causes radiation pattern distortion and effects antennas and behaviour. Therefore, electromagnetic waves suffered from multiple reflections and large attenuation when they pass through the human body. Furthermore, depending on the surrounding body tissue, the performance and the antenna gain are decreased dramatically. Therefore,

an efficient antenna design and new techniques to overcome the lossy media effects and to improve implantable antennas performance are required.

High performance implanted antenna should be compact size, light in weight, wide bandwidth, high gain and, in case of capsule endoscopy, has to be omni-directional radiation pattern. However, most of the previous implantable antennas satisfied some of these conditions and most of them suffer from some problems of low gain, high SAR and narrow bandwidth. Moreover, in case of capsule endoscopy antennas, most of proposed implanted antennas have a large difference between the maximum and minimum gain. Thus, more power needs to be delivered to the antenna to get efficient wireless communication to the external devices. Therefore, new antennas that satisfy all the requirements for implanted antennas design performance are required.

2.9 References

[1] N. Townsend, K. Wickramasinghe, P. Bhatnagar, K. Smolina, M. Nichols, J. Leal*, et al.*, "Coronary heart disease statistics 2012 edition," *British Heart Foundation: London,* p. P107, 2012.

[2] W. H. Organization, *World health statistics 2010*: World Health Organization, 2010.

[3] J. Perk, G. De Backer, H. Gohlke, I. Graham, Ž. Reiner, M. Verschuren*, et al.*, "European Guidelines on cardiovascular disease prevention in clinical practice (version 2012)," *European heart journal,* vol. 33, pp. 1635-1701, 2012.

[4] A. Alwan, *Global status report on noncommunicable diseases 2010*: World Health Organization, 2011.

[5] C. Borger, S. Smith, C. Truffer, S. Keehan, A. Sisko, J. Poisal*, et al.*, "Health spending projections through 2015: changes on the horizon," *Health Affairs,* vol. 25, pp. w61-w73, 2006.

[6] B. Lo and G.-Z. Yang, "Key technical challenges and current implementations of body sensor networks," in *Proc. 2nd International Workshop on Body Sensor Networks (BSN 2005)*, 2005.

[7] S. Ullah, H. Higgin, M. A. Siddiqui, and K. S. Kwak, "A study of implanted and wearable body sensor networks," in *Agent and Multi-Agent Systems: Technologies and Applications*, ed: Springer, 2008, pp. 464-473.

[8] J. Gutierrez, M. Naeve, E. Callaway, M. Bourgeois, V. Mitter, and B. Heile, "IEEE 802.15. 4: a developing standard for low-power low-cost wireless personal area networks," *network, IEEE,* vol. 15, pp. 12-19, 2001.

[9] P. Hall, Y. Hao, and K. Ito, "Guest editorial for the special issue on antennas and propagation on body-centric wireless communications," *Antennas and Propagation, IEEE Transactions on,* vol. 57, pp. 834-836, 2009.

[10] G.-Z. Yang and M. Yacoub, "Body sensor networks," 2006.

[11] B. Lo and G.-Z. Yang, "Architecture for body sensor networks," in *Perspectives in Pervasive Computing*, 2005, pp. 23-28.

[12] A. Milenković, C. Otto, and E. Jovanov, "Wireless sensor networks for personal health monitoring: Issues and an implementation," *Computer communications,* vol. 29, pp. 2521-2533, 2006.

[13] D. Andre and D. L. Wolf, "Recent advances in free-living physical activity monitoring: a review," *Journal of diabetes science and technology,* vol. 1, pp. 760-767, 2007.

[14] F. Braunschweig, P. T. Mortensen, D. Gras, W. Reiser, T. Lawo, H. Mansour*, et al.*, "Monitoring of physical activity and heart rate variability in patients with chronic heart failure using cardiac resynchronization devices," *The American journal of cardiology,* vol. 95, pp. 1104-1107, 2005.

[15] M. Gerritsen, J. Jansen, and J. Lutterman, "Performance of subcutaneously implanted glucose sensors for continuous monitoring," *The Netherlands journal of medicine,* vol. 54, pp. 167-179, 1999.

[16] P. Kupelian, T. Willoughby, A. Mahadevan, T. Djemil, G. Weinstein, S. Jani*, et al.*, "Multi-institutional clinical experience with the Calypso System in localization and continuous, real-time monitoring of the prostate gland during external radiotherapy," *International Journal of Radiation Oncology* Biology* Physics,* vol. 67, pp. 1088-1098, 2007.

[17] *Body-Centric Wireless Communications*. Available: http://antennas.eecs.qmul.ac.uk/research/body-centric-wireless-commnication-and-networks/

[18] O. Garcia-Morchon, T. Falck, T. Heer, and K. Wehrle, "Security for pervasive medical sensor networks," in *Mobile and Ubiquitous Systems: Networking & Services, MobiQuitous, 2009. MobiQuitous' 09. 6th Annual International*, 2009, pp. 1-10.

[19] P. Zweifel, S. Felder, and M. Meiers, "Ageing of population and health care expenditure: a red herring?," *Health economics,* vol. 8, pp. 485-496, 1999.

[20] J. A. Von Arx, M. D. Amundson, W. R. Mass, R. Balczewski, and W. J. Linder, "Telemetry apparatus and method for an implantable medical device," ed: Google Patents, 2003.

[21] A. J. Maniglia and W. H. Ko, "Totally implantable cochlear implant for improvement of partial and total sensorineural hearing loss," ed: Google Patents, 2000.

[22] K. Gosalia, M. S. Humayun, and G. Lazzi, "Impedance matching and implementation of planar space-filling dipoles as intraocular implanted antennas in a retinal prosthesis," *Antennas and Propagation, IEEE Transactions on,* vol. 53, pp. 2365-2373, 2005.

[23] J. Rigelsford and C. Davenport, "A passive RFID implant for soft tissue trauma monitoring," in *Antennas and Propagation Conference (LAPC), 2013 Loughborough*, 2013, pp. 127-130.

[24] T. Karacolak, A. Z. Hood, and E. Topsakal, "Design of a dual-band implantable antenna and development of skin mimicking gels for continuous glucose monitoring," *Microwave Theory and Techniques, IEEE Transactions on,* vol. 56, pp. 1001-1008, 2008.

[25] R. D. Beach, R. W. Conlan, M. C. Godwin, and F. Moussy, "Towards a miniature implantable in vivo telemetry monitoring system dynamically configurable as a potentiostat or galvanostat for two-and three-electrode biosensors," *Instrumentation and Measurement, IEEE Transactions on,* vol. 54, pp. 61-72, 2005.

[26] L. Thuc, "Human implanted spiral antenna for a 2.45 GHz wireless temperature and pressure SAW sensor system," in *2008 IEEE Antennas and Propagation Society International Symposium*, 2008, pp. 1-4.

[27] C. Gabriel, "Compilation of the Dielectric Properties of Body Tissues at RF and Microwave Frequencies," DTIC Document1996.

[28] D. Andreuccetti, R. Fossi, and C. Petrucci, "Calculation of the dielectric properties of body tissues," *Institute for Applied Physics, Italian National Research Council,* 2007.

[29] P. Zakavi, N. C. Karmakar, and I. Griggs, "Wireless Orthopedic Pin for Bone Healing and Growth: Antenna Development," *Antennas and Propagation, IEEE Transactions on,* vol. 58, pp. 4069-4074, 2010.

[30] R. W. P. King, G. S. Smith, M. Owens, and T. T. Wu, "Antennas in matter: Fundamentals, theory, and applications," *NASA STI/Recon Technical Report A,* vol. 81, p. 29690, 1981.

[31] A. Kiourti and K. S. Nikita, "Miniature scalp-implantable antennas for telemetry in the MICS and ISM bands: Design, safety considerations and link budget analysis," *Antennas and Propagation, IEEE Transactions on,* vol. 60, pp. 3568-3575, 2012.

[32] A. Alomainy and Y. Hao, "Modeling and characterization of biotelemetric radio channel from ingested implants considering organ contents," *Antennas and Propagation, IEEE Transactions on,* vol. 57, pp. 999-1005, 2009.

[33] L. J. Chu, "Physical Limitations of Omni-Directional Antennas," *Journal of applied physics,* vol. 19, pp. 1163-1175, 1948.

[34] R. F. Harrington, "Effect of antenna size on gain, bandwidth, and efficiency," *J. Res. Nat. Bur. Stand,* vol. 64, pp. 1-12, 1960.

[35] J. S. McLean, "A re-examination of the fundamental limits on the radiation Q of electrically small antennas," *Antennas and Propagation, IEEE Transactions on,* vol. 44, p. 672, 1996.

[36] K. M. Jones, J. Mechling, J. W. Strohbehn, and B. S. Trembly, "Theoretical and experimental SAR distributions for interstitial dipole antenna arrays used in hyperthermia," *Microwave Theory and Techniques, IEEE Transactions on,* vol. 37, pp. 1200-1209, 1989.

[37] D. Kurup, W. Joseph, G. Vermeeren, and L. Martens, "Specific absorption rate and path loss in specific body location in heterogeneous human model," *IET Microwaves, Antennas & Propagation,* vol. 7, pp. 35-43, 2013.

[38] R. Kohno, K. Hamaguchi, H.-B. Li, and K. Takizawa, "R&D and standardization of body area network (BAN) for medical healthcare," in *Ultra-Wideband, 2008. ICUWB 2008. IEEE International Conference on*, 2008, pp. 5-8.

[39] I. C. U. (ITU-R). *Sharing between the meteorological aids service and medical implant*. Available: https://www.itu.int/rec/R-REC-SA.1346-0-199802-S/en

[39] K. Thotahewa, J.-M. Redouté, and M. R. Yuce, "SAR, SA, and temperature variation in the human head caused by IR-UWB implants operating at 4 GHz," *Microwave Theory and Techniques, IEEE Transactions on,* vol. 61, pp. 2161-2169, 2013.

[40] E. T. S. Institute, "Electromagnetic compatibility and Radio spectrum Matters " 2002.

[41] H. S. Savci, A. Sula, Z. Wang, N. S. Dogan, and E. Arvas, "MICS transceivers: regulatory standards and applications [medical implant communications service]," in *SoutheastCon, 2005. Proceedings. IEEE*, 2005, pp. 179-182.

[42] A. Sani, A. Alomainy, and Y. Hao, "The effect of various human body tissue models on radiowave propagation from a bladder implanted wireless source," in *Antennas and Propagation Society International Symposium, 2009. APSURSI'09. IEEE*, 2009, pp. 1-4.

[43] E. R. Committee, "ERC recommendation 70-03 relating to the use of short range devices," ed, 2002.

[44] A. Kiourti and K. S. Nikita, "Detuning issues and performance of a novel implantable antenna for telemetry applications," in *Antennas and Propagation (EUCAP), 2012 6th European Conference on*, 2012, pp. 746-749.

[45] J. Lee and S. Nam, "Q evaluation of small insulated antennas in a lossy medium and practical radiation efficiency estimation," in *Microwave Conference, 2007. KJMW 2007. Korea-Japan*, 2007, pp. 65-68.

[46] N. Cho, T. Roh, J. Bae, and H.-J. Yoo, "A planar MICS band antenna combined with a body channel communication electrode for body sensor network," *Microwave Theory and Techniques, IEEE Transactions on,* vol. 57, pp. 2515-2522, 2009.

[47] C. Buratti, R. D'Errico, M. Maman, F. Martelli, R. Rosini, and R. Verdone, "Design of a body area network for medical applications: the WiserBAN project," in *Proceedings of the 4th International Symposium on Applied Sciences in Biomedical and Communication Technologies*, 2011, p. 164.

[48] S. Manafi and H. Deng, "Design of a Small Modified Minkowski Fractal Antenna for Passive Deep Brain Stimulation Implants," *International Journal of Antennas and Propagation,* vol. 2014, 2014.

[49] J. Tak, K. Kwon, S. Kim, and J. Choi, "Dual-band on-body repeater antenna for in-on-on WBAN applications," *International Journal of Antennas and Propagation,* vol. 2013, 2013.

[50] Y. Ahmed, Y. Hao, and C. Parini, "A 31.5 GHz patch antenna design for medical implants," *International Journal of Antennas and Propagation,* vol. 2008, 2008.

[51] W. Huang and A. A. Kishk, "Embedded spiral microstrip implantable antenna," *International Journal of Antennas and Propagation,* vol. 2011, 2011.
[52] Y.-W. Yang, H.-L. Su, K.-H. Lin, H.-H. Lin, and C.-Y. Wu, "Spiral-like implanted antenna for biotelemetry," in *Microwave Conference Proceedings (APMC), 2012 Asia-Pacific*, 2012, pp. 409-411.
[53] J. Abadia, F. Merli, J.-F. Zurcher, J. R. Mosig, and A. K. Skrivervik, "3D-spiral small antenna design and realization for biomedical telemetry in the MICS band," *Radioengineering,* vol. 18, pp. 359-367, 2009.
[54] C.-Y. Huang, C.-L. Tsai, and C.-L. Yang, "Compact Folded Meander PIFA Antennas in MedRadio Bands," *Session 3A5 Microstrip and Printed Antenna, Antenna Theory,* p. 457.
[55] J. Kim and Y. Rahmat-Samii, "Implanted antennas inside a human body: Simulations, designs, and characterizations," *Microwave Theory and Techniques, IEEE Transactions on,* vol. 52, pp. 1934-1943, 2004.
[56] P. Soontornpipit, C. M. Furse, and Y. C. Chung, "Miniaturized biocompatible microstrip antenna using genetic algorithm," *Antennas and Propagation, IEEE Transactions on,* vol. 53, pp. 1939-1945, 2005.
[57] C. Sánchez-Fernández, O. Quevedo-Teruel, J. Requena-Carrión, L. Inclán-Sánchez, and E. Rajo-Iglesias, "Dual-band microstrip patch antenna based on short-circuited ring and spiral resonators for implantable medical devices," *IET microwaves, antennas & propagation,* vol. 4, pp. 1048-1055, 2010.
[58] J. Kim and Y. Rahmat-Samii, "SAR reduction of implanted planar inverted F antennas with non-uniform width radiator," in *Antennas and Propagation Society International Symposium 2006, IEEE*, 2006, pp. 1091-1094.
[59] P. Soontornpipit, C. M. Furse, and Y. C. Chung, "Design of implantable microstrip antenna for communication with medical implants," *Microwave Theory and Techniques, IEEE Transactions on,* vol. 52, pp. 1944-1951, 2004.
[60] A. Abbosh, M. Bialkowski, M. Jacob, and J. Mazierska, "Design of a compact ultra-wideband antenna," *Microwave and optical technology letters,* vol. 48, pp. 1515-1518, 2006.
[61] F. Merli, "Implantable antennas for biomedical applications," 2011.
[62] P. M. Izdebski, H. Rajagopalan, and Y. Rahmat-Samii, "Conformal ingestible capsule antenna: A novel chandelier meandered design," *Antennas and Propagation, IEEE Transactions on,* vol. 57, pp. 900-909, 2009.
[63] Y. Mahe, A. Chousseaud, M. Brunet, and B. Froppier, "New flexible medical compact antenna: Design and analysis," *International Journal of Antennas and Propagation,* vol. 2012, 2012.
[64] R. Alrawashdeh, Y.-P. Huang, and P. Cao, "Flexible meandered loop antenna for implants in MedRadio and ISM bands," *Electronics Letters,* vol. 49, pp. 1515-1517, 2013.
[65] J. C. Wang, E. G. Lim, Z. Wang, Y. Huang, T. Tillo, M. Zhang*, et al.*, "UWB planar antennas for wireless capsule endoscopy," in *Antenna Technology (iWAT), 2013 International Workshop on*, 2013, pp. 340-343.

[66] W. Seo, U. Kim, S. Lee, K. Kwon, and J. Choi, "A meandered inverted-f capsule antenna for an ingestible medical communication system," *Microwave and Optical Technology Letters,* vol. 54, pp. 1761-1765, 2012.

[67] Y. Rahmat-Samii and J. Kim, "Implanted antennas in medical wireless communications," *Synthesis Lectures on Antennas,* vol. 1, pp. 1-82, 2005.

[68] A. Sani, M. Rajab, R. Foster, and Y. Hao, "Antennas and propagation of implanted RFIDs for pervasive healthcare applications," *Proceedings of the IEEE,* vol. 98, pp. 1648-1655, 2010.

[69] W. C. Liu, F. M. Yeh, and M. Ghavami, "Miniaturized implantable broadband antenna for biotelemetry communication," *Microwave and Optical Technology Letters,* vol. 50, pp. 2407-2409, 2008.

[70] W.-C. Liu, S.-H. Chen, and C.-M. Wu, "Implantable broadband circular stacked PIFA antenna for biotelemetry communication," *Journal of Electromagnetic Waves and Applications,* vol. 22, pp. 1791-1800, 2008.

[71] A. Kiourti, M. Tsakalakis, and K. S. Nikita, "Parametric study and design of implantable PIFAs for wireless biotelemetry," in *Wireless Mobile Communication and Healthcare*, ed: Springer, 2012, pp. 96-102.

[72] C. M. Lee, T. C. Yo, F. J. Huang, and C. H. Luo, "Bandwidth enhancement of planar inverted-F antenna for implantable biotelemetry," *Microwave and Optical Technology Letters,* vol. 51, pp. 749-752, 2009.

[73] T. Karacolak, R. Cooper, and E. Topsakal, "Electrical properties of rat skin and design of implantable antennas for medical wireless telemetry," *Antennas and Propagation, IEEE Transactions on,* vol. 57, pp. 2806-2812, 2009.

[74] F.-J. Huang, C.-M. Lee, C.-L. Chang, L.-K. Chen, T.-C. Yo, and C.-H. Luo, "Rectenna application of miniaturized implantable antenna design for triple-band biotelemetry communication," *Antennas and Propagation, IEEE Transactions on,* vol. 59, pp. 2646-2653, 2011.

[75] T. Karacolak, R. Cooper, J. Butler, S. Fisher, and E. Topsakal, "In vivo verification of implantable antennas using rats as model animals," *Antennas and Wireless Propagation Letters, IEEE,* vol. 9, pp. 334-337, 2010.

[76] X. Qing, T. S. P. See, Z. N. Chen, T. M. Chiam, and C. K. Goh, "Characterization of in-and near-body radio frequency transmission loss for biomedical implants," *Journal of Medical Imaging and Health Informatics,* vol. 3, pp. 112-119, 2013.

[77] C.-K. Wu, T.-F. Chien, C.-L. Yang, and C.-H. Luo, "Design of novel s-shaped quad-band antenna for MedRadio/WMTS/ISM implantable biotelemetry applications," *International Journal of Antennas and Propagation,* vol. 2012, 2012.

[78] Y. Hao, K. Ito, and P. Hall, "Electromagnetic properties and modeling of human body," in *Antennas and propagation for Body centric Communication Systems*, P. S. Hall and Y. Hao, Eds., ed Norwood, MA, U SA: Artech Hous, 2006, pp. 1-7.

[79] T. Yilmaz, T. Karacolak, and E. Topsakal, "Characterization of Muscle and Fat Mimicking Gels at MICS and ISM Bands (402-405MHz and 2.40-2.48 GHz)," *XXIX Gen. Assoc. Int. Union Rad. Sci,* 2008.

Chapter 3

Improved Performance of Implanted Antennas Using External Planar Elements[1, 2]

3.1 Introduction:

Chapter two outlined the current progress towards implanted antenna and presented the challenges of getting high performance implanted antenna. It presented that current research into ways to improve implantable antenna performance focused on using new and different designs of antennas. This chapter presents the performance improvement of simple and available implanted antenna using external element techniques that been detailed in chapter two. This chapter proposes the design, characterisation and simulation of probe and patch implanted antennas for body wireless communication.

---

[1] AlAmoudi, A.O.; Alamri, S.; Zhu, S.; Langley, R.J., "Improved performance of 2.45 GHz implanted antenna for wireless communication," *2012 IEEE Asia-Pacific Conference on Applied Electromagnetics (APACE),* vol., no., pp.308,312, 11-13 Dec. 2012

[2] Alamri, S.; Langley, R.J.; AlAmoudi, A.O., "Improved performance of 2.45 GHz implanted patch antenna for wireless communication," *Antennas and Propagation Conference (LAPC), 2013 Loughborough* , vol., no., pp.27,30, 11-12 Nov. 2013

The design scenarios investigated the parasitic coupling of the EM wave to external elements to improve antenna performance. It shows that a length of strip line and/or a grid structure or an external ring could be used in order to enhance the performance of the implanted antenna. These are monitored by calculating the S_{11} for all scenarios.

This chapter is organized as follows: Section 3.2 presents a probe implanted antenna under investigation using a grid structure and parasitic resonator as external elements to improve its performance. These external elements are further investigated in Section 3.3 to improve a patch implanted antenna performance. In addition, an external ring is used to increase the gain of the patch antenna and is presented in Section 3.3 and, finally, conclusions are drawn in Section 3.4.

3.2 Improved Performance Implanted 2.45 GHz Probe Antenna

3.2.1 Antenna Design and Human body model

This section proposes the design, characterisation and simulation of a probe implanted antenna for body wireless communication. A simple probe wire antenna is employed as it can be easily made from a semi-rigid cable. The antenna in Figure 3.1 is embedded underneath the skin layer of a simplified biological tissue model, as shown in Figure 3.2. This body model consists of three layers of human tissue: skin, fat and muscle. The electrical properties of these body tissues at 2.45GHz are listed in Table 3.1. The antenna is designed to operate at 2.45 GHz, which is one of the industrial-scientific-medical (ISM) bands.

The design is investigated based on the Finite integration technique FIT technique using CST software. The simulation environment was setup for a hexahedral mesh, the

time domain solver and the frequency range was set from 0.1 to 3 GHz. Used hexahedral mesh properties are: 20 lines per wavelength, 6 lower mesh limit and 10 mesh line ratio limit. It should be noted that this settings is used throughout this thesis unless a different sitting is mentioned. Moreover, to take in account losses, in this thesis, wherever the gain is mentioned, it means the realised gain which "*reduced by the losses due to the mismatch of the antenna input impedance to specified impedance*" [13].

Table 3.1: Electromagnetic prosperities of human body tissue at 2.45 GHz [1, 2]

	Permittivity εr	Conductivity σ S/m	Loss Tangent δ
Skin	37.952	1.4876	0.28184
Fat	5.2749	0.10672	0.14547
Muscle	52.668	1.773	0.24205

The implanted antenna is surrounded by lossy tissues with high permittivity. Therefore, the wavelength is shorter than the wavelength in free space. For this reason, implantable antennas can be designed with compact dimensions compared to antennas in free space. To find out the antenna length, the following equation can be used [3]:

$$\lambda = \frac{c}{f\sqrt{\varepsilon_r}} \qquad (3\text{-}0)$$

Where λ is the wavelength, c is the light speed, ε_r is the effective permittivity and *f* is the frequency. Antenna length is affected by the surrounding tissues and the effective permittivity will be a combination of the different surrounding tissues permittivity. Therefore, the effective permittivity can be calculated as below [4]:

$$\varepsilon_{rc} = \frac{\sum_{i=1}^{n} h_i}{\sum_{i=1}^{n} \frac{h_i}{\varepsilon_{ri}}} \qquad (3\text{-}1)$$

Where ε_{rc} the combination permittivity, *n* is the number of layers of substrates (if there is) and tissues surrounding the antenna, *h* is the thickness of the substrate or tissue and *i* is the layer number. Now, the result of equation (3-1) is used in equation (3-0) as $\varepsilon_r = \varepsilon_{rc}$.

When the antenna length is calculated based only on the fat layer (ε_r = 5.27 at 2.45 GHz), the half wavelength is 26.65 mm. However, the optimized antenna length is 16 mm which is lower than the half wavelength in the fat media. This behaviour is due to the strong affect of the skin and muscle where they have higher permittivity (ε_r = 37.952 and 52.668 respectively). Hence in reality the effective permittivity is higher than the fat permittivity and, therefore, the antenna length should be shorter than 26.65 mm as expected.

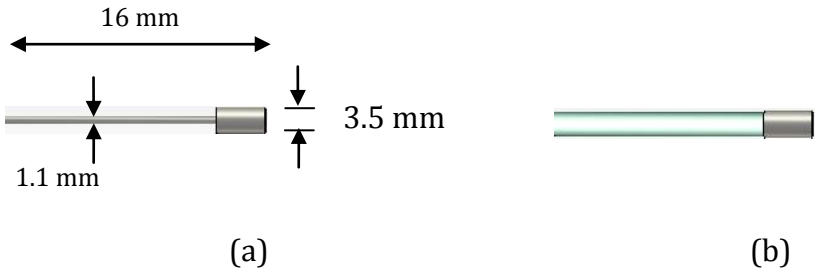

Figure 3.1: Antenna (a) without dielectric coating (b) with the dielectric coating

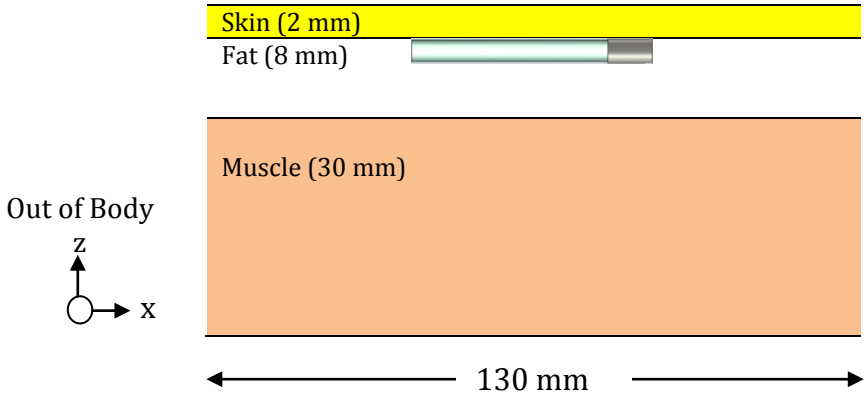

Figure 3.2: The probe antenna in three layers human body model

3.2.2 Implanted Probe Antenna Performance

Antenna performance in Figure 3.1 is investigated in two cases: when the wire is surrounded by human lossy tissue (Figure 3.1 (a)) and when a coating layer is added to the wire (Figure 3.1 (b)). The coat used is of a dielectric material (Teflon: $\varepsilon r=2.08$). Both of the antennas are tuned to work at around 2.45 GHz.

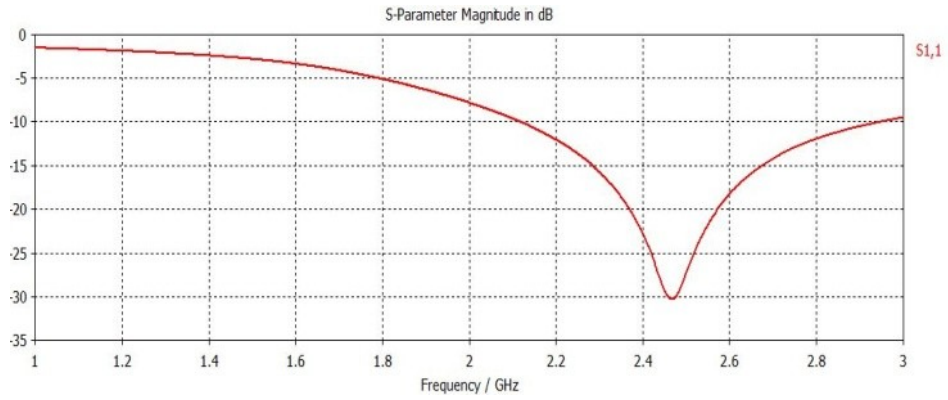

Figure 3.3: Simulated S11 of the probe antenna.

Figure 3.3 shows the S11 performance of the antenna. The -10 dB bandwidth achieved is about 32.6%. Far-field radiation patterns of the implanted antenna are plotted in Figure 3.4. It shows that the gain achieved is -9.3 dB towards the out the body. However, it shows that when the antenna is directly placed into the lossy human tissue, the near field power loss is high. Due to the higher permittivity, the resonant frequency is shifted down in case of the antenna without dielectric coating. Therefore, dielectric coat it is an effective technique to improve the performance of the implanted antenna. This is due to the lower permittivity of the surrounded material than the human body tissue.

Figure 3.4 shows that a valuable amount of power is wasted in the backward direction. That indicates that an amount of the power will be lost and this design could be inadequate to realise a sufficient communication between the implants and an external monitor.

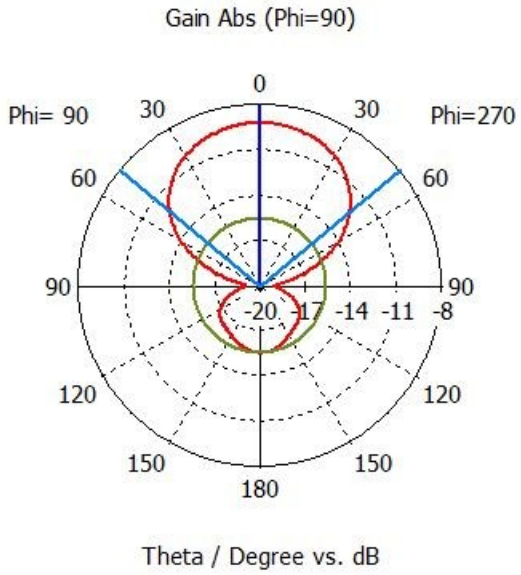

Figure 3.4: Far-Field pattern of the probe antenna.

From the radiation patterns, it is also notice that when the antenna is placed into the fat and very close to the skin layer which has a high permittivity and high loss tangent, a high power is radiated towards the back direction of the skin. This indicates that to realize sufficient communication between the implants and an external monitor, it is important to think about another way to enhance the performance with external elements and this is what this chapter presents in the next section.

3.2.3 Performance Improvement of Implanted Probe Antenna

3.2.3.1 Implanted Probe Antenna with External Grid

To improve the implanted antenna performance, particularly the forward gain, an external grid structure is designed and investigated, combined with the implanted antenna as shown in Figure 3.5. The Grid has a very simple structure of a 3x3 inductive grid forming a band pass filter as shown in Figure 3.6. The radiated power

can then be directed by the filter and the beam formed in the desired direction. The grid structure is designed to have a greater dimension than the inner antenna, so that more EM waves can be captured from inside the body. The distance from the grid layer to the skin is observed from 0 mm, which indicates the grid directly printed on the skin, to several millimetres. A 1.1 mm thickness felt fabric with a relative dielectric permittivity εr = 1.22 is used as a substrate to separates the grid and skin. The effect of the felt on the gain is investigated and found that the felt have no effect on the antenna performance. It is found that the combined structure is able to improve the gain, and the best result occurs at the separation when the two elements have the strongest coupling. Here, the results of a 4.4 mm distance from the grid to the skin will be presented because any larger separation is not easily achievable in practice.

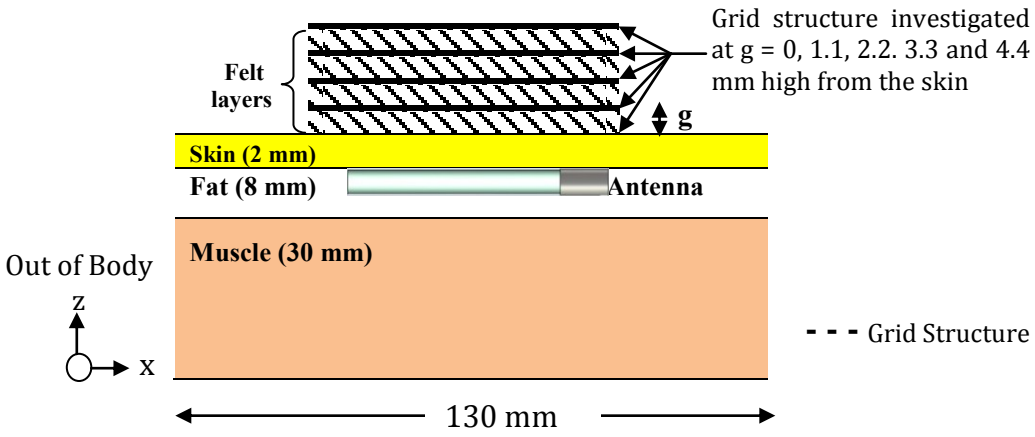

Figure 3.5: The implanted antenna with an external grid structure in the human body model side view

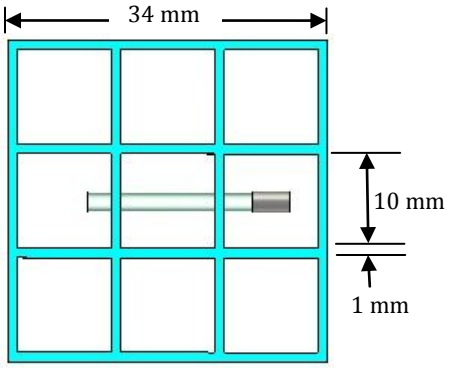

Figure 3.6: The implanted antenna with an external grid structure top view.

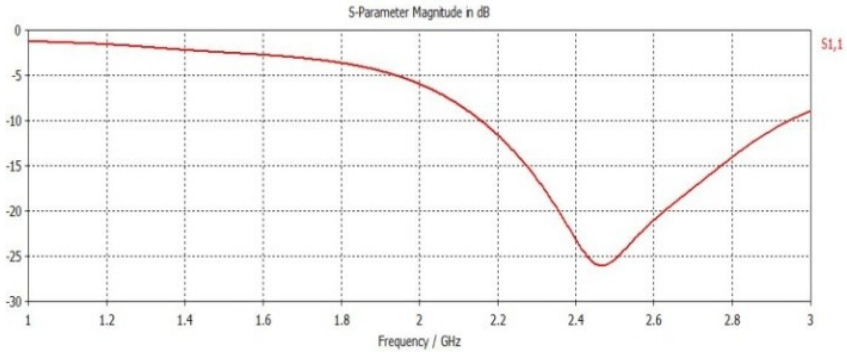

Figure 3.7: Simulated S11 of the probe antenna with an external grid.

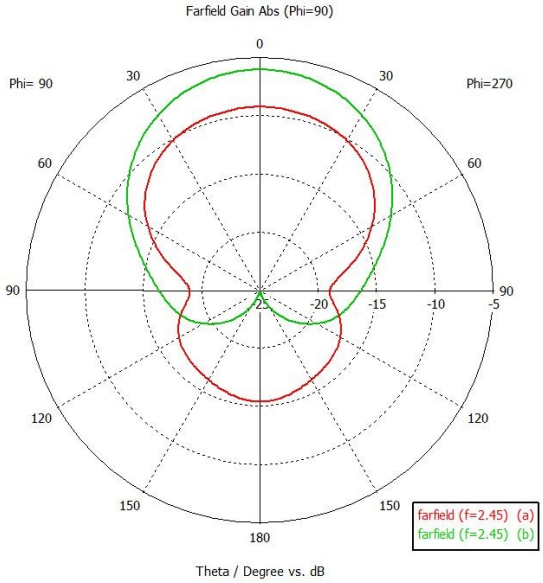

Figure 3.8: Far-Field pattern of the probe antenna (a) without and (b) with an external grid structure.

Figure 3.7 shows the S11 performance of the antenna with the grid. The bandwidth achieved is about 32.6% calculated -l0 dB bandwidth. The far-field radiation pattern of the implanted antenna with the grid is plotted in Figure 3.8 . It is very clear that the main power radiation is enhanced and the gain achieved is -6.1 dBi. Moreover, it shows that the power wasted in the backward direction is reduced and shifted from the back of the body to the front of the body. However, more enhancements could be achieved using an external strip line which will be shown in the following section.

3.2.3.2 Effect of parasitic grid structure height

The effects of parasitic grid structure height from the skin on the performance of the antenna have been studied and the simulation is performed at 2.45 GHz. The gap, g, between the parasitic grid structure and the skin varied, in order to analyse its impact on antenna radiated power. The investigation is carried out at the multiples of the felt layer thickness (1.1 mm). To maintain a reasonable overall thickness of the felt, a maximum of 4 layers was investigated. Thus, the investigation is carried out on g = 0, 1.1, 2.2, 3.3 and 4.4 mm. Figure 3.9 shows the gain investigation results at different heights of the grid from skin. It shows that the antenna gain increases as the gap between the grid structure and skin increases and the higher gain achieved at g = 4.4 mm. Therefore, for the improvement scenario, the grid structure is chosen to be at 4.4 mm height from the skin.

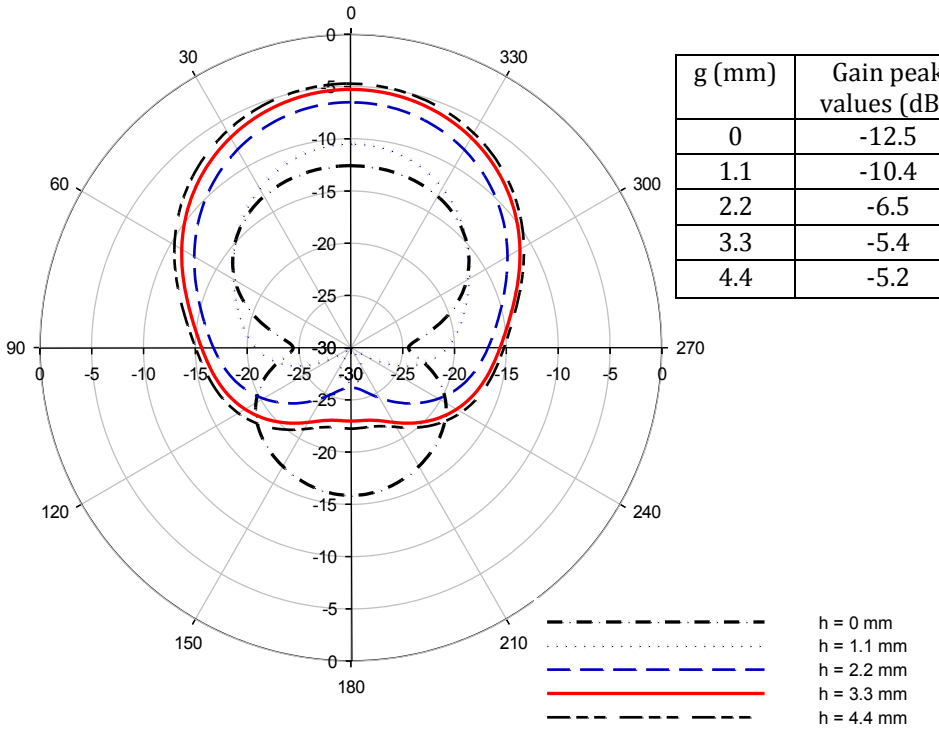

g (mm)	Gain peak values (dBi)
0	-12.5
1.1	-10.4
2.2	-6.5
3.3	-5.4
4.4	-5.2

Figure 3.9: Investigated gain of the gap between the grid structure and skin

3.2.3.3 Implanted Antenna with External Grid and Strip Line

To enhance the performance of the antenna further and make the whole structure more practicable, a new model is established in the software. Instead of leaving the gap between the grid and the skin as free space, a fabric material - felt - is used to fill the gap as the substrate of the grid. A single layer of felt has a thickness of 1.1 mm, relative permittivity of 1.38 and loss tangent of 0.02. In addition, another parasitic element, a printed line, as shown in Figure 3.10, is inserted in between the inner implant and the grid to enhance the coupling. The printed line length and position are tuned to achieve the optimum results.

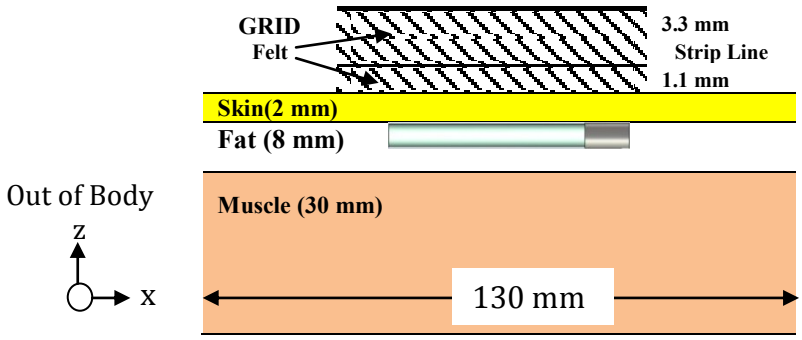

Figure 3.10: The implanted antenna with an external grid structure and printed line.

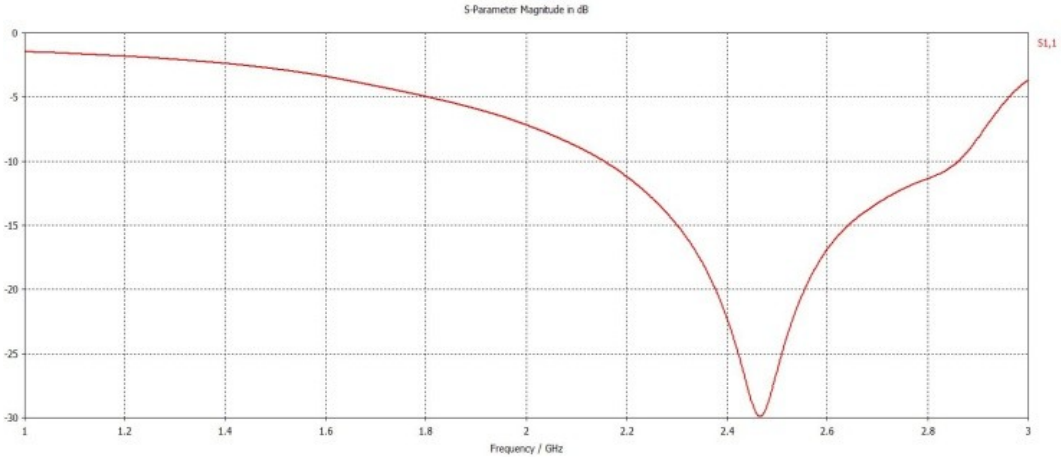

Figure 3.11: Simulated S11 of the probe antenna with an external GRID and strip line.

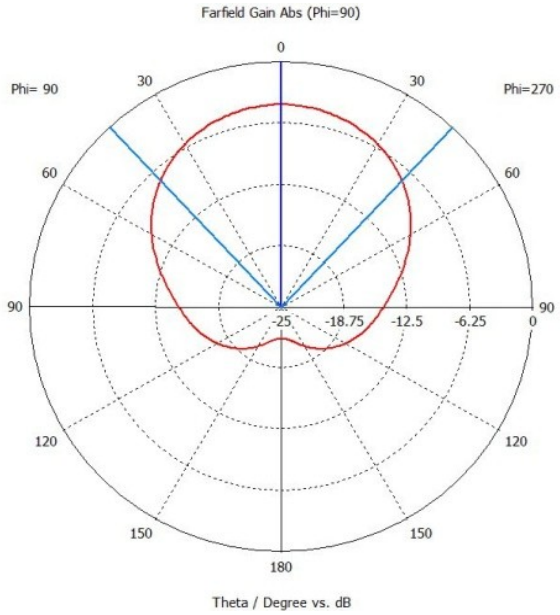

Figure 3.12: Far-Field pattern of the probe antenna with an external grid and printed line.

The bandwidth achieved is about 30.6% calculated -10 dB bandwidth. Far-field radiation pattern of the implanted antenna with the grid and the printed line is plotted in Figure 3.12. It shows a significant enhancement towards outside the body and the gain achieved is -4.4 dBi. Moreover, it shows a good reduction in the power wasted in the backward direction.

3.2.3.4 Effect of parasitic elements rotation

The effects of parasitic grid and printed line rotation on the performance of the antenna have been investigated. The angle, θ, from the horizontal position varied, in order to analyse its impact on antenna radiated power. As seen in Figure 3.13, the angel, θ, varied on 8 positions from 0 to 360 with $\theta = 45^0$ step. Figure 3.14 shows the

gain of investigated different angles and shows that the maximum difference between the highest and lowest gain is 1.14 dBi. This indicates that the antenna has a low sensitivity toward the rotation of the parasitic elements.

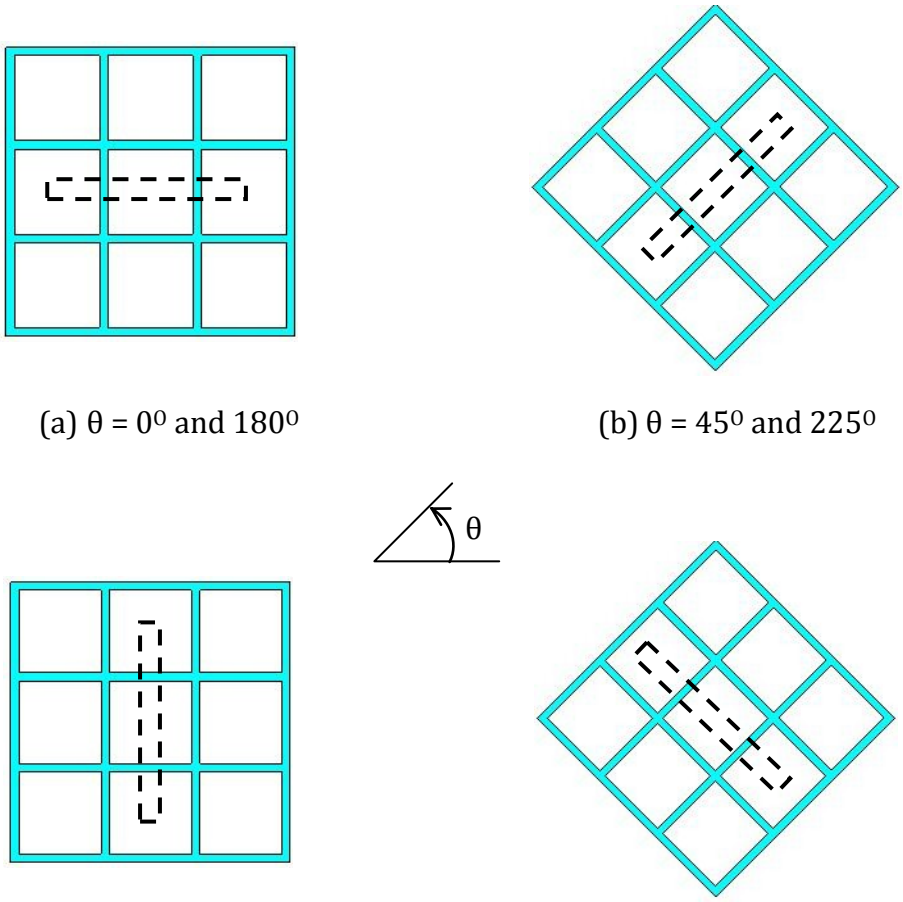

(a) $\theta = 0^0$ and 180^0 (b) $\theta = 45^0$ and 225^0

(c) $\theta = 90^0$ and 270^0 (d) $\theta = 135^0$ and 315^0

Figure 3.13: Investigation of the parasitic elements rotation

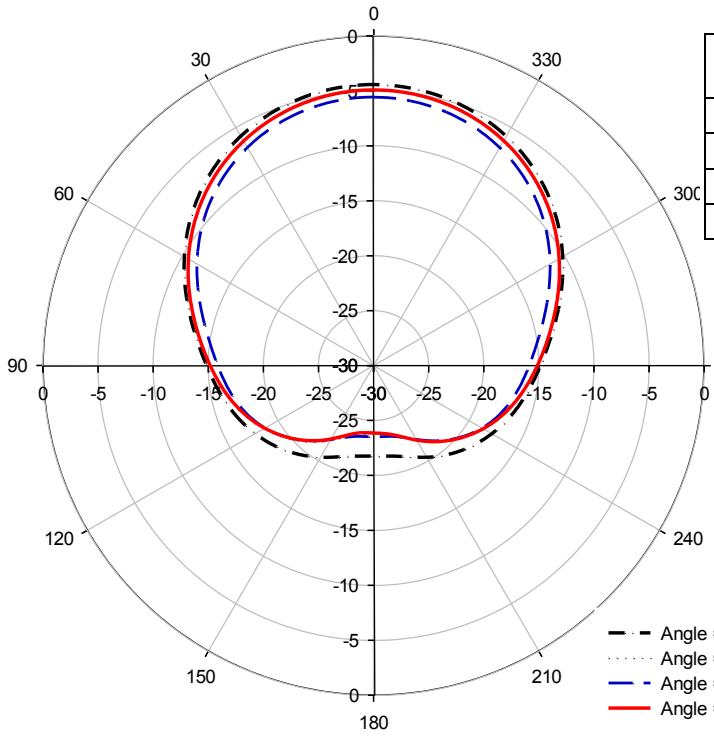

Angle ^{0}	Gain peak values (dBi)
0 or 180	-4.43
45 or 225	-4.92
90 or 270	-5.57
135 or 315	-4.92

Figure 3.14: Investigated gain of the parasitic elements rotation

3.2.4 Results Analysis

To compare these results with those of some other published material, Table 3.2 show results of three other types of antenna from referenced literature, published in [9] and [10]. Moreover, the power radiated from the body and the antenna gain towards the transceiver and the overall radiation efficiency are compared. It is important to note that some data on some antennas was not found. From the comparison, it can be seen that using the external grid and strip line elements, the implanted probe antenna maximum radiated power is increased by 160% in the direction of the body. Perhaps the most useful and informative result is that for the gain which is improved by 12 dB in the desired direction. This proves that by adding external parasitic elements, the power of the implant antenna can be dramatically decreased.

Table 3.2: Comparisons of the radiation characteristics of different types of implanted antennas (input power = 1W)

Antenna type	P_{max} (W) out of Body	Gain dBi out of Body	Radiation efficiency
Probe antenna (this work)	0.0016	- 16.83	9.8%
Probe antenna + Grid+Parasitic resonator (this work)	0.02275	- 4.4	14.1%
Cavity slot antenna [5]	0.0025	-13.69	3.5%
Microstrip antenna [6]			0.16%
PIFA [6]			0.25%

As detailed in Chapter 2, absorption of EM waves generate heat effect in the human body and this is measured by the Specific Absorption Rate (SAR) which can be calculated as following:

$$SAR = \frac{\sigma|E|^2}{\rho} \text{ W/kg} \qquad (3\text{-}2)$$

Where, σ is the electric conductivity of the tissue [S/m], ρ is the density of the tissue [kg/m^3], and E is the amplitude of electric-field strength (r. m. s.) inside the tissue [V/m]. For SAR calculation, maximum input power is assumed to be one watt for normalisation. Figure 3.15 shows the calculated peak SAR of 1-gram tissue for the probe antenna with external elements is 89.2 W/kg.

Figure 3.16 shows the calculated maximum 1-g SAR as a function of distance from the antenna toward the inside and outside the body for the implanted antenna with and without external elements. It shows that the SAR is reduced in the direction of the body by more than 28% when the grid and parasitic resonator is used with the

antenna. The SAR decreases rapidly from 89.2 W/kg to 9 W/kg for a distance on 1 cm and to less than 1.6 W/kg for 1.5 cm. However, 89.2 W/kg is higher than the peak 1-g SAR standard value of ANSI (1.6 W/kg). Therefore, in order to satisfy the peak 1-g SAR limitation, the maximum power has to be reduced using the following equation:

$$P_{max} = \frac{1.6\ \text{W/kg}}{\text{SAR (1g)}} = \frac{1.6}{89.2} = 0.0179 = 17.9\ \text{mW} \qquad (3\text{-}3)$$

where P_{max} is the maximum radiated power, g is gram, kg is kilogram, W is watt and mW is milliwatt. This equation shows that the maximum power can be delivered to the antenna is 17.9 mW to satisfy the SAR limitation of the ANSI. This value of the input power also generates smaller radiated power than the 100 mW EIRP limitation.

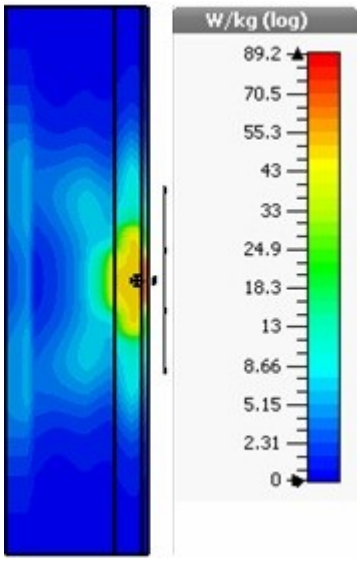

Figure 3.15: 1-g SAR distribution of the probe antenna with external elements

It can be noted in Figure 3.16 that zero position is co-located at the air-body interface. The radiation is implied as propagating inwards in the case where the base of the antenna is located at the zero position. The second co-located zero position is

referenced to the top of the antenna, and radiation is implied to be propagating outwards from the air-body interface.

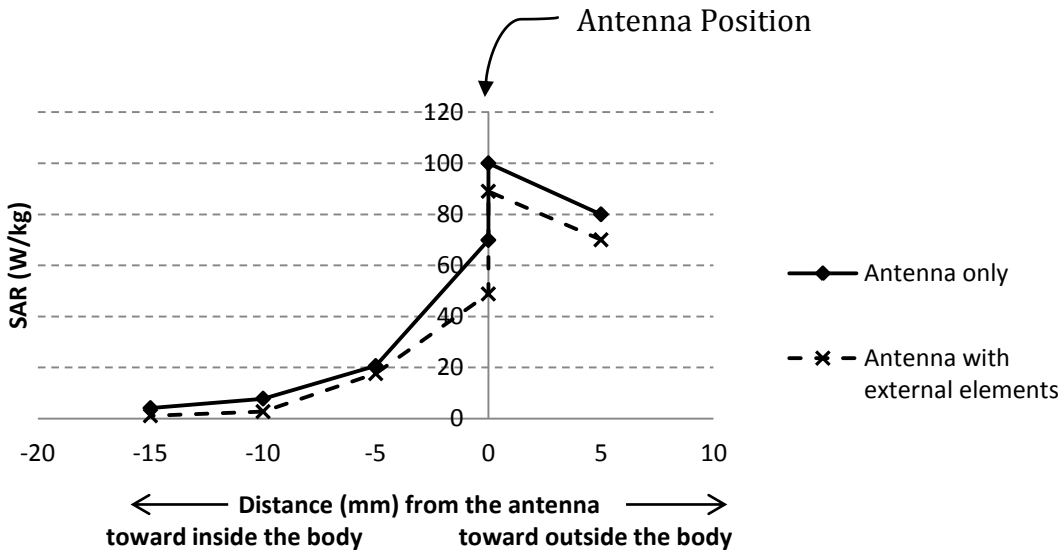

Figure 3.16: Maximum 1-g SAR calculated as a function of distance from the antenna toward inside the body

3.3 Improved Performance 2.45 GHz Implanted Patch Antenna

3.3.1 Implanted Microstrip Patch Antenna Design

In this section a microstrip patch antenna is designed and investigated as the implant antenna. The antenna is embedded under the skin layer of a simplified biological tissue model, as shown in Figure 3.17. The designed antenna is a compact size simple structure as shown in Figure 3.18 fed by a coaxial pin. The antenna is embedded inside the fat layer of a simplified biological tissue model which consists of three layers of human tissue: skin (2 mm), fat (8 mm) and muscle (30 mm). This antenna is designed on a 0.8 mm thick FR4 substrate with thin copper layers etched on each side.

The antenna is designed to operate at 2.45 GHz, which is one of the industrial-scientific-medical (ISM) bands and the design is investigated using CST software.

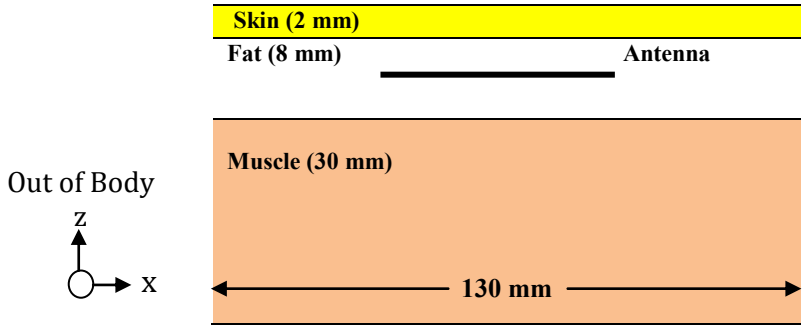

Figure 3.17: The implanted patch antenna placed in the middle of the fat layer of a simple human body model

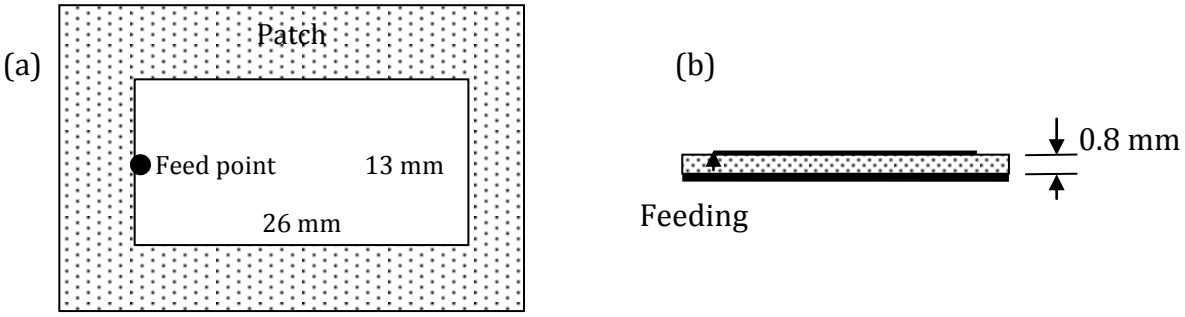

Figure 3.18: Patch Antenna (a) Top view and (b) side view

The design process starts with the determination of the overall dimensions of the antenna using commonly used mathematical formulation of patch antennas. Then, the final dimensions of the microstrip patch antenna were optimized using the CST software. The resonant frequency for patch antenna can be calculated approximately using the equation below [3]:

$$L = \frac{C}{2f\sqrt{\varepsilon_{eff}}} \tag{3-4}$$

$$W = \frac{C}{2f}\sqrt{\frac{2}{\varepsilon_r + 1}} \tag{3-5}$$

Where L is the patch antenna length, W is the patch antenna width, C is the light speed, ε_r is the substrate permittivity, ε_{eff} is the effective permittivity and f is the frequency. The patch length is a function of the effective permittivity which is given by [7]:

$$\varepsilon_{reff} = \frac{\varepsilon_r + 1}{2} + \frac{\varepsilon_r - 1}{2}\left[1 + 12\frac{h}{W}\right]^{-1/2} \tag{3-6}$$

However, the patch antenna size is affected by the surrounding tissues and the effective permittivity will be a combination of the substrate permittivity and surrounding tissues. Therefore, the effective permittivity can be calculated as below [4]:

$$\varepsilon_{rc} = \frac{\sum_{i=1}^{n} h_i}{\sum_{i=1}^{n} \frac{h_i}{\varepsilon_{ri}}} \tag{3-7}$$

Where ε_{rc} the combination permittivity, n is is the number of layers of substrates and tissues surrounding the antenna, h is the thickness of the substrate or tissue and i is the layer number. Now, the result of equation (3-7) is to be used in equation (3-6) as $\varepsilon_r = \varepsilon_{rc}$.

Since the antenna is mainly surrounded by fat, two layers will be used to solve equation (3-7); the substrate and the fat. Thereafter, by solving equations (3-4) to (3-7) and using CST for the optimisation, it is founded that the implanted patch antenna dimensions are 26.4 x 13 mm and has an overall size including the ground of 34 x 30 x 1 mm^3 and tuned at around 2.45 GHz.

3.3.2 Implanted Patch Antenna Performance

Figure 3.19 shows the S11 performance of the antenna. The bandwidth achieved is about 6.1% calculated for -l0 dB bandwidth. The two principle planes are plotted in Figure 3.20 which shows that the gain achieved is - 9.3 dB out the body and the Far-field radiation pattern of the implanted antenna is plotted in 3D in Figure 3.21.

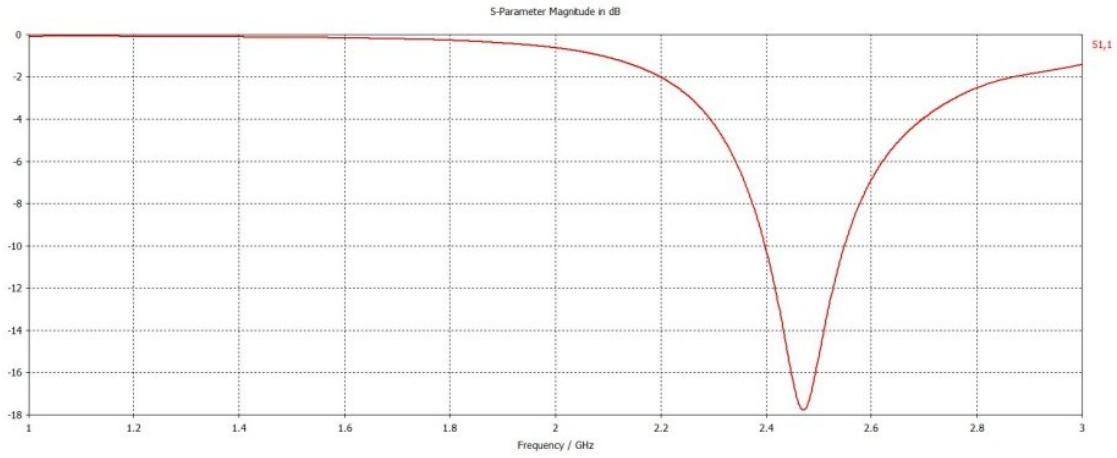

Figure 3.19: Simulated S11 of the patch implanted antenna

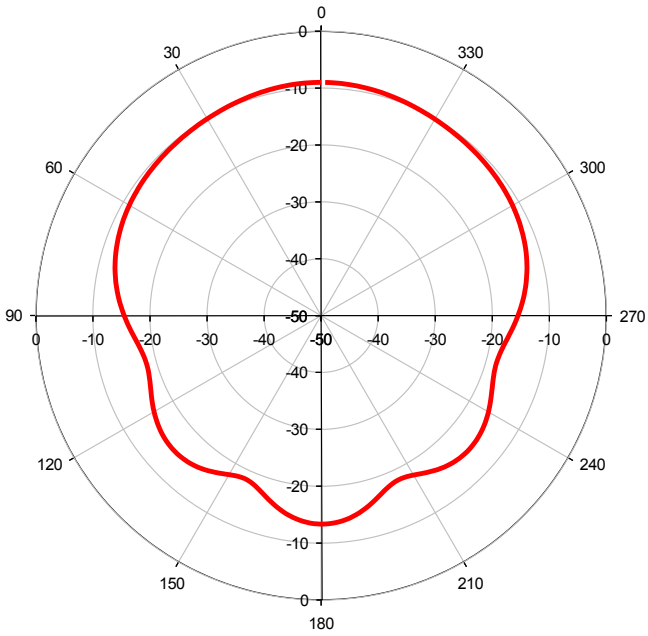

(a)

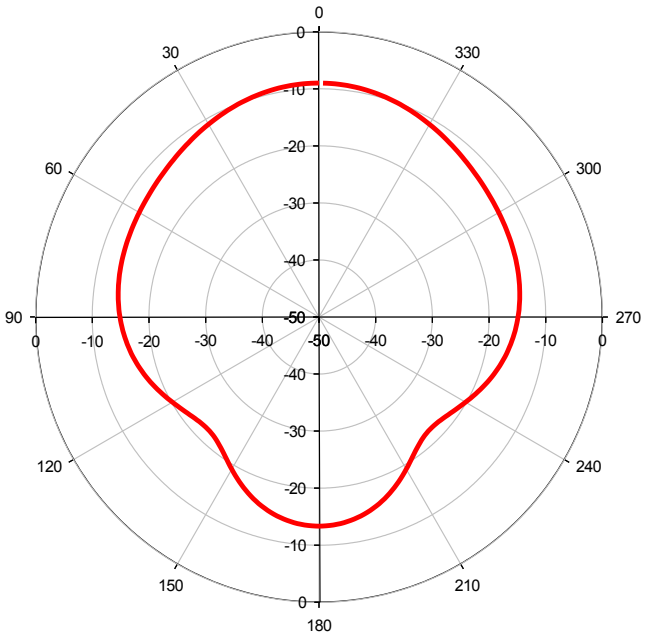

(b)

Figure 3.20: Far-Field pattern (in dBi) of the patch antenna (a) E-plane and (b) H-plane Performance Improvement of Implanted Patch Antenna

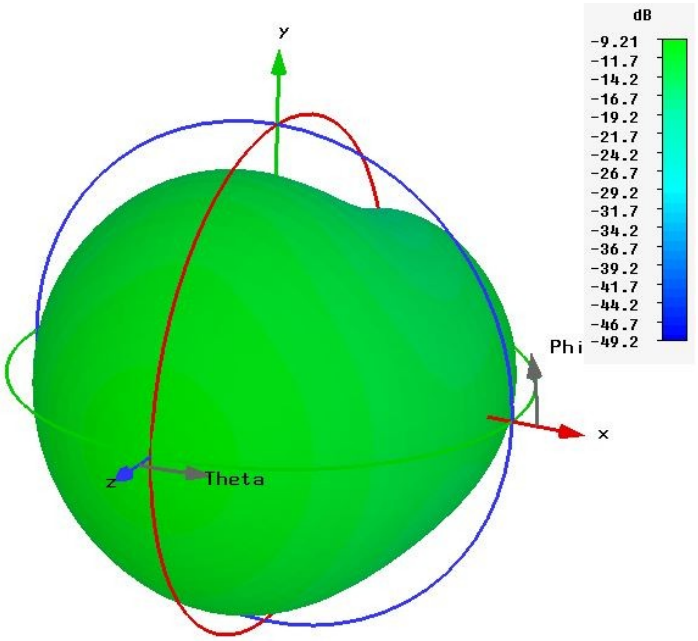

Figure 3.21: 3D Far-Field pattern of the patch antenna

3.3.2.1 Implanted Antenna Improvements with External Grid

To improve the implanted antenna performance, particularly the forward gain, an external grid structure is designed and investigated, combined with the implanted antenna. As shown in Figure 3.22, the simple structure grid of 3 x 3 inductive grids forming a matching surface with dimension of 28 x 28 mm^2. The radiated power can then be directed by the filter and beam formed in the desired direction. A fabric material 'felt' which has a permittivity of 1.38 was used as a substrate for the grid with a thickness of 4.4 mm.

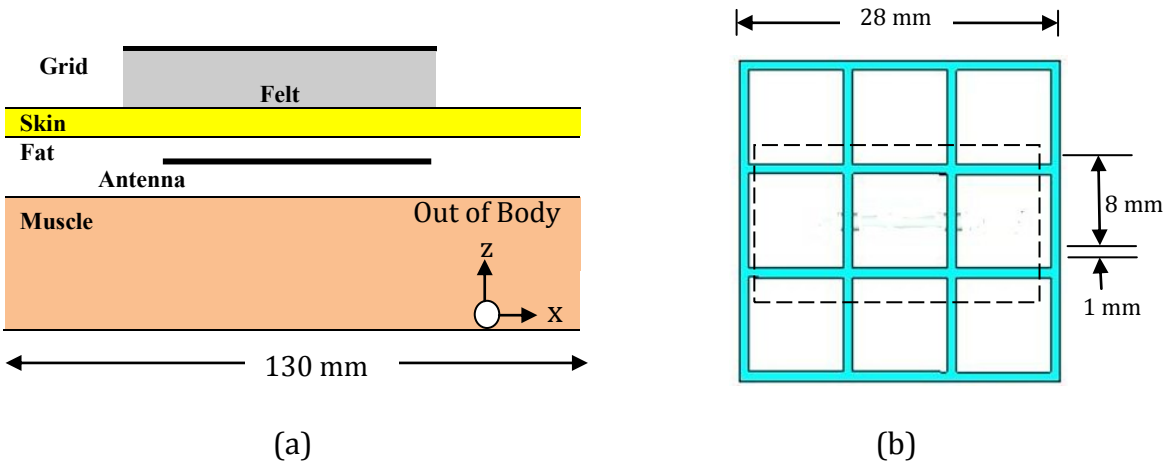

(a) (b)

Figure 3.22: The implanted antenna with an external Grid structure

(a) Side view (b) Top view

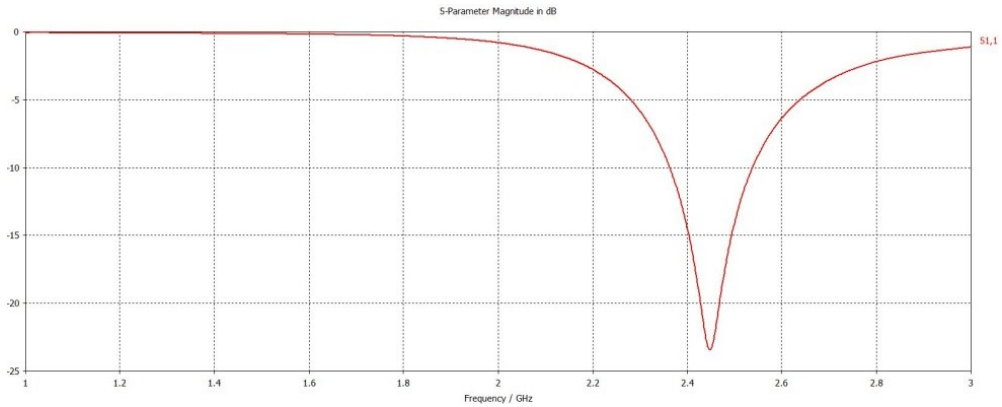

Figure 3.23: Simulated S11 of the patch antenna with an external Grid

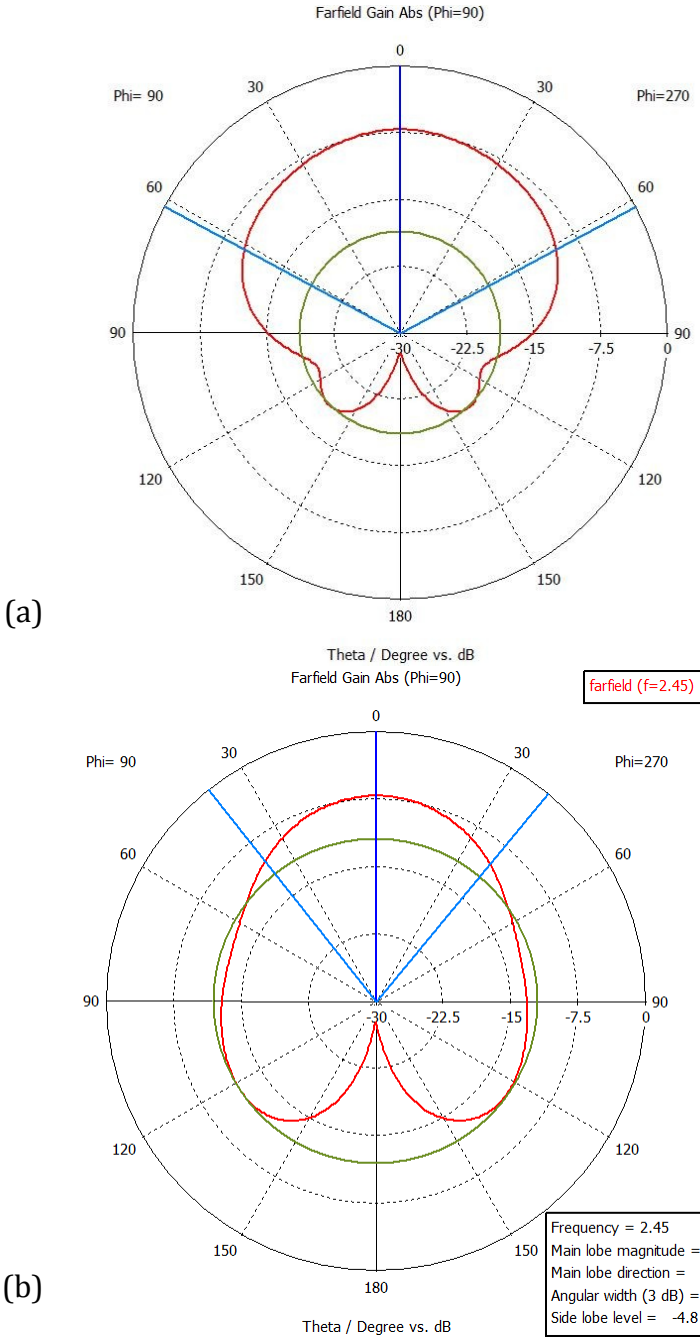

Figure 3.24: Far-Field pattern of the antenna with an external Grid E-plane (a) and H-plane (b)

Figure 4.3Figure 3.23 shows the S11 performance of the antenna with the grid. The bandwidth achieved is about 8.2% calculated for -l0 dB bandwidth which improved by about 33% over the bandwidth of the antenna without the grid. The far-field radiation

pattern of the implanted antenna with the grid is plotted in Figure 3.24. It is very clear that the main power radiation is enhanced and the gain achieved is -7.2 dBi towards out of the body. However, more enhancements could be achieved using an external strip line which will be shown in the following section.

3.3.2.2 Implanted Antenna with External Grid and Parasitic Resonator

To enhance the performance of the patch antenna further, another parasitic element is inserted in between the inner implant and the grid to enhance the coupling. As shown in Figure 3.25 the strip line length and position are tuned to achieve the optimum results with 16 mm length and 1 mm width.

Figure 3.26 shows the simulated S11 of the antenna with the GRID and strip line. The bandwidth achieved is about 8.2% calculated for the -10 dB bandwidth. Far-field radiation pattern of the implanted antenna with the grid is plotted in Figure 3.28. It shows a significant enhancement and the gain achieved is -5.3 dB out of the body.

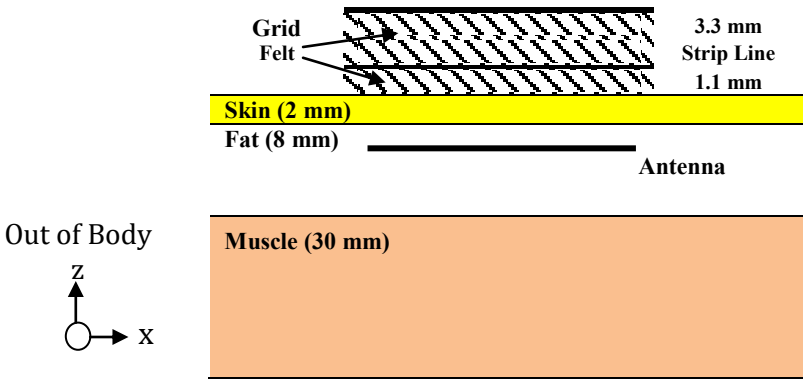

Figure 3.25: The implanted patch antenna with an external GRID structure and strip line.

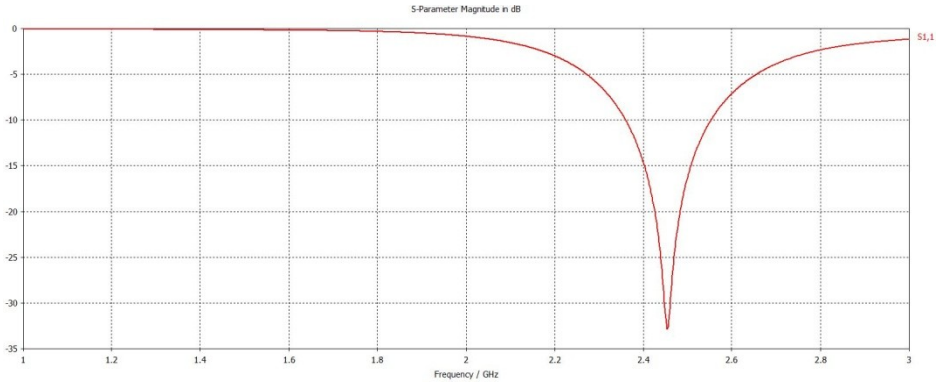

Figure 3.26: Simulated S11 of the patch antenna with an external GRID and strip line.

3.3.3 Results Analysis

Figure 3.27 and Figure 3.28 show the comparison of the S11 and radiation pattern. From this comparison, it can be seen that using the external grid and strip line elements, the implanted patch antennas performance is improved. The most useful and informative result is that for the gain which is improved by up to 4.5 dB in the desired direction using the parasitic elements. The calculated -l0 dB bandwidth improved by about 33%. This proves that by adding external parasitic elements, the output power of the implant antenna can be dramatically decreased by at least 3 times. Therefore, the battery life can be increased by a similar factor.

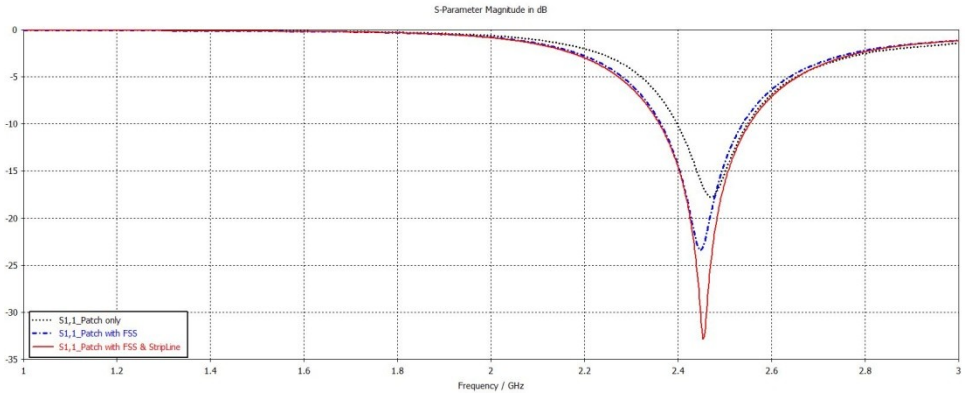

Figure 3.27 Simulated S11comparison of the patch antenna

(a)

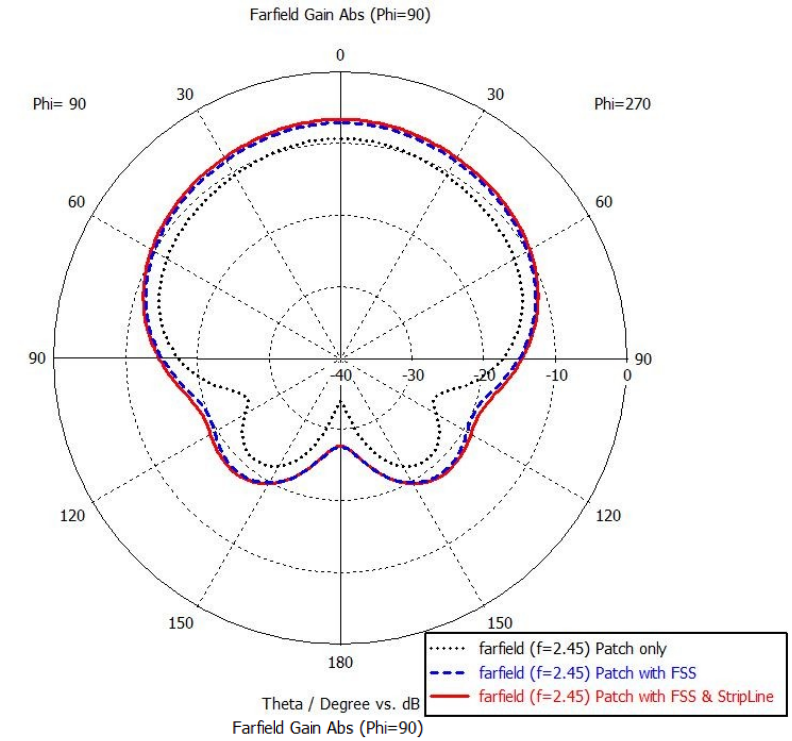

(b)

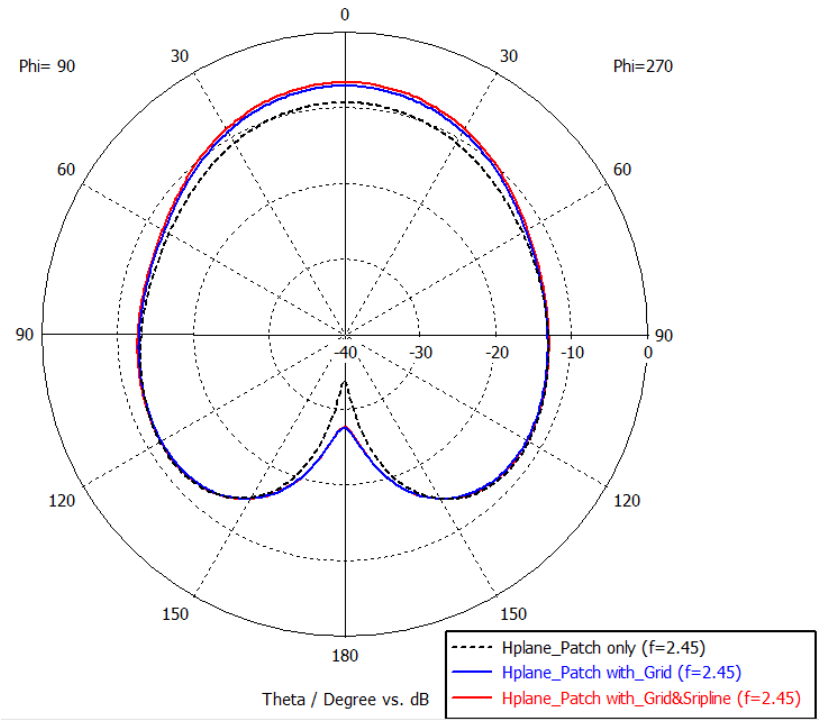

Figure 3.28: Far-Field pattern comparison of the patch antenna (a) E-plane and (b) H-plane

Figure 3.29 shows the calculated peak SAR of 1-gram tissue for the patch antenna with external elements is 72.3 W/kg. Figure 3.30 shows the calculated maximum 1-g SAR as a function of distance from the antenna toward inside and outside the body for the implanted antenna with and without external elements. It shows that the SAR is reduced in the direction of the body by almost 10% when the grid and parasitic resonator is used with the antenna. The SAR decreases rapidly from 45 W/kg to 2 W/kg where SAR is less by more than 60% when the external elements are used. However, 72.3 W/kg is higher than the peak 1-g SAR standard value of ANSI (1.6 W/kg) as detailed in Chapter 2. Therefore, in order to satisfy the peak 1-g SAR limitation, the maximum transmitted power has to be reduced using the following equation:

$$P_{max} = \frac{1.6\ \text{W/kg}}{\text{SAR (1g)}} = \frac{1.6}{72.3} = 0.022.1 = 22{,}1\ \text{mW} \qquad (3\text{-}8)$$

Where P_{max} is the maximum power. This equation shows that the maximum power can be delivered to the antenna is 22.1 mW to satisfy the SAR limitation of the ANSI and EIRP.

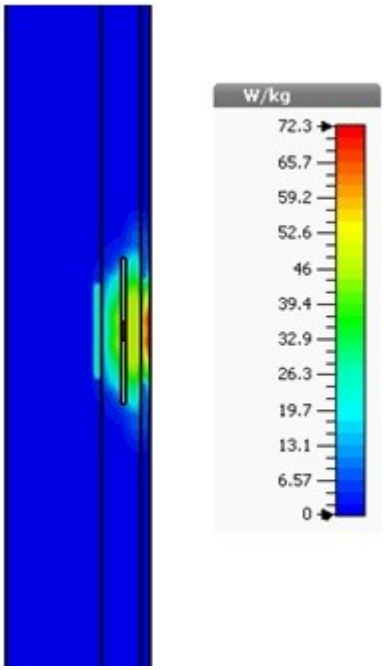

Figure 3.29: 1-g SAR distribution of the probe antenna with external elements

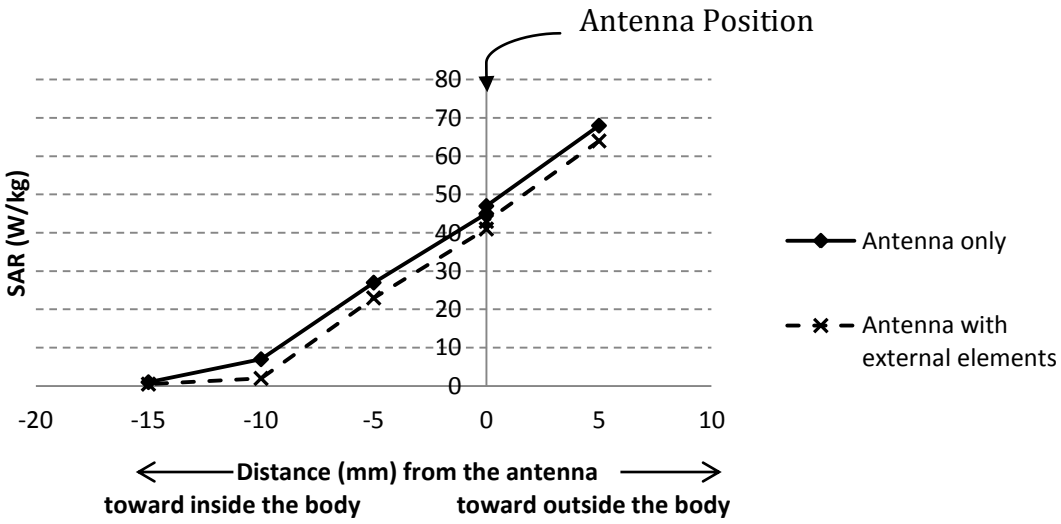

Figure 3.30: Maximum 1-g SAR calculated as a function of distance from the antenna toward inside the body

In order to validate this work, the work in [6] was implemented using CST. The objective of this is to verify that the used simulation package, CST, is working correctly

by comparing its results with other work results. Results show that CST results are very similar to the published results in the original work as detailed in Appendix C.

3.3.4 Microstrip Patch Antenna Measurements

The simulations for the microstrip patch antenna were verified by measurements where pork meat was used to simulate a human body and the patch antenna has been fabricated and measured. Figure 3.31 measurements setup for S11 where the antenna inserted inside the 3-layers pork cut and the cable connected from the bottom of the cut. Figure 3.32 show the measurements setup for antenna far-field where the pork cut fixed on a rigid foam material and the cable connected from the back. The patch antenna was embedded in a piece of pork meat with similar dimensions to the human model Figure 3.17. Pork meat has close but not identical electromagnetic characteristics to the human body [8]. However the pork meat used for the measurements did not have uniformly thick layers nor were the layers parallel and the meat sample were only approximate.

Figure 3.31: S-parameter measurements of the patch antenna

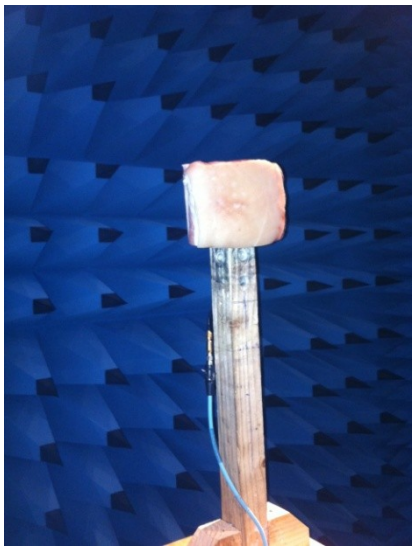

Figure 3.32: Far Field pattern measurements of the patch antenna

3.3.5 Results Analysis

Figure 3.33 to Figure 3.35 show the measurements results. For the S11, the measurements results are agree with the simulations. When the grid and parasitic resonator are used, the gain increased by 7.5 dBi (simulated) and 3 dBi (measured). Figure 3.34 shows the comparison between normalised measured and simulated far-

field. Generally, measurements show that the implanted antenna performance is improved when the parasitic elements are used and measurements results are in satisfactory agreement with simulations. Figure 3.33 shows the measured versus the simulated S11 of the antenna where the measured band width is almost 75 MHz at VSWR 2:1.

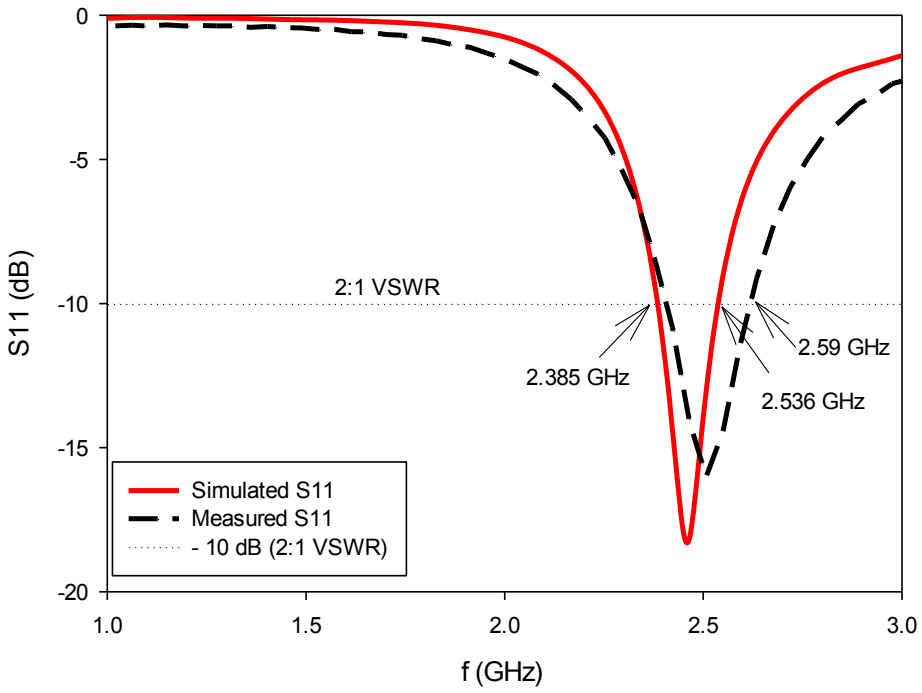

Figure 3.33: Measured vs. Simulated S11 of the patch antenna

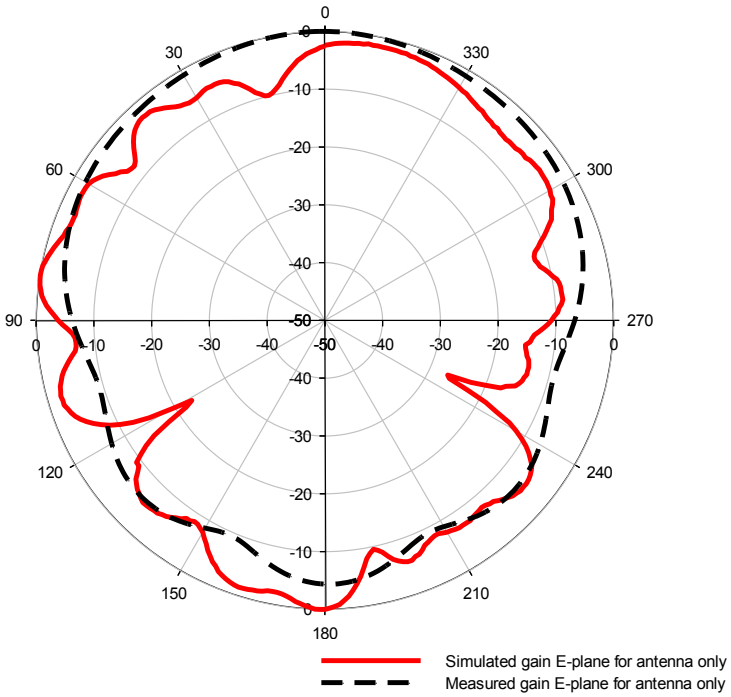

(a)

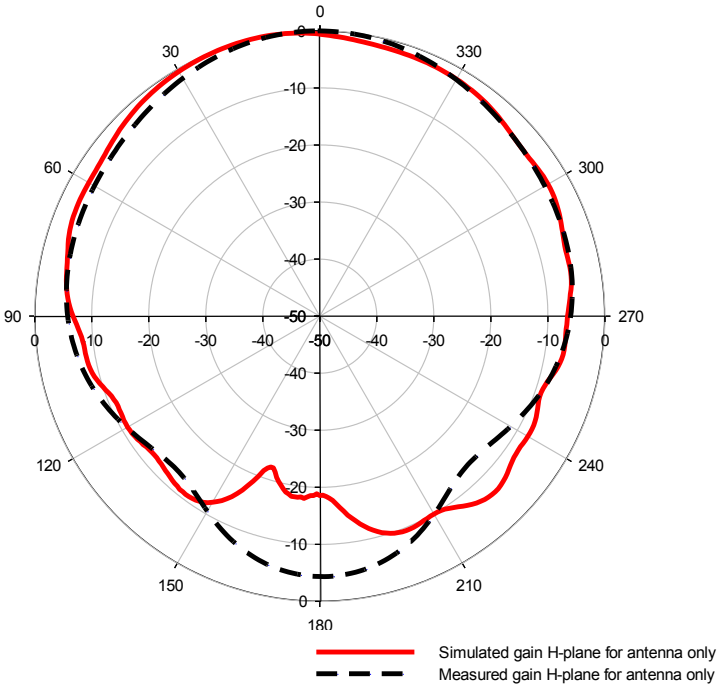

(b)

Figure 3.34: Measured vs. simulated normalised Far-Field pattern of the antenna only

(a) E-plane (b) H-plane

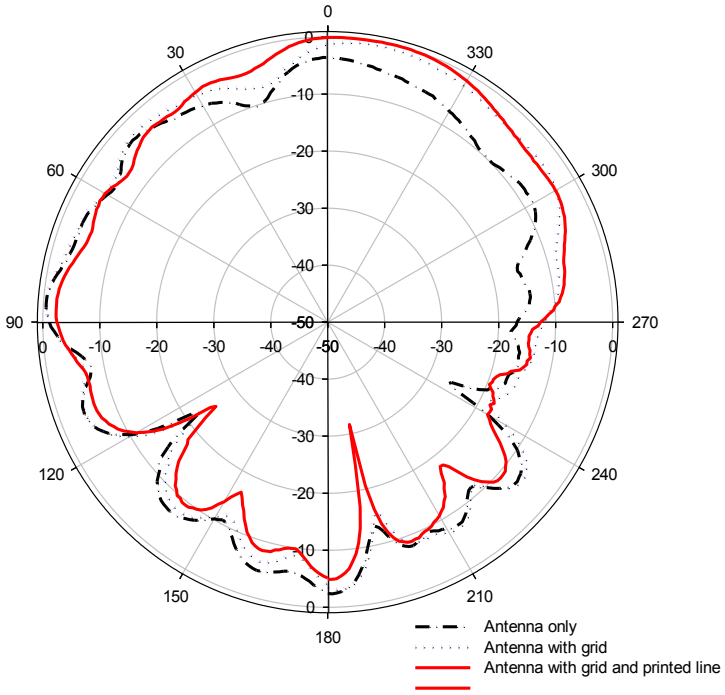

(a)

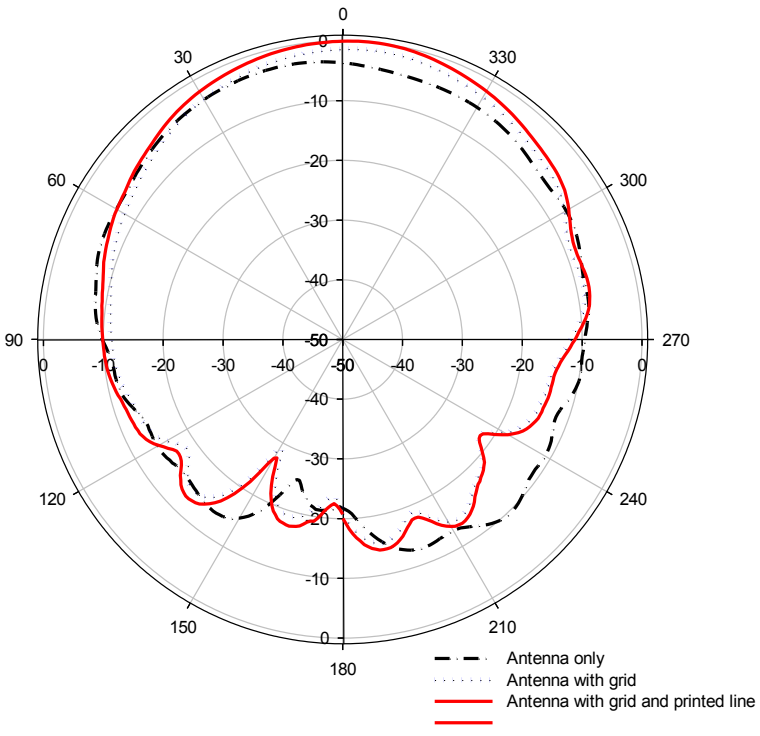

(b)

Figure 3.35: Measured Far-Field pattern comparison of the patch antenna without and with external elements (a) E-plane and (b) H-plane

3.4 Conclusions

In this Chapter, a probe and patch implanted antenna designed to work at the ISM band for biomedical applications is presented. A 3-layer (skin, fat and muscle) human model was constructed in the CST simulation to represent a simple human body. External elements were designed to enhance the performance of such implanted antennas. This approach yields a significant improvement in the antenna gain. To compare these results with those of some other published material, Table 3.3 show results of three other types of antenna from referenced literature, published in [5] and [6].

Table 3.3: Comparisons of the radiation characteristics of different types of implanted antennas (input power = 1W)

Antenna type	P_{max} (W) out of Body	Gain dBi out of Body	Radiation efficiency
Probe antenna (this work)	0.0016	- 16.83	9.8%
Probe antenna + Grid + Parasitic resonator (this work)	0.02275	- 4.4	14.1%
Patch antenna + Grid + Parasitic resonator (this work)	0.0075	- 4	14.6%
Cavity slot antenna [5]	0.0025	-13.69	3.5%
Microstrip antenna [6]			0.16%
PIFA [6]			0.25%

Both simulation and measurement have shown that the simple external grid can significantly improve the implanted antenna gain out of the body by up to 6 dBi (12 dBi calculated). In case of the probe antenna, the gain increased by 6 dB and 28%

overall SAR reduction. In case of the microstrip patch antenna, the gain increased by 7.5 dBi (simulated) and 4.5 dBi (measured).

Such external elements could be manufactured in a sticking plaster form and applied to the skin giving much improved implant communication performance and significantly reduced battery power consumption. In both antennas, the SAR values can satisfy the safety standards for medical implant applications.

3.5 References

[1] Y. Hao, K. Ito, and P. Hall, "Electromagnetic properties and modeling of human body," in *Antennas and propagation for Body centric Communication Systems*, P. S. Hall and Y. Hao, Eds., ed Norwood, MA, U SA: Artech Hous, 2006, pp. 1-7.

[2] C. Gabriel, "Compilation of the Dielectric Properties of Body Tissues at RF and Microwave Frequencies," DTIC Document1996.

[3] C. A. Balanis, *Antenna theory: analysis and design* vol. 1: John Wiley & Sons, 2005.

[4] Z.-F. Liu, P.-S. Kooi, L.-W. Li, M.-S. Leong, and T.-S. Yeo, "A method for designing broad-band microstrip antennas in multilayered planar structures," *Antennas and Propagation, IEEE Transactions on,* vol. 47, pp. 1416-1420, 1999.

[5] H. Usui, M. Takahashi, and K. Ito, "Radiation characteristics of an implanted cavity slot antenna into the human body," in *Antennas and Propagation Society International Symposium 2006, IEEE*, 2006, pp. 1095-1098.

[6] K. Jaehoon and Y. Rahmat-Samii, "Implanted antennas inside a human body: simulations, designs, and characterizations," *Microwave Theory and Techniques, IEEE Transactions on,* vol. 52, pp. 1934-1943, 2004.

[7] R. Garg, *Microstrip antenna design handbook*: Artech House, 2001.

[8] C.-K. Wu, T.-F. Chien, C.-L. Yang, and C.-H. Luo, "Design of novel s-shaped quad-band antenna for MedRadio/WMTS/ISM implantable biotelemetry applications," *International Journal of Antennas and Propagation,* vol. 2012, 2012.

[9] P. K. A. a. N. Y. Joshi, " Design and Fabrication of Microwave Metallic Lens " *ICAT,* 2005.

[10] R. Shavit, "Dielectric spherical lens antenna for wireless millimeter-wave communications," *Microwave and Optical Technology Letters,* vol. 39, pp. 28-33, 2003.

[11] C. A. Balanis, *Antenna theory: analysis and design* vol. 1: John Wiley & Sons, 2005.

[12] J. C. Lin, "Safety standards for human exposure to radio frequency radiation and their biological rationale," *Microwave Magazine, IEEE,* vol. 4, pp. 22-26, 2003.

[13] Standard Definitions of Terms for Antennas," in *IEEE Std 145-1993* , vol., no., pp.1-32, July 18 1993

Chapter 4

Gain Enhancement of Implanted Antennas Using Lens and Parasitic Ring[1]

4.1 Introduction

The last chapter presents an improvement of implantable antennas performance using different external parasitic elements. In this chapter, a novel hemispherical lens and a printed parasitic ring are proposed to improve the performance of implantable antennas externally.

The design and characteristics of hemispherical lens to improve an implantable 2.45 GHz microstrip patch antenna are investigated using simulation and practical experiments. The results show that the hemispherical lens can be used to enhance the performance of a subcutaneous implantable antenna. This is shown by calculating the S_{11} for all scenarios and the antenna performance is characterized by antenna gain and SAR calculations.

[1] Alamri, S.; Langley, R.J.; AlAmoudi, A.O., "Gain Enhancement of Implanted Antennas Using Lens and Parasitic Ring". Electronics Letters. (Submitted)

This chapter is organized as follows: section 4.2 introduces the concept of lens antennas and the design of the hemispherical lens to be used for implantable antenna improvement. Thereafter, section 4.3 presents an additional improvement technique using a parasitic ring resonator combined with the hemispherical lens. The realisation, findings and measurement results are discussed in section 4.6 and 4.7 respectively. Finally, conclusions are drawn in Section 4.8.

4.2 Performance Improvement of Implanted Patch Antenna Using External Lens

Antenna gain enhancement methods for free space applications have included using metamaterials at millimetre waves [1] or using a square aperture superstrate [2]. In [3] the performance of an implanted antenna was enhanced by up to 10 dB using a parasitic monopole and a matching printed grid surface placed on the skin of the patient. This chapter presents a simple way to improve the antenna gain using a parasitic ring and glass hemispherical lens placed on the skin.

Recently, lens antennas have attracted researchers for antennas gain enhancement in many free space microwaves applications [4-7]. For example, lenses have used to improve the gain of patch antenna for WiMAX applications from 3.87 dBi to 7.71 dBi and 11.07 dBi respectively [4]. A four element and eight elements Microstrip array have use the lens to enhance the gain by 4 dBi [5]. Dielectric lens antennas are more popular in MMW applications at higher frequencies where lens dimensions and weight become small enough and allow easy system integration [5-8].

4.2.1 Lens Antennas

Dielectric lens antenna has been investigated during the early developments of microwave antennas. However the interests have declined due to the large size of lenses at low frequencies. Recently, an increasing interest in dielectric lenses research due to the rapidly growing of number of applications for millimeter waves where the lenses physical dimensions have reasonable sizes. Lens antennas are mainly used to collimate incident divergent energy to prevent it from spreading in undesired directions. They are effective at producing highly directive beams by transforming of divergent energy to plane waves [6, 7, 9, 10]. Figure 4.1 shows the principle of antenna with hemispherical lens where it works to directive the antenna waves [11].

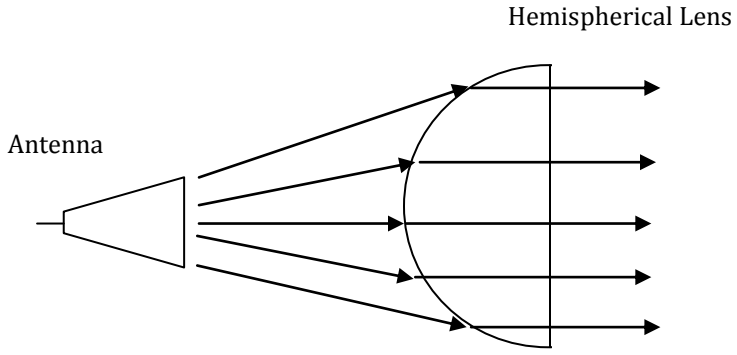

Figure 4.1: An antenna with a hemispherical lens (adopted from [11])

For effective lens antennas, it is important to select a material which is mechanically and electromagnetically stable. A typical choice if material can be selected depend on relative permittivity vary from about 1.2 to 13. Figure B.1 in Appendix B list the permittivity and loss tangent of some well know materials [7].

Although lenses have been widely used on the MMW applications, literature reviews have indicated that there was no published work for using such technique to improve implantable antennas performance. Therefore, section 4.2.2 briefly presents a model for to use a hemispherical lens that could be used to improve implantable antennas performance.

4.2.2 Antenna and Lens Design

As presented in Chapter 3, a patch antenna was designed at 2.45 GHz as the implant antenna using CST Microwave Studio. The antenna is embedded inside the fat layer of a simplified biological tissue model which consists three layers of human tissue: skin, fat and muscle. The electrical properties of these body tissues and the patch antenna configuration are presented in Chapter 3. This chapter presents methods for improving the gain of a microstrip patch antenna operating at 2.45 GHz implanted in the fat layer of the human body using an external hemispherical lens and parasitic ring.

To improve the implanted antenna performance an external hemispherical lens was designed and investigated to be placed on the skin over the implanted antenna as in Figure 4.2. Numerical simulations are carried out using CST microwave studio design software.

There are various factors that affect the design of the lenses to be used for antennas performance improvements. This includes electromagnetic properties of the lens material, shape of the lens, orientation, size and antenna operating frequency [7]. Several simulations have been performed using CST Microwave studio to achieve the

optimal material type suitable for this applications. For the same size of lens, it was found that Glass (Pyrex) of permittivity 4.82 is the most suitable for improving the gain of implanted antenna.

Since the size is very important factor in biomedical application, the spherical lens is excluded from the design in this chapter.

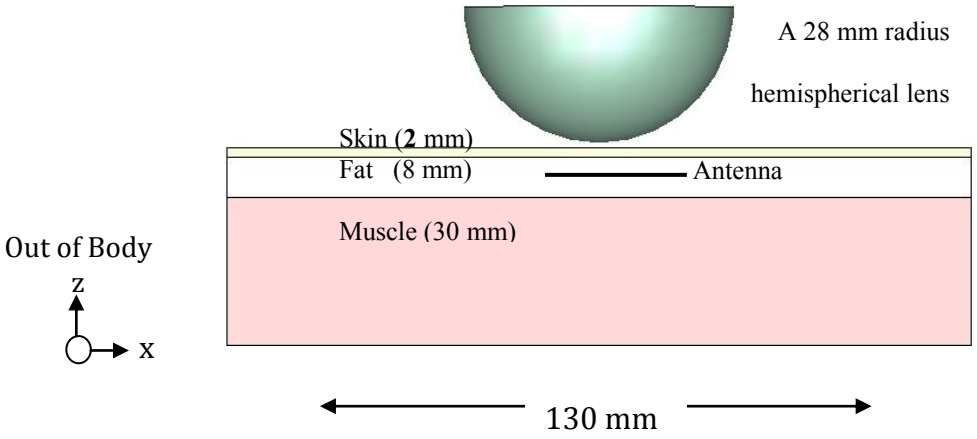

Figure 4.2: The proposed antenna with a hemispherical Lens over the body model

Table 4.1: Optimizing lens radius for optimal antenna gain (the bold font shows the best results)

Hemispherical Lens Radius (mm)	Gain (dB)
20	-5.57
22	-4.69
24	-3.38
26	-3.09
27	-2.82
28	**-2.26**
29	2.40
30	-2.39
32	-2.46
38	-2.42

The hemispherical lens radiuses and orientation are investigated for the highest gain using CST software. Table 4.1 shows the antenna gain optimised against the hemispherical lens radius. It shows that the hemispherical lenses with radius of 28 mm and larger are providing the highest gain. To conclude, the optimised hemispherical lens for this design is a Glass (Pyrex) with 4.82 primitively, the hemisphere curve is in the body side with 56 mm diameter.

4.2.3 Improvement results

Figure 4.3 shows the simulated S11 of the patch antenna with a hemispherical lens. Radiation pattern results show that there is a significant gain enhancement when the hemispherical lens is implemented. The improvement of normalized gain is nearly 6.5 dB as illustrated in Figure 4.4. This gain improvement is obtained when the dielectric lens is implemented where it is work to focus the radiation energy and, thus, the antenna gain is improved [6]. Figure 4.4 shows clearly that the radiation pattern is focused in out of the body direction, where the lens is implemented. It is clear that antenna outward radiation directivity and gain enhanced while total backward radiation levels are similar.

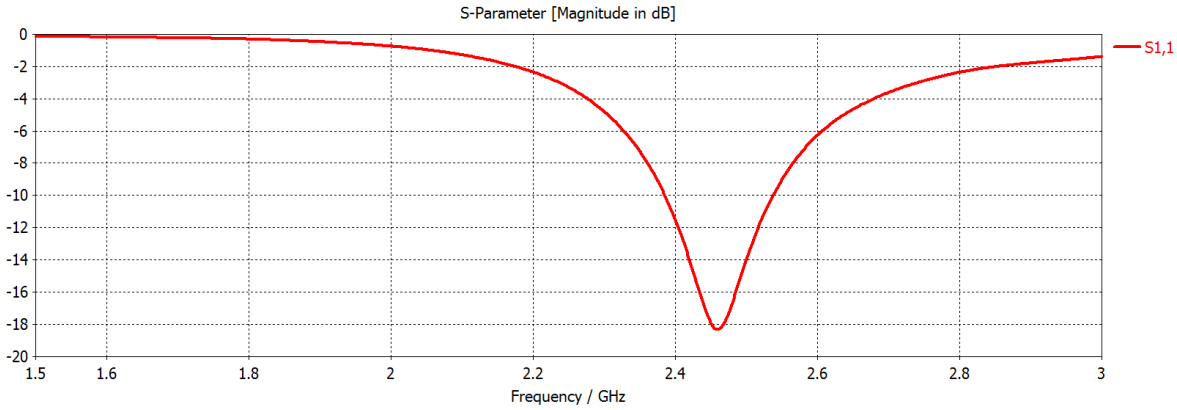

Figure 4.3: Simulated S11 of the patch antenna with a hemispherical lens

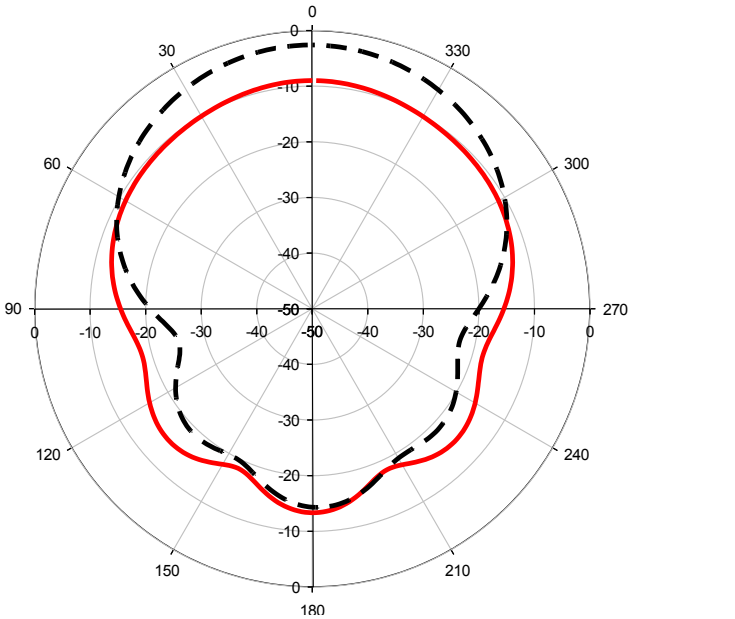

(a)

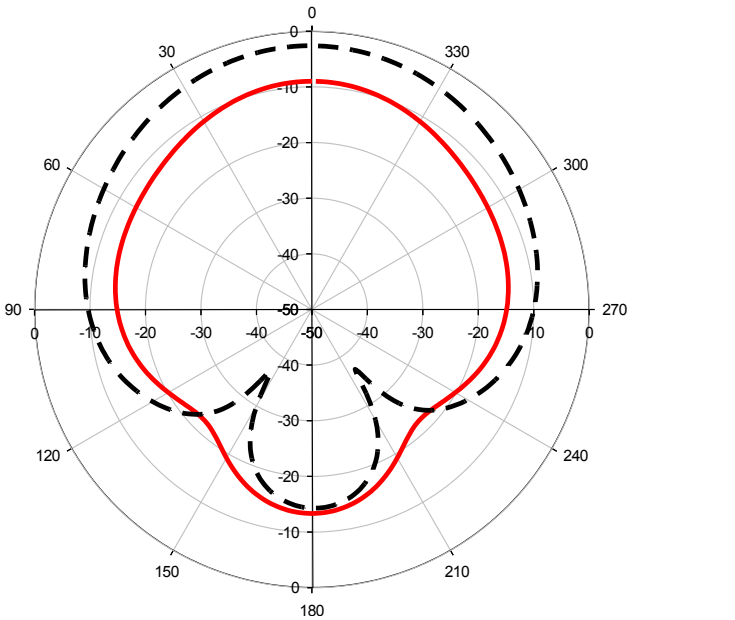

(b)

Figure 4.4: Simulated implanted antenna Far-Field pattern with/without a hemispherical lens E-plane (a) and H-Plane (b)

4.3 Performance Improvement of Implanted Patch Antenna Using External Lens and Parasitic Ring

Studies were carried out to further improve the implanted antenna gain by coupling the exiting EM wave to an external parasitic ring in addition to the lens. As best of the researcher knowledge, this is the first time that a parasitic ring is used for implantable antenna gain enhancement. A lens and a parasitic ring resonator were placed on the skin as shown in Figure 4.5. The parasitic ring resonator radius was optimised for the highest gain using CST software. Optimisation of the ring radius for optimal antenna gain is shown in Table 4.1 where the bold font shows the optimum radius. The best results obtained when the ring had a radius of 30 mm and 3 mm wide and was printed on a layer of felt. The felt layer material has a thickness of 1.1 mm, relative permittivity of 1.38 and loss tangent of 0.02.

As shown in Figure 4.5 and Figure 4.6, a simple ring of 30 mm radius (R) and 3 mm width (W) is placed on the the skin. Figure 4.7 shows that the simulations indicated that there should be a significant gain enhancement of almost 8.5 dB when both lens and parasitic ring resonator are used compared to the implanted antenna alone.

To investigate the impact of the body sample size, the gain is also investigated when the body sample is 150 mm and 200 mm length. Figure 4.8 shows that the normalised gain is enhanced from - 8.33 dB for the antenna alone to – 1.77 dB when the lens is used and to 0 dB when lens and parasitic ring resonator are used for 150 mm body sample length. Figure 4.9 shows a similar improvement when the body sample is 200 mm length. This investigation shows that using a lens and parasitic ring resonator provides a significant gain enhancement regardless the body sample size.

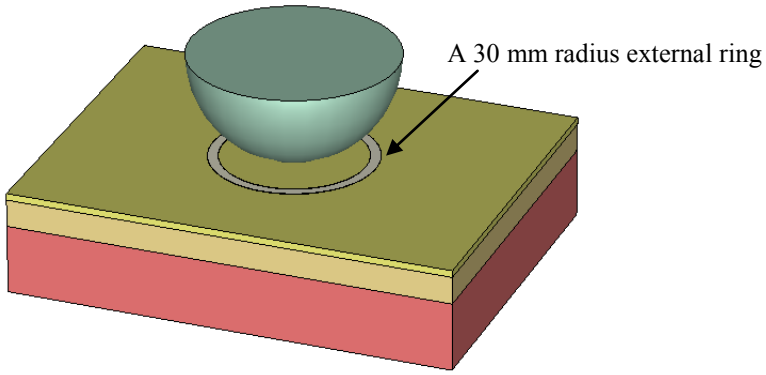

Figure 4.5: The proposed antenna with a hemispherical Lens and Ring over the body model

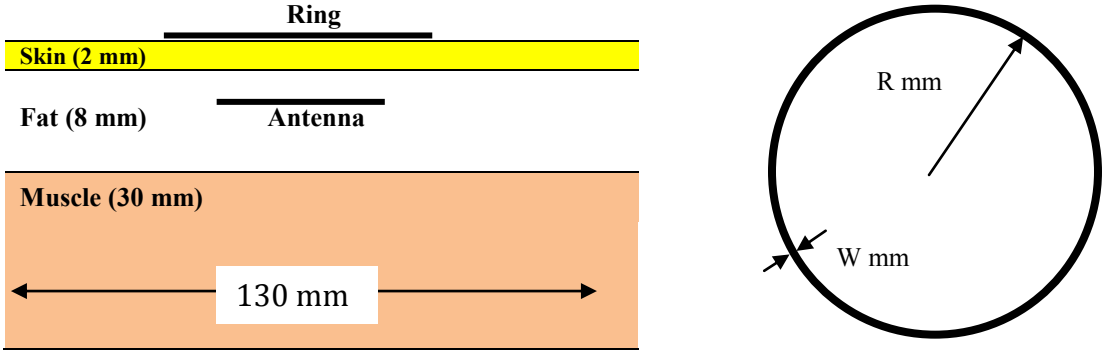

(a) (b)

Figure 4.6: (a) The implanted patch antenna with an external Ring (b) Ring design

Table 4.2: Optimizing ring radius for optimal antenna gain where the bold font shows the optimum radius

Ring Radius (R) (mm)	Gain (dB) at 2.45 GHz
22	-16.06
24	-15.23
25	-14.67
26	-14.03
27	-13.42
28	-12.91
30	**-12.46**
35	-13.85

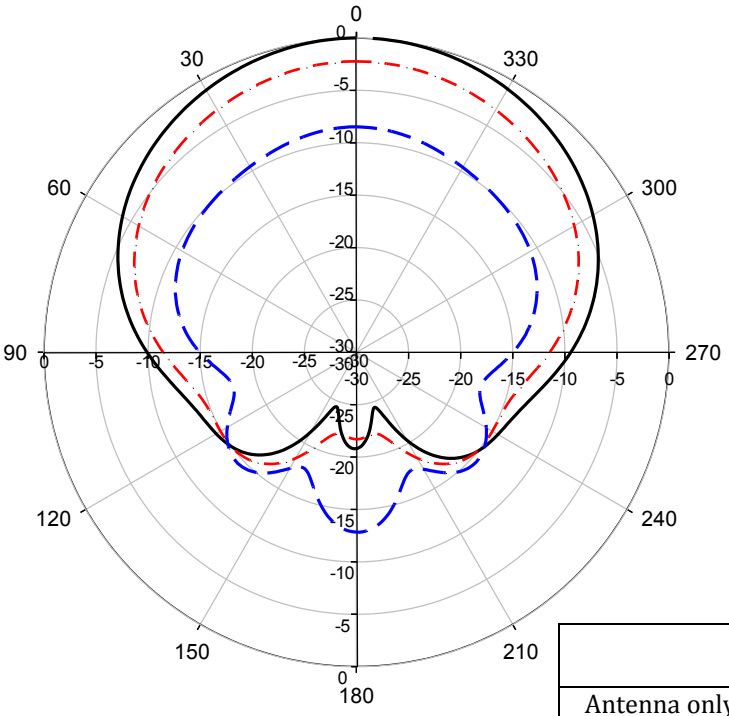

(a)

	Gain peak values (dBi)
Antenna only	- 8.48
Antenna with lens	- 2.23
Antenna with Lens & Ring	0

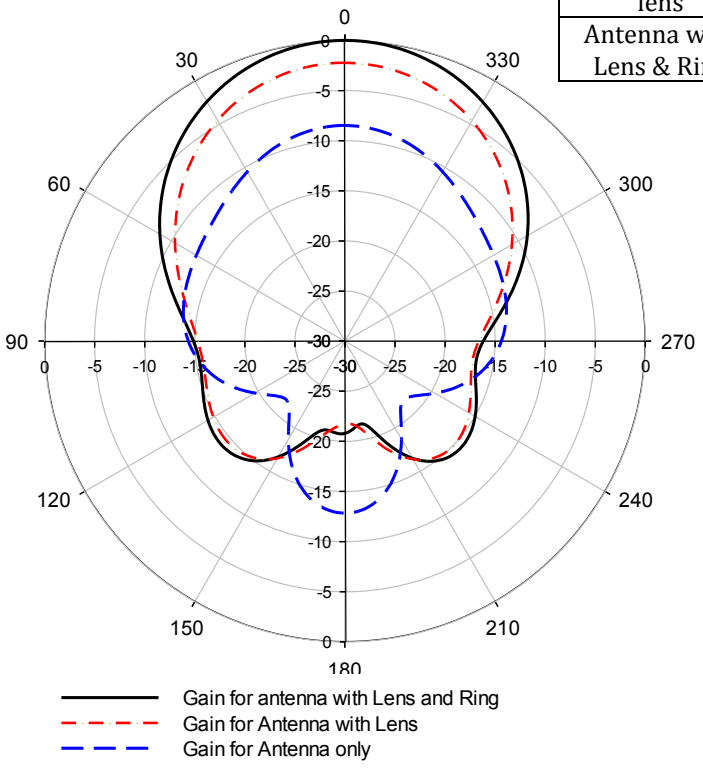

(b)

Figure 4.7: Normalised simulated implanted antenna Far-Field pattern with/without a hemispherical lens and parasitic ring (a) E-plane and (b) H-Plane when the body sample is 130 mm length

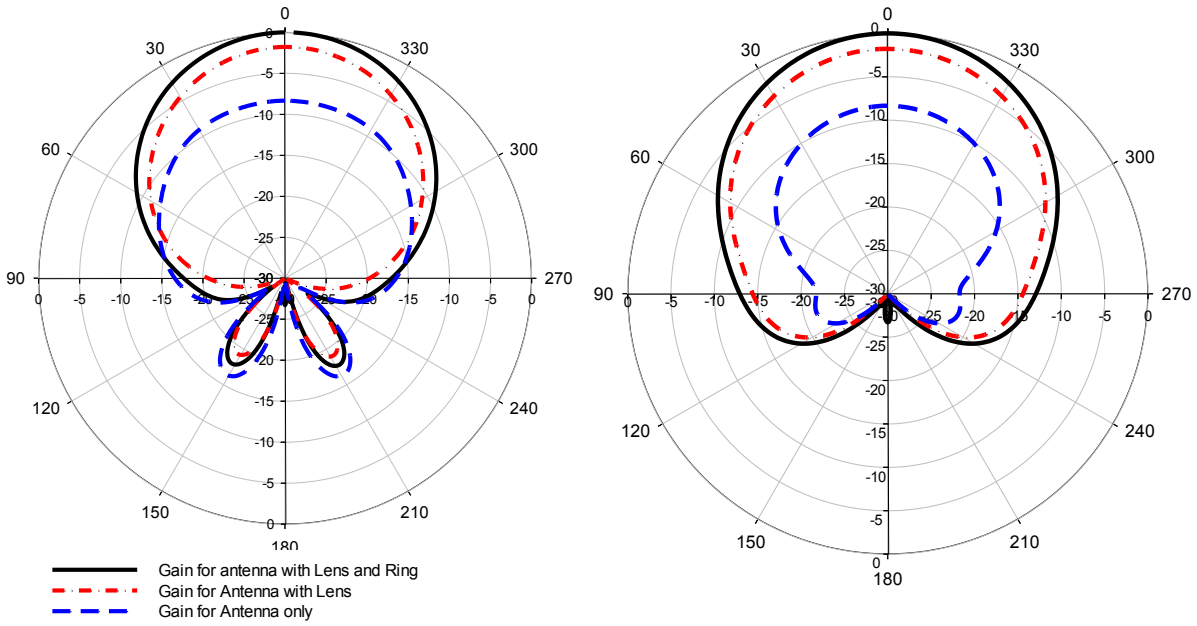

(a) (b)

Figure 4.8: Normalised simulated implanted antenna Far-Field pattern at 150 mm length body sample with/without a hemispherical lens and parasitic ring (a) E-plane and (b) H-Plane

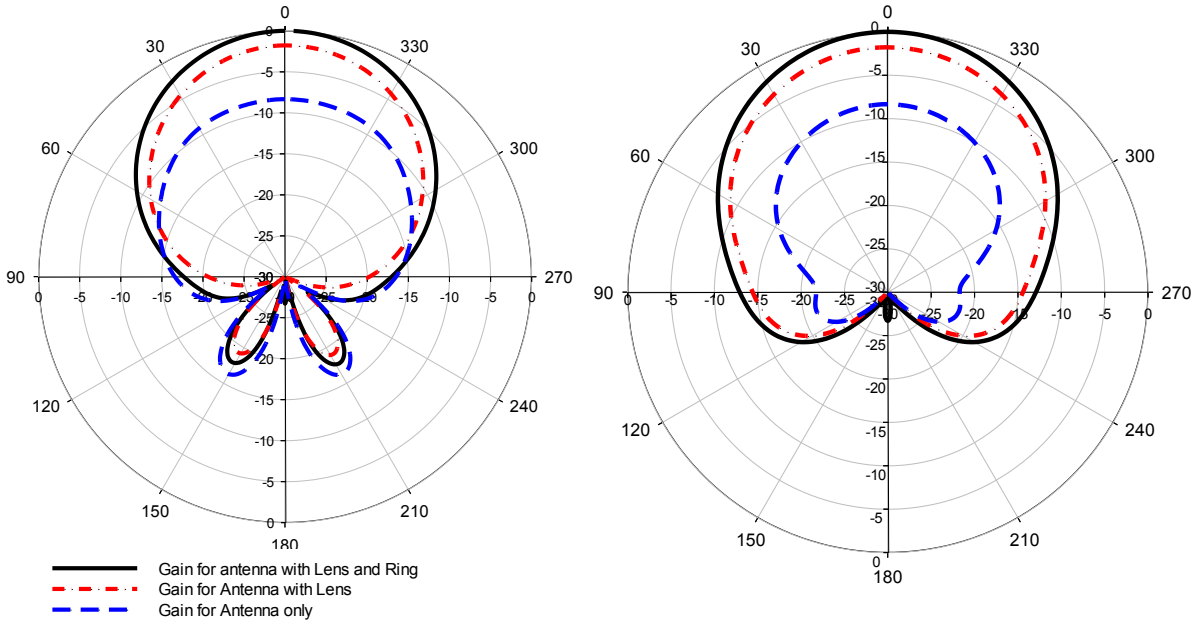

(a) (b)

Figure 4.9: Normalised simulated implanted antenna Far-Field pattern at 200 mm length body sample with/without a hemispherical lens and parasitic ring (a) E-plane and (b) H-Plane

4.4 Impact of the Antenna depth on the performance of using the external lens

The effects of implant depth on the performance of the antenna particularly inside the fat and muscle layers have been studied. The implanted depth of the antenna was tested and compared in three places to show and analyse its impact on antenna performance as shown in Figure 4.10. The S11 of the implanted antenna in the three places is shown in Figure 4.11. It can be seen that there is a small change in the resonant frequency of the implant when the antenna is still in the fat layer. However, the frequency is shifted down to 1.63 GHz when the antenna is inserted deeper in the muscle. This is due to the new higher permittivity surrounding the antenna which is muscle.

In order to investigate whether the lens still improves the gain even if the antenna is deeper in muscle, the Far-field pattern was analysed for both frequencies, 2.45 GHz and 1.63 GHz, in both cases (with and without hemispherical lens). Figure 4.12 and Figure 4.13 show the simulated Far-Field pattern of the antenna in muscle with/without a hemispherical lens at 2.45 GHz and at 1.63 GHz, respectively. Both figures show that the implanted antenna gain is improved when the lens is used even if the antenna is placed in muscle.

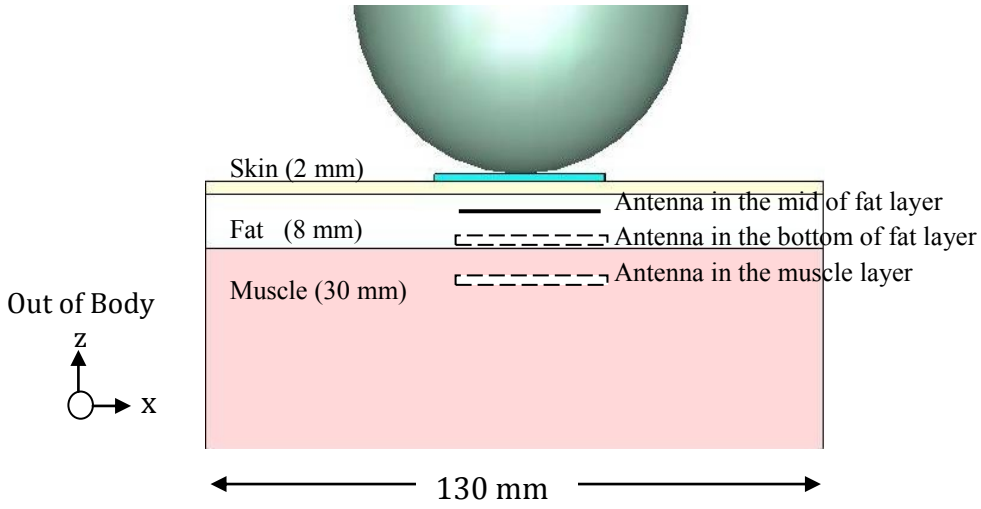

Figure 4.10: The implanted antenna in different depth with a hemispherical Lens

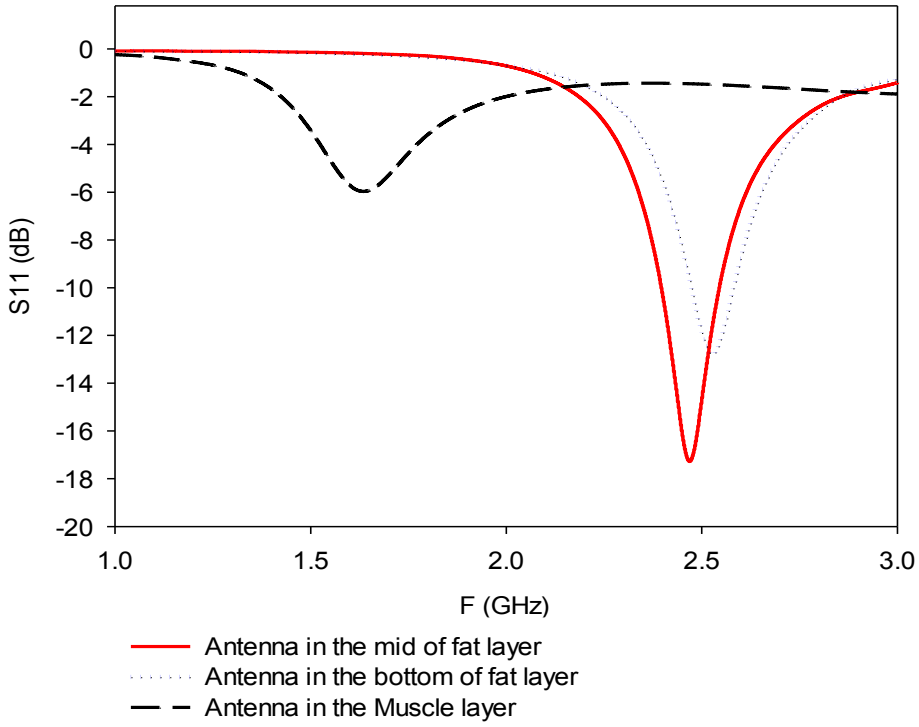

Figure 4.11: Simulated S11 of the implanted antenna in different depth

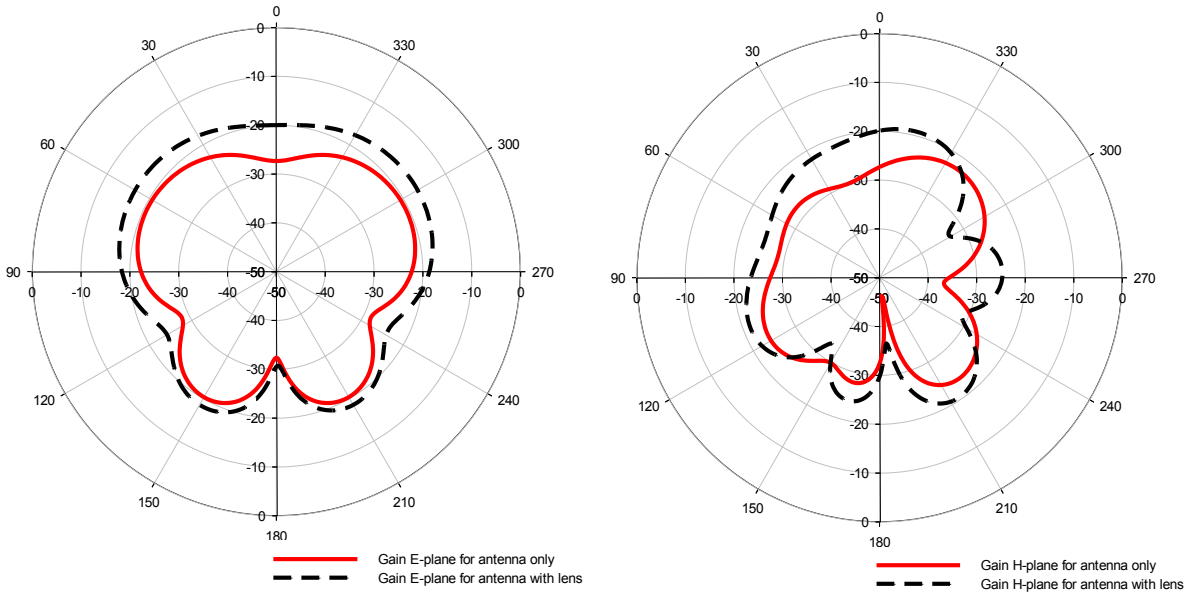

(a) (b)

Figure 4.12: Simulated Far-Field pattern of the antenna in muscle with/without a hemispherical lens E-plane (a) and H-Plane (b) at f = 2.45 GHz

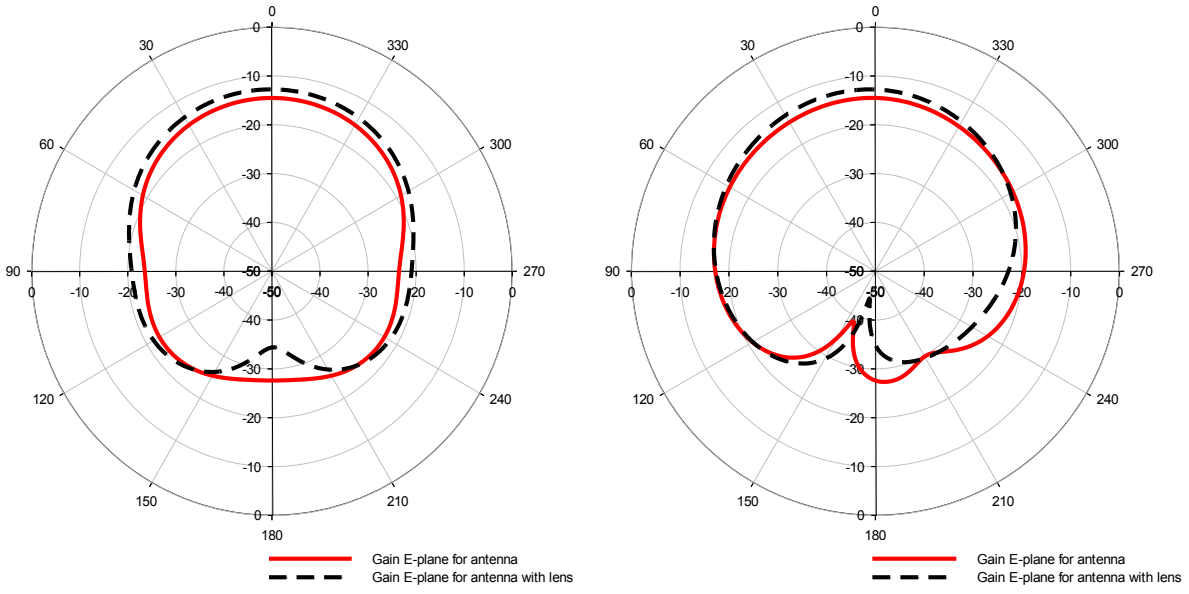

(a) (b)

Figure 4.13: Simulated Far-Field pattern of the antenna in muscle with/without a hemispherical lens E-plane (a) and H-Plane (b) at f = 1.63 GHz

4.5 SAR Analysis

Figure 4.14 shows the distribution of the Specific Absorption Rate (SAR) of 1-gram tissue along the model sample. It shows that the calculated peak SAR of 1-gram tissue is 69.6 W/kg for the antenna only and 67 W/kg when the hemispherical lens was implemented. The results show that the maximum SAR is reduced by 4.3% when the hemispherical lens is used with the antenna. Figure 4.15 shows the calculated maximum 1-g SAR as a function of distance from the antenna toward inside and outside the body at a cut along the centre of the body model for the implanted antenna with and without lens. The SAR decreases rapidly from 17.4 W/kg to 1.6 W/kg for a distance of 1 cm and to less than 1.6 W/kg for 1.5 cm. In many points, SAR is reduced by 20% to 40% when the hemispherical lens is used with the antenna. However, the peak SAR (67 W/kg) is higher than the peak 1-g SAR standard value of ANSI (1.6 W/kg) [12]. Therefore, in order to achieve the peak of 1-g SAR limit, the maximum power has to be reduced using the following equation:

$$P_{max} = \frac{1.6\ \text{W/kg}}{\text{SAR (1g)}} = \frac{1.6}{67} = 0.0238 = 23.8\ \text{mW} \qquad (4.9)$$

Where P_{max} is the maximum power. This equation shows that the maximum power can be delivered to the antenna is 23.8 mW to satisfy the SAR limit of the ANSI.

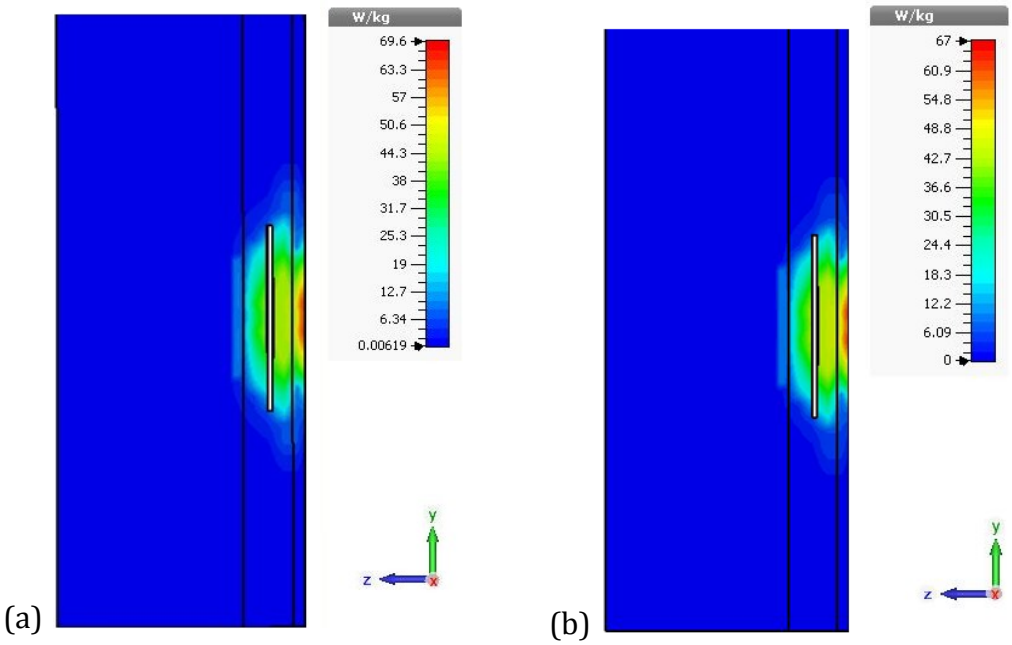

Figure 4.14: 1-g SAR distribution of the microstrip antenna without (a) and with (b) hemispherical lens

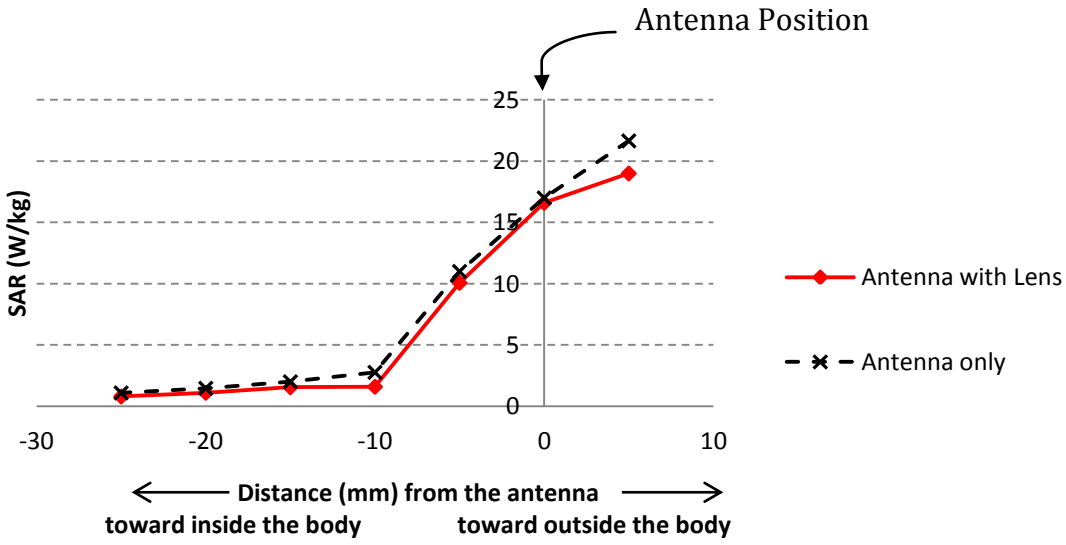

Figure 4.15: Maximum 1-g SAR calculated as a function of distance from the antenna toward inside the body

4.6 Measurements Setup

The simulated results obtained in the last sections using CST Microwave Studio are experimentally validated. Measurements were carried out in an anechoic chamber and the patch antenna was embedded in a piece of pork meat with similar skin, fat and muscle dimensions to the human model shown in Figure 4.16. Pork meat has close but not identical electromagnetic characteristics to the human body. However, the thicknesses of the various layers in the meat sample were only approximate and the layers were not completely uniform in thickness. The S11 and far-field for the antenna with and without the hemispherical lens and parasitic ring resonator are measured.

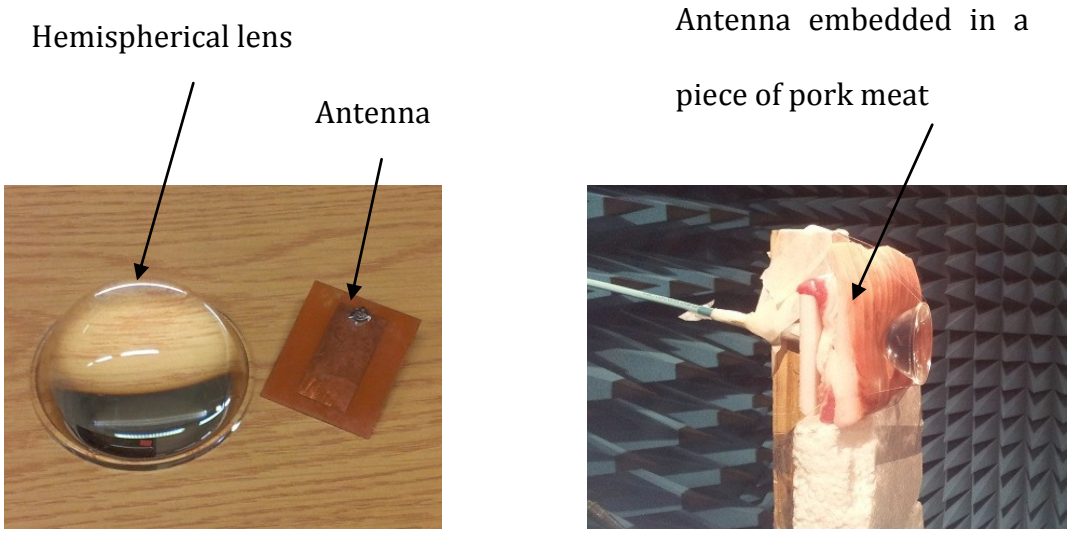

Figure 4.16: The hemispherical lens (left) and the far-field measurements (right)

4.7 Analysis of Measured Results

Figure 4.17 and Figure 4.18 show that measured results are similar with simulation. Figure 4.17 shows the measured versus the simulated S11 of the antenna with hemispherical lens where the measured band width is almost 70 MHz at VSWR 2:1.

Results show that the resonant frequency of the implanted antenna was not affected by placing the lens and/or parasitic element on the skin over the antenna. The measurements show that the antenna performance is significantly improved. However, the radiation pattern levels at the rear of the antenna are not accurate due to the stand used to support the antenna and meat sample.

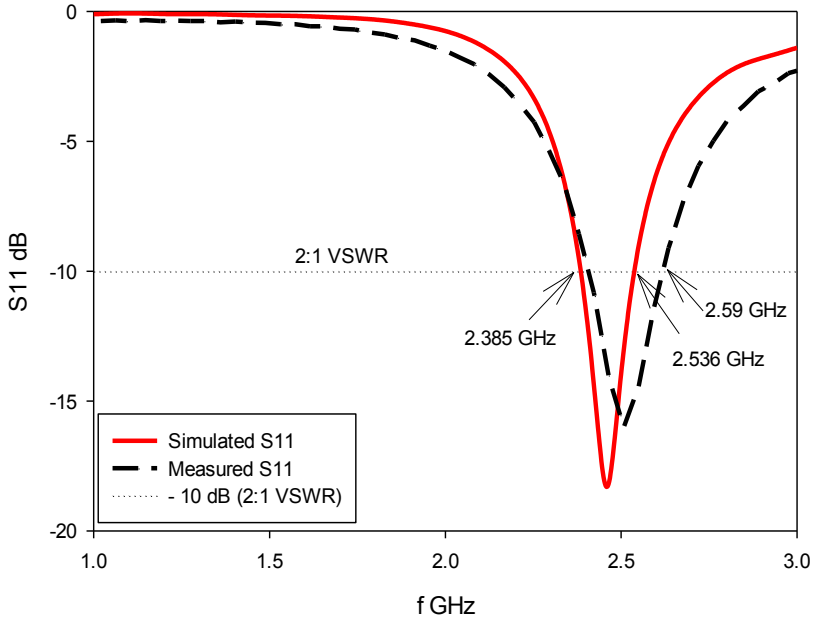

Figure 4.17: Measured vs. Simulated S11 of the implanted antenna with lens

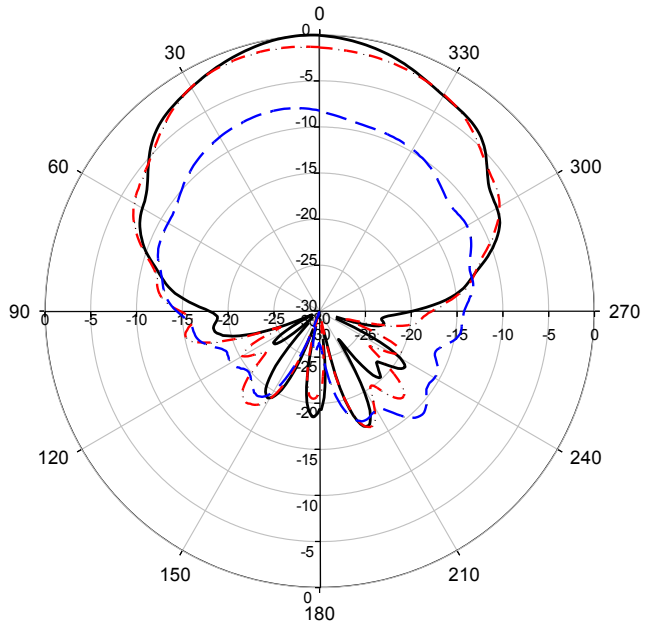

(a)

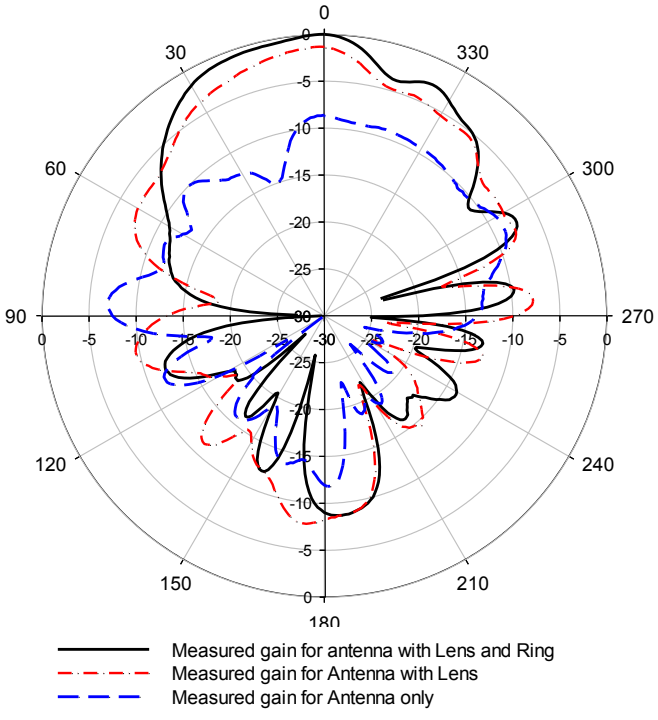

(b)

Figure 4.18: Measured radiation patterns in two planes for implanted antenna with/without lens and/or ring at 2.45 GHz (a) H-plane (b) E-plane

4.8 Summary

This chapter presented a new method to improve the gain of the implanted antenna and this method is numerically and experimentally investigated. The simulation and practical results show that combining an external hemispherical lens with a parasitic ring placed on the skin above the implanted antenna can enhance the performance of an implantable antenna. This approach yields a significant improvement in the antenna gain which was increased by up to 8.5 dB and hence provides better communication ability and reduces the power consumption for the implant. Moreover, it can also reduce SAR values to comply with the safety standards for medical implant applications.

The results showed that the antenna gain was increased by 8.5 dB and between 4% to 40% SAR reduction were achieved. In both cases, the SAR values can satisfy the safety standards for medical implant applications. Such an external lens is quit cheap, easy to implement and has a significant impact on the medical applications by improving the communication link between the implanted antenna and the nearest hotspot.

4.9 References

[1] Y. Lee*, et al.*, "Narrow-beam azimuthally omni-directional millimetre-wave antenna using freeformed cylindrical woodpile cavity," *IET microwaves, antennas & propagation,* vol. 4, pp. 1491-1499, 2010.

[2] P. Jirasakulporn*, et al.*, "Gain enhancement of microstrip antenna using square aperture superstrate," in *Electrical Engineering/Electronics, Computer, Telecommunications and Information Technology (ECTI-CON), 2012 9th International Conference on*, 2012, pp. 1-4.

[3] S. Zhu*, et al.*, "Implanted antenna efficiency improvement," in *Antennas and Propagation (EuCAP), 2013 7th European Conference on*, 2013, pp. 3247-3248.

[4] D. T. S. R. Manjunath G., Rajine Swetha R, "Gain Enhancement of Microstrip Patch Antenna Using Hemispherical and Spherical Dielectric Lens Structure for WiMAX Applications " *International Journal of Emerging Technology and Advanced Engineering* vol. 2, March 2012.

[5] A. Mahesh*, et al.*, "The gain enhancement of Microstrip array antenna with dielectric lens-A comparative study," in *Applied Electromagnetics Conference (AEMC), 2009*, 2009, pp. 1-4.

[6] T. Komljenovic and Z. Sipus, "Dielectric lens antennas design at millimeter waves," in *ELMAR, 2008. 50th International Symposium*, 2008, pp. 621-624.

[7] J. Thornton and K.-C. Huang, *Modern lens antennas for communications engineering* vol. 39: John Wiley & Sons, 2013.

[8] W. Chih-Kuang*, et al.*, "A Low Profile Dual Band Antenna for Implanted ZigBee Based Biosensors," in *Intelligent Computation and Bio-Medical Instrumentation (ICBMI), 2011 International Conference on*, 2011, pp. 253-255.

[9] P. K. A. a. N. Y. Joshi, " Design and Fabrication of Microwave Metallic Lens " *ICAT,* 2005.

[10] R. Shavit, "Dielectric spherical lens antenna for wireless millimeter-wave communications," *Microwave and Optical Technology Letters,* vol. 39, pp. 28-33, 2003.

[11] C. A. Balanis, *Antenna theory: analysis and design* vol. 1: John Wiley & Sons, 2005.

[12] J. C. Lin, "Safety standards for human exposure to radio frequency radiation and their biological rationale," *Microwave Magazine, IEEE,* vol. 4, pp. 22-26, 2003.

Chapter 5

Compact Dual-Band Implanted Antenna with Gain Enhancement[1, 2]

5.1 Introduction:

Different gain enhancement techniques have been used in Chapter 3 and Chapter 4 to enhance the gain of a simple implanted patch antenna. This chapter presents a compact dual-band implanted antenna with gain enhancement. Some of performance improvement techniques that used in last two chapters are used here to improve this antenna gain.

The design, analysis and measurements of a compact dual band implanted antenna for biotelemetry subcutaneous applications with gain enhancement are presented in this chapter. The desired ISM operating frequencies were 915 MHz and 2.45 GHz with a total size of 13 mm x 13 mm (1/25 λ = 0.04 λ) of the lower frequency band. The investigated gain improvements techniques show that an external hemispherical lens and parasitic ring can produce up to 7 dB gain enhancement.

---

[1] Alamri, S.; Langley, R.J.; AlAmoudi, A.O., "Compact Dual-Band Implanted Antenna for Wireless Communication," *Antennas and Propagation Conference (LAPC), 2014 Loughborough* , vol., no., pp.333, 335, 11-12 Nov. 2014

[2] Alamri, S.; Langley, R.J.; AlAmoudi, A.O., " Gain Enhancement of Implanted Antenna for Medical Applications," ICEAA - IEEE APWC 2015, September 7-11, Torino, Italy

This chapter is organized as follows: Section 5.2 presents a brief review of the research on size reduction of implanted dual-band antennas. Section 5.3 proposes a compact dual-band implanted antenna for medical wireless applications. To improve this antenna gain, an external hemispherical lens is used and illustrated in 5.4. In addition, an external parasitic ring is used to increase the gain of the dual-band antenna. The realisation and measurements are presented in 5.5. Finally, results analysis and discussions and conclusions are drawn in Sections 5.6 and 5.7 respectively.

5.2 Size Reduction of Implanted Dual-Band Antennas

Antenna size and gain are extremely important especially for implanted systems and, therefore, researchers apply extra effort to reduce implanted antenna size and to improve their performance. However, antenna electrical size directly affects the electromagnetic performance where the reduction of antenna size reduces the antenna performance [1-3]. For microstrip antennas the wavelength could be as big as 0.75 m for 403 MHz and 0.315 m for 915 MHz which cannot be used for an implant with such dimensions. Therefore, some researchers uses high frequencies bands, such as 5.2, 5.8 GHz or even as high as 31.5 GHz, to presents applicable size for implanted antennas for biomedical applications [4-6]. The other technique to overcome the size problem is to design a conducting microstrip antenna with meandered, folded or spiralled surface along the substrate either in one layer or multi layers [7-10]. The resonant frequency of the microstrip antenna is then proportional to the total length of the meandered, folded or spiral.

A recently presented antenna to be subcutaneous has 0.2 λ overall size operating at 2.45 GHz with a maximum gain of – 6 dBi [11]. A two research papers proposed a multiband implanted RFID antenna to be used for healthcare applications work at the ISM band: 433 MHz, 866 MHz and 2.45 GHz [12, 13]. Both antennas are 0.06 λ length for antennas design at 866 MHz with – 16 dB maximum gain at the same frequency. A dual band antenna operating at 405 MHz and 2.45 GHz with an overall dimension of 22.5 mm x 22.5 mm (0.06 λ) and a maximum gain of -25 dBi is presented in [14]. One of the presented antennas has an overall size of 0.1 λ operating at 700 MHz and 1.4 GHz with a maximum gain of – 29 dB [15]. A dual band antenna operating at 405 MHz and 2.45 GHz with an overall dimension of 13 mm x 8 mm x 5.2 mm (multilayer) and a maximum gain of -30 dBi is presented in [16].

It is clear from the literature, as mentioned, that reduction of antenna electrical size affects the electromagnetic performance and reduces the antenna performance. Therefore, to maintain a combination of low profile antenna and a reasonable performance, this chapter presents a compact size dual-band implanted antenna with gain enhancement.

5.3 Antenna Design

5.3.1 Antenna Size Reduction

Designing a microstrip patch antenna for implanted systems could be acceptable in the high frequency bands and a considerable amount of literature has been published. Several studies investigating high frequencies have studied microstrip patches antennas with sizes varies from 30 millimetres down to few millimetres for

frequencies from 2.45 GHz to 31.5 GHz [6, 17]. However, the antenna size is proportional to the wavelength. Thus the antenna size could be unrealistic for lower frequency such as 403 MHz and 915 MHz.

In this chapter, antenna designed to be working at 915 MHz and 2.45 GHz where ZigBee is allocated as a wireless technology based upon the IEEE 802.15.4 standard for wireless personal area networks (WPAN) [18]. Recent researches highlight the importance of ZigBee technology for next generation of wireless medical devices [19-22]. This is due a number of features that this technology has such as covering large distance, supporting a large number of nodes and low transmitter power.

The proposed antenna is inserted in a simplified 3 layers human body model that used in used in chapters 3 and 4. The configuration of the proposed antenna is shown in Figure 5.1.

Using the CST Microwave simulation software, a novel dual band antenna was designed for biotelemetry applications over the ISM bands (915 MHz and 2.45 GHz). As shown in Figure 5.1 and Table 5.1, the proposed antenna is S-shaped spiral antenna constructed on a 0.8 mm thick FR4 substrate as a patch grounded antenna, where F is the feeding point and S is the shorting point. The operating frequencies of this antenna are 915 MHz and 2.45 GHz. It has an overall size of the antenna is 13 mm x 13 mm (1/25 = 0.04) of the wavelength of the lowest frequency. The resonant frequency (915 MHz) can be tuned by changing the length of 915 branch, while the frequency 2.45 GHz can be tuned by changing the length of 2.45 branch.

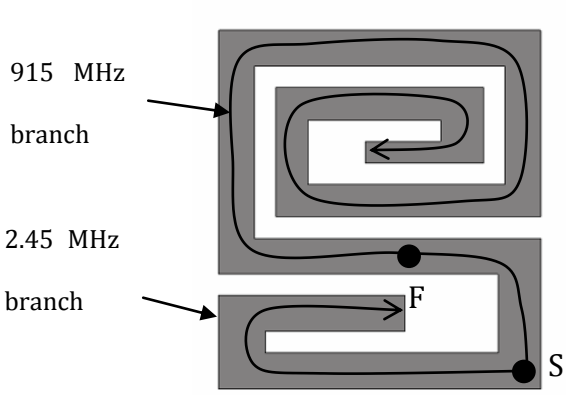

(a)

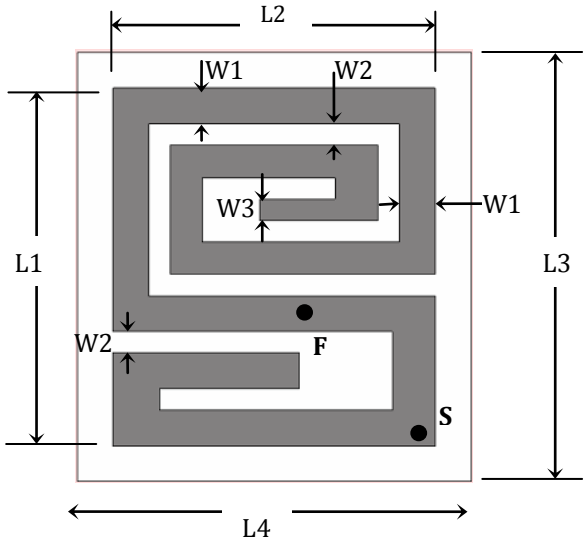

(b)

Figure 5.1: Proposed Antenna Design (a) the two branches of the dual-band antenna (b) antenna structure and dimensions

Table 5.1: Antenna parameters dimensions

Parameter	**Dimension (mm)**	**Parameter**	**Dimension (mm)**
W1	1	L1	11
W2	0.5	L2	11
W3	0.6	L3	13
		L4	13

5.3.2 Antenna Simulation Results

As shown in Figure 5.2, the simulated S11 of the proposed antenna shows that the antenna is resonating at 915 MHz and 2.45 GHz. The antenna has 72 MHz bandwidth at 915 MHz and 259 MHz bandwidth for 2.45 GHz calculated at 2.5:1 VSWR. Figure 5.3 shows the simulated far-field of antenna at 2.45 GHz (a) H-plane (b) E-plane. It shows that the maximum gain of this antenna is – 25 dBi.

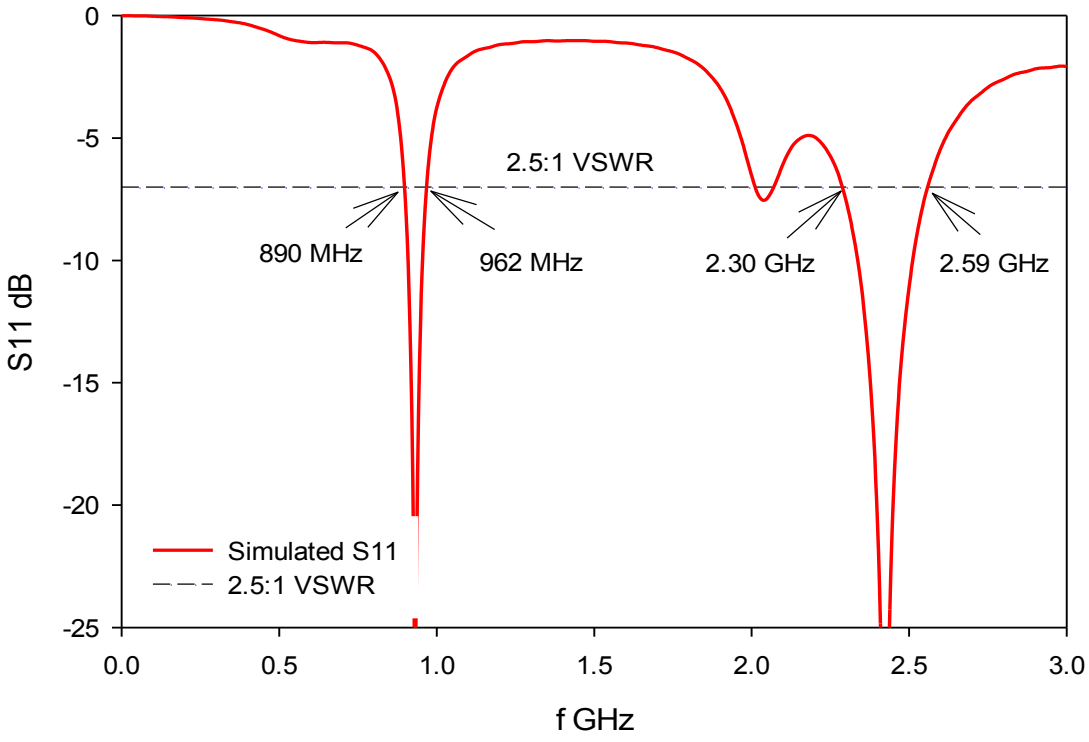

Figure 5.2: Simulated S11 of the dual-band antenna

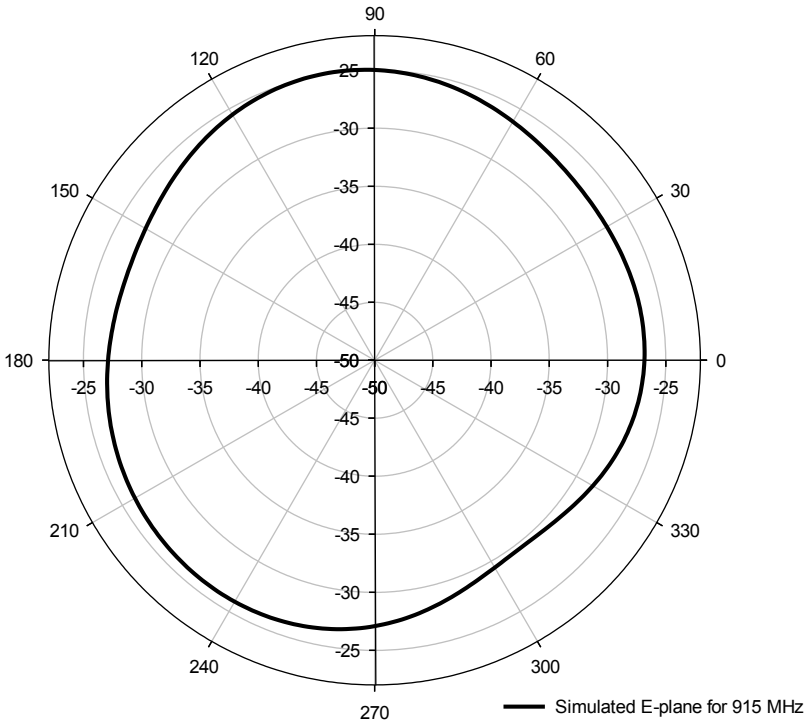

(a)

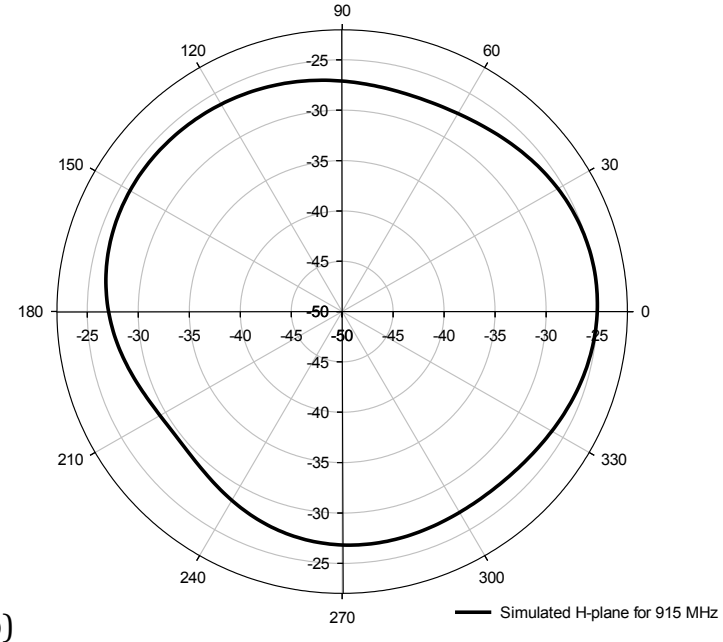

(b)

Figure 5.3: Simulated far-field of antenna at 915 MHz (a) E-plane (b) H-plane

5.4 Gain Enhancement of Implanted Dual-Band Antenna

In this section, two gain enhancement techniques for dual-band implanted antennas are presented. A hemispherical dielectric lens and parasitic ring are used on the top of patient skin with different scenarios as presented in the following two subsections.

5.4.1 Gain Enhancement of Implanted Dual-Band Antenna Using External Ring

A ring, as external parasitic resonator element, is investigated to improve the implanted dual-band antenna performance combined with the implanted antenna. The dual-band implanted antenna with ring over the skin model is shown in Figure 5.4. The ring is optimised to work for both resonant frequency; 915 MHz and 2.45 GHz. Table 5.2 shows optimisation of the ring radius for optimal antenna gain where the bold font shows the optimum radius and Table 5.3 shows optimisation of the ring width where the bold font shows the optimum ring width. As shown in Figure 5.4, the simple ring of 26 mm Radius (R) and 3 mm width (W) is placed on the top of the skin.

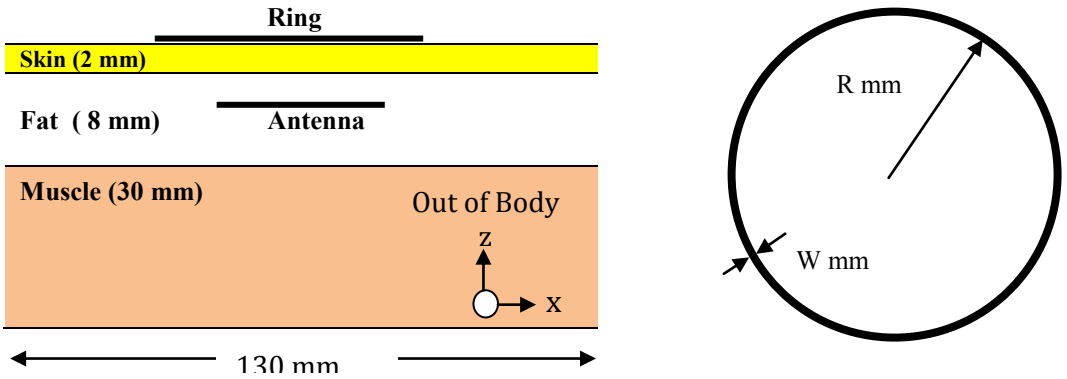

Figure 5.4: (a) The implanted patch antenna with an external Ring (b) Ring design

Table 5.2: Optimizing Ring Radius for Optimal Antenna Gain where the bold font shows the optimum radius

Ring Radius (R) (mm)	Gain (dB)	
	915 MHz	2.45 GHz
20	-19.79	-16.63
22	-16.48	-16.06
24	-14.37	-15.23
25	**-14.20**	**-14.67**
26	**-14.50**	**-14.03**
27	-15.21	-13.42
28	-16.29	-12.91
30	-18.17	-12.46
35	-21.21	-13.85

Table 5.3: Optimizing Ring Thickness for Optimal Antenna Gain where the bold font shows the optimum ring width

Ring Width (W) (mm)	Gain (dB)	
	915 MHz	2.45 GHz
1	-18.78	-13.91
2	-15.92	-14.23
3	**-14.20**	**-14.67**
4	-14.93	-15.12
5	-17.08	-15.54

5.4.2 Gain Enhancement of Implanted Dual-Band Antenna Using Hemispherical Lens and parasitic ring

To investigate another improvement possibility, the implanted antenna performance an external hemispherical glass lens was designed and investigated using CST software, to be placed on the skin over the implanted antenna. The hemispherical lens material used was Pyrex glass of permitivity 4.82 and its radius is 28 mm. The simulation results showed that there was a significant gain enhancement when the hemispherical lens was implemented of about 6.5 dB.

For further improvements, the hemispherical lens and parasitic ring resonator were combined together. The simulations indicated that there should be a significant gain enhancement of almost 8.5 dB compared to the implanted antenna alone.

5.5 Measurements

The simulated results are experimentally validated and measurements were carried out in an anechoic chamber. The antenna was inserted into pork meat joints whose fat and muscle layers varied in thickness but approximated the model as shown in Figure 5.5. The body sample was assigned to a slab of cork to be fixed. The cable is connected to the antenna through the cork and the meat. The measurements were carried out using Agilent Vector Network Analyser (VNA) with a start frequency of 300 KHz, a stop frequency of 3 GHz, 201 points and 70 kHz IFBW.

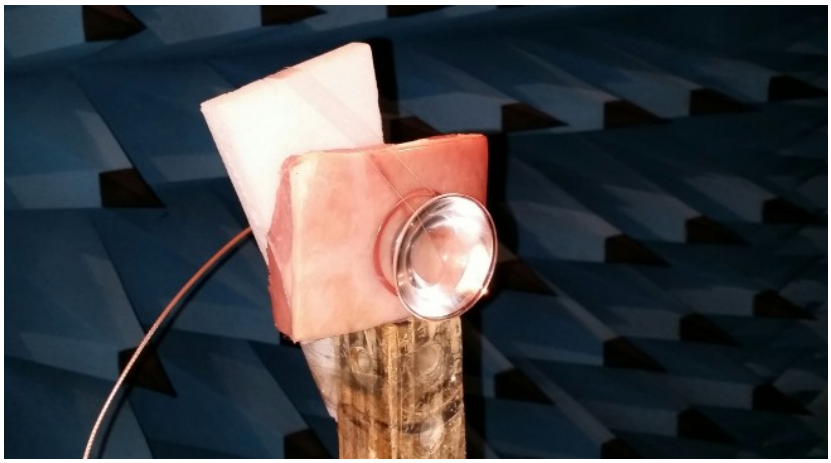

Figure 5.5: Measurements Setup embedding antenna in a pork meat with hemisphere lens and parasitic ring.

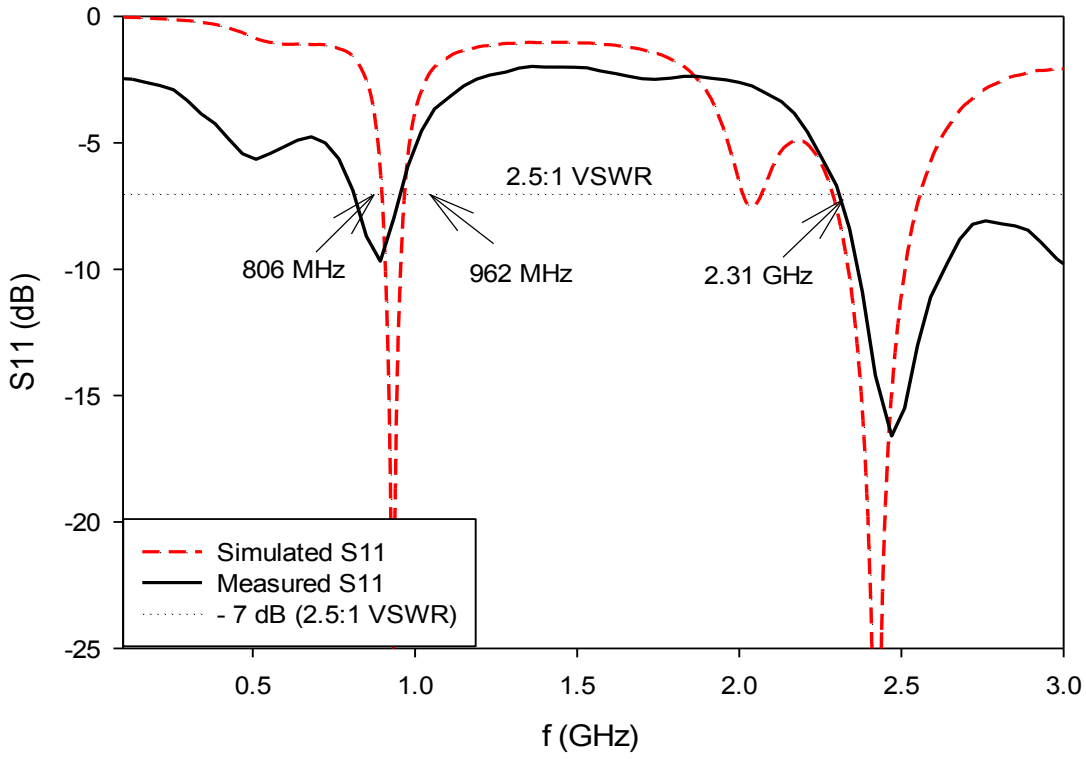

Figure 5.6: Measured versus simulated S11 for the dual-band antenna

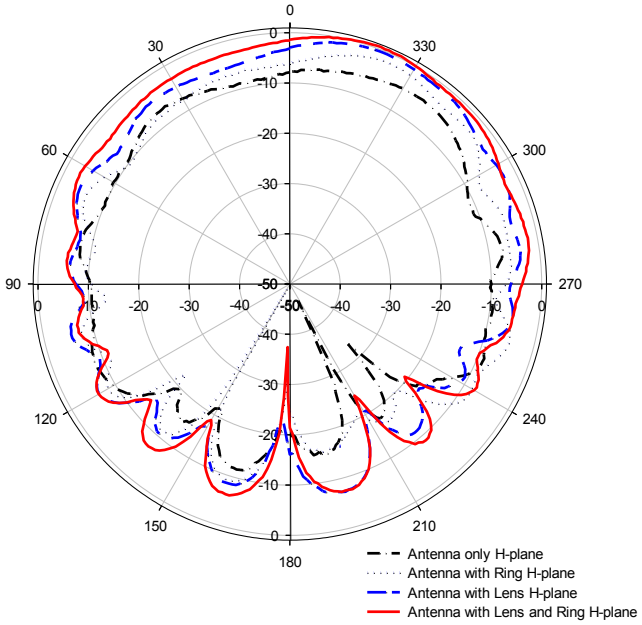

(a)

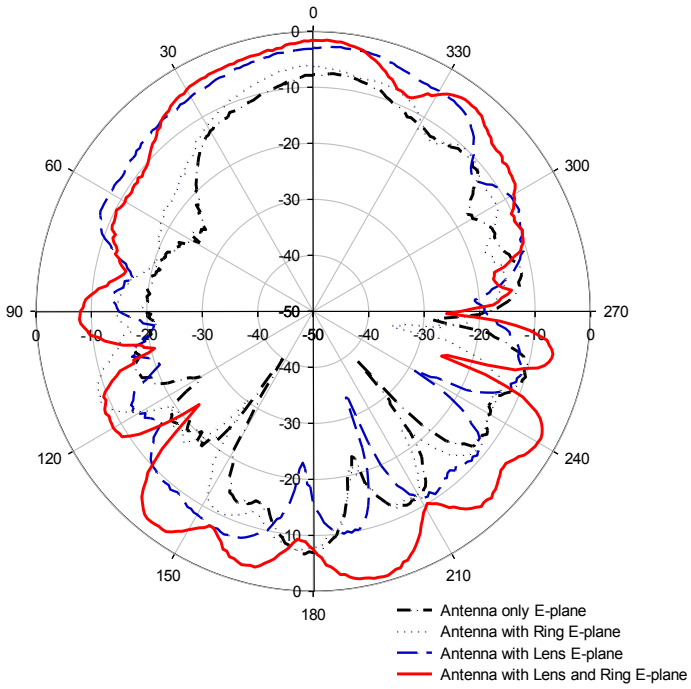

(b)

Figure 5.7: Measured normalised gain comparison of implanted antenna with/without ring and/or lens for 2.45 GHz (a) H-plane (b) E-plane

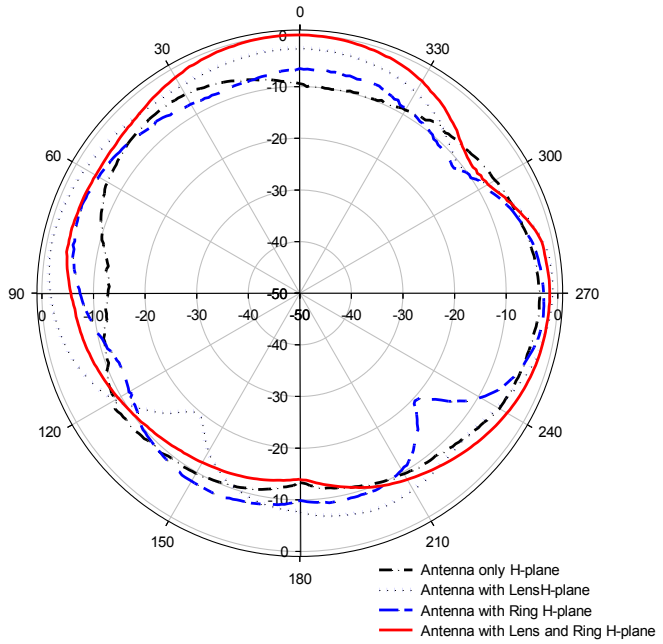

(a)

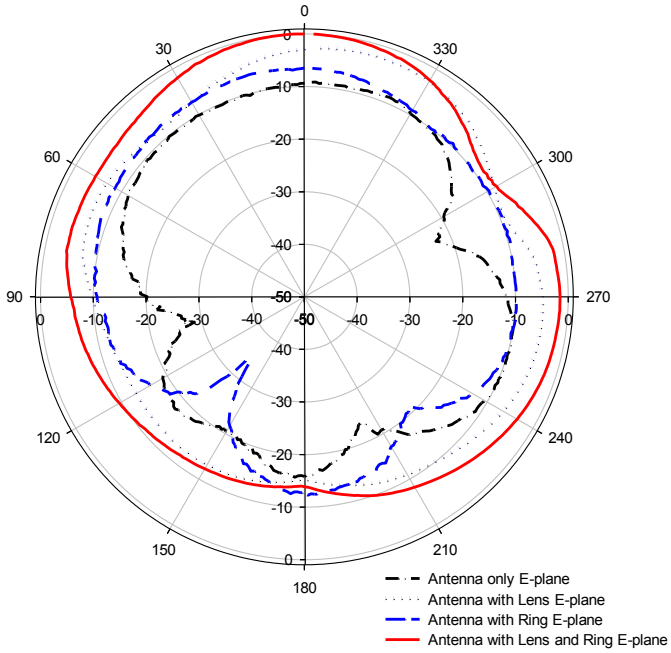

(b)

Figure 5.8: Measured normalised realised gain comparison of antenna with/without ring and/or lens for 915 MHz (a) H-plane (b) E-plane

5.6 Results Analysis and Discussions

As shown in Figure 5.6 the design achieves good matching at 915 MHz and 2.45 GHz. Figure 5.7 shows the measured 2.45 GHz far field radiation pattern for the antenna in the two principal planes compared to the simulated far field radiation pattern. Figure 5.8 shows a comparison between the measured and simulated far field at 915 MHz. The patterns are not symmetrical due to the pork samples used but the antenna. Maximum gains achieved in the body front are -22.8 dB at 2.45 GHz and -27.3 dB at 915 MHz.

By using parasitic ring on the top of skin, the gain has improved by 3 dBi for 915 MHz and by 1.5 dBi for 2.45 GHz. In addition, when a hemispherical dielectric lens is used, the gain has improved by 6 dBi and 4 dBi for frequencies 915 MHz and 2.45 GHz respectively. When the hemispherical dielectric lens and the parasitic ring are combined together, this antenna has improved by almost 9 dBi for the 915 MHz frequency and nearly 6 dBi for the 2.45 GHz.

It should be mentioned that the thicknesses of the various layers in the meat sample were only approximate and the layers were not completely uniform in thickness. Moreover, the radiation pattern levels at the rear of the antenna are not accurate due to the stand used to support the antenna and meat sample.

5.7 Summary

In this Chapter, the design, analysis and measurements of a novel compact dual band implanted antenna for biotelemetry subcutaneous applications is presented. The desired ISM operating frequencies were 915 MHz and 2.45 GHz. Miniaturization is

achieved by bending the spiral as S-shaped antenna. The total size of the antenna is 13 mm x 13 mm (1/25 λ = 0.04 λ) of the lower frequency band. Maximum gains achieved in the body front are -22.8 dB at 2.45 GHz and -27.3 dB at 915 MHz.

A hemispherical dielectric lens and parasitic ring resonator are used on the top of patient skin are simulated with different scenarios and verified by measurements. The simulation and measurements results showed that there is a significant improvement in the antenna gain by using these techniques which are not very expensive and easy to manufacture. The gain has improved by 9 dB and 6.5 dBi for the frequencies 915 MHz and 2.45 GHz respectively. The antennas are considered to be co-designed for a medical applications environment and a communication systems perspective for optimum LAN/WAN connectivity and minimum SAR exposure level.

5.8 References

[1] L. J. Chu, "Physical Limitations of Omni- Directional Antennas," *Journal of applied physics,* vol. 19, pp. 1163-1175, 1948.

[2] R. F. Harrington, "Effect of antenna size on gain, bandwidth, and efficiency," *J. Res. Nat. Bur. Stand,* vol. 64, pp. 1-12, 1960.

[3] J. S. McLean, "A re-examination of the fundamental limits on the radiation Q of electrically small antennas," *Antennas and Propagation, IEEE Transactions on,* vol. 44, p. 672, 1996.

[4] S. Manafi and H. Deng, "Design of a Small Modified Minkowski Fractal Antenna for Passive Deep Brain Stimulation Implants," *International Journal of Antennas and Propagation,* vol. 2014, 2014.

[5] J. Tak, K. Kwon, S. Kim, and J. Choi, "Dual-band on-body repeater antenna for in-on-on WBAN applications," *International Journal of Antennas and Propagation,* vol. 2013, 2013.

[6] Y. Ahmed, Y. Hao, and C. Parini, "A 31.5 GHz patch antenna design for medical implants," *International Journal of Antennas and Propagation,* vol. 2008, 2008.

[7] W. Huang and A. A. Kishk, "Embedded spiral microstrip implantable antenna," *International Journal of Antennas and Propagation,* vol. 2011, 2011.

[8] Y.-W. Yang, H.-L. Su, K.-H. Lin, H.-H. Lin, and C.-Y. Wu, "Spiral-like implanted antenna for biotelemetry," in *Microwave Conference Proceedings (APMC), 2012 Asia-Pacific*, 2012, pp. 409-411.

[9] J. Abadia, F. Merli, J.-F. Zurcher, J. R. Mosig, and A. K. Skrivervik, "3D-spiral small antenna design and realization for biomedical telemetry in the MICS band," *Radioengineering,* vol. 18, pp. 359-367, 2009.

[10] C.-Y. Huang, C.-L. Tsai, and C.-L. Yang, "Compact Folded Meander PIFA Antennas in MedRadio Bands," *Session 3A5 Microstrip and Printed Antenna, Antenna Theory,* p. 457.

[11] S. A. Kumar and T. Shanmuganantham, "Implantable CPW-fed rectangular patch antenna for ISM band biomedical applications," *Microwave and Optical Technology Letters,* vol. 56, pp. 1060-1065, 2014.

[12] A. Sani, M. Rajab, R. Foster, and H. Yang, "Antennas and Propagation of Implanted RFIDs for Pervasive Healthcare Applications," *Proceedings of the IEEE,* vol. 98, pp. 1648-1655, 2010.

[13] A. Sani, M. Rajab, R. Foster, and Y. Hao, "Antennas and propagation of implanted RFIDs for pervasive healthcare applications," *Proceedings of the IEEE,* vol. 98, pp. 1648-1655, 2010.

[14] T. Karacolak, A. Z. Hood, and E. Topsakal, "Design of a Dual-Band Implantable Antenna and Development of Skin Mimicking Gels for Continuous Glucose Monitoring," *Microwave Theory and Techniques, IEEE Transactions on,* vol. 56, pp. 1001-1008, 2008.

[15] P. M. Izdebski, H. Rajagopalan, and Y. Rahmat-Samii, "Conformal ingestible capsule antenna: A novel chandelier meandered design," *Antennas and Propagation, IEEE Transactions on,* vol. 57, pp. 900-909, 2009.

[16] F. Merli, L. Bolomey, E. Meurville, and A. Skrivervik, "Implanted Antenna for Biomedical Applications F. Merli*, L. Bolomey2, E. Meurville2, and AK Skrivervik1 Laboratory of Electromagnetics and Acoustics 2 Laboratory of Microengineering for Manufacturing 2 Ecole Polytechnique Fédérale de Lausanne, Switzerland," 2008.

[17] S. Almari, R. J. Langley, and A. O. AlAmoudi, "Improved performance of 2.45 GHz implanted patch antenna for wireless communication," in *Antennas and Propagation Conference (LAPC), 2013 Loughborough*, 2013, pp. 27-30.

[18] Z. Alliance and Z. Specifications, "ZigBee Document 053474r17," *ZigBee Specification, ZigBee Alliance,* 2008.

[19] D. Li and Y. Chen, *Computer and Computing Technologies in Agriculture VII: 7th IFIP WG 5.14 International Conference, CCTA 2013, Beijing, China, September 18-20, 2013, Revised Selected Papers* vol. 419: Springer, 2014.

[20] F. Qiang, L. Shuenn-Yuh, H. Permana, K. Ghorbani, and I. Cosic, "Developing a Wireless Implantable Body Sensor Network in MICS Band,"

Information Technology in Biomedicine, IEEE Transactions on, vol. 15, pp. 567-576, 2011.

[21] S. Ullah, H. Higgin, M. A. Siddiqui, and K. S. Kwak, "A study of implanted and wearable body sensor networks," in *Agent and Multi-Agent Systems: Technologies and Applications*, ed: Springer, 2008, pp. 464-473.

[22] P. Valdastri, A. Menciassi, and P. Dario, "Transmission Power Requirements for Novel ZigBee Implants in the Gastrointestinal Tract," *Biomedical Engineering, IEEE Transactions on,* vol. 55, pp. 1705-1710, 2008.

Chapter 6

Implantable Loop Antenna for Capsule with Gain Enhancement

6.1 Introduction

The last chapters present different antennas that can be implanted under the skin with performance improvement, particularly improved gain, using different external elements. In this chapter, a novel flexible and omni-directional loop antenna is proposed to be used in ingestible capsule systems. In addition a novel technique is used to improve the performance of this antenna.

The design and characteristics of an implantable 403 MHz loop antenna with gain enhancement are investigated using simulation and practical experiments. The results show that the technique can be used to significantly enhance the performance of the capsule loop antenna. This was shown by calculating the S_{11} and the antenna performance is characterized by antenna gain.

This chapter is organized as follows: section 6.2 briefly introduces the topic of an antenna for ingestible capsule systems. Then, the human body modelling is reviewed with the development of a novel formula to implement a human body liquid phantom are illustrated in section 6.3. The size and far-field issues of capsule antenna is

discussed in section 6.4. Thereafter, section 6.5 presents a flexible loop antenna to be used for capsule systems and, then, a novel improvement technique is presented in 6.6. The realisation, findings and measurement results are discussed in section 6.8 and 6.9 respectively. Finally, conclusions are drawn in Section6.10.

6.2 Capsule Antennas for Biomedical Applications

Gastroenterology (GI) diseases are one of the most prevalent diseases. Examples include, stomach ulcers and bowel cancer, chronic abdominal pain, unexplained weight loss or anemia, and/or GI bleeding ... etc. Many of these can be avoided by early detection of complications, especially cancer. Current early detection mechanisms are considered expensive, painful and a discomfort for patients [1, 2]. Recently, Capsule endoscopy is recognized as one of the least invasive procedures that offers a feasible non-invasive way to detect diseases along the gastrointestinal (GI) tract [2-4].

In 2000, a paper published in the journal Nature presented a new form of gastrointestinal endoscopy with a small camera that can be swallowed and can send photos of the GI tract to an external receiver [5]. It is similar to vitamin capsule size, and the wireless capsule endoscopy consists of batteries, sensors, a light source, camera, transmitter and antenna. Moreover, the wireless Capsule promises significant improvements in patients' care and quality of life [2, 6].

6.3 Development of a Homogeneous Liquid Phantom

In chapter 3, the human body model consists of three biological layers; skin, fat and muscle is presented to simulate the human body. This model can be used for modelling an subcutaneous antenna to be implanted in a specific and fixed area of the human body. However, this model would be inappropriate to model moving devices, such as ingestible capsules, or devices that would be located in an area with many overlapping biological tissues. Examples of these devices include heart pacemakers [7] and implants that can be used for monitoring the healing of soft tissue trauma and early stage diagnosis of infection [8].

The human body consists of of a large number of systems with different electromagnetic characteristics for every part of the body. Figure 6.1 shows that the human body's electromagnetic characteristics vary from 70 to 0 overlapping tissues [9, 10]. Table A.1 in Appendix A lists the 30 tissues electromagnetic characteristics. Therefore, researchers propose a different human body model and a homogeneous body model to simulate the human body [11, 12]. A number of recent studies prove that the homogeneous body model is close enough to the real one [13].

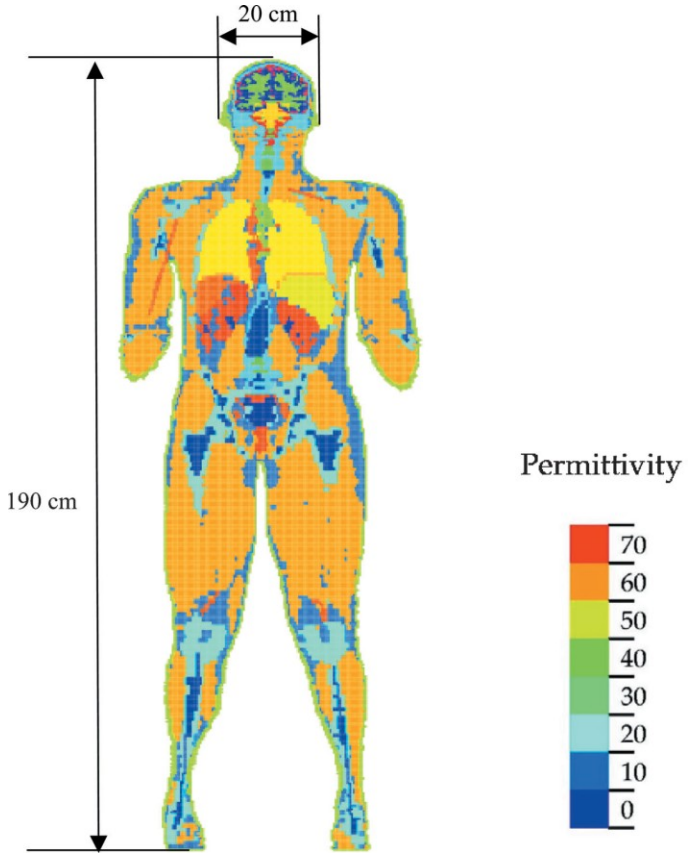

Figure 6.1: A human body model represented by different relative permittivity [9]

As mentioned in chapter 2, the literature proposes a complicated phantom formula to be used for homogeneous body model measurements using polyethylene powder, TX-151, Sodium oxide, deionised water, sodium chloride and agar [11]. Moreover, a gel phantom formula was proposed for skin, fat and muscle using deionised water, sodium chloride, sugar and agar [12]. However, some of the first formula components are not easy to find and the sodium oxide is poisonous and extreme caution is needed and, therefore, the second formula was proposed for skin, fat and muscle.

6.3.1 Proposed liquid phantom formula for homogeneous body model:

A simple liquid phantom formula for the homogeneous human body model at 403 MHz is proposed using deionised water, sodium chloride and sugar. The electromagnetic properties for the homogeneous human body model are: $\varepsilon = 56.4$ and conductivity = 0.82 [10, 14]. Many mixtures were tried in order to give as close as possible electromagnetic properties of the homogeneous model. Mixtures content is weighted using a sensitive scale and Table 6.1 shows the amounts of chosen integrants for the equivalent body phantom formula.

Table 6.1: shows the integrants for the equivalent body phantom formula

Integrants	Concentration
deionised water	44.5%
sodium chloride	0.5%
Sugar	55%

6.3.2 Dielectric properties measurements

Figure 6.2 shows the dielectric properties measurement setup. An Agilent 85070E Dielectric Probe Kit is used with a Vector Network Analyser (VNA) in order to measure the dielectric properties of the liquid phantom with a start frequency of 300 KHz, a stop frequency of 8.5 GHz, 201 points and 70 kHz IFBW. The measurements are carried out as following:

- The VNA is connected to the Dielectric Probe and permittivity measurement presented using software provided by Agilent.

- The calibration is carried out using 85052D calibration kit.

- The measurement system is calibrated using an open circuit (air), a shorting block (provided with Dielectric Probe Kit) and deionised water.

- The prepared liquid phantom (in section 6.3.1) is, then, measured using the Dielectric Probe Kit and results presented using software provided by Agilent.

A number of phantom mixtures were tried taking into account that permittivity decreases significantly as sugar concentration increases in the mixture and only a slight increase in conductivity as the sugar concentration increases. However, there is a clear increase in conductivity as the sodium chloride concentration increases. The formula in Table 6.1 gives the closest electromagnetic properties to the electromagnetic properties of the homogeneous model and the formula permittivity is $\varepsilon = 53.96$. This result fairly satisfies the phantom properties, since it is very difficult to produce exact values [11, 12].

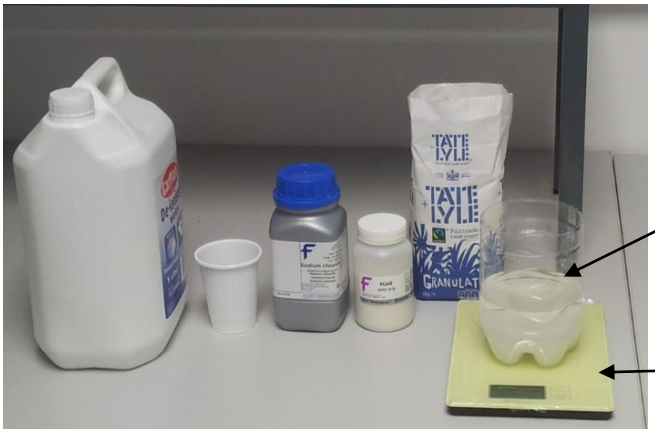

(a)

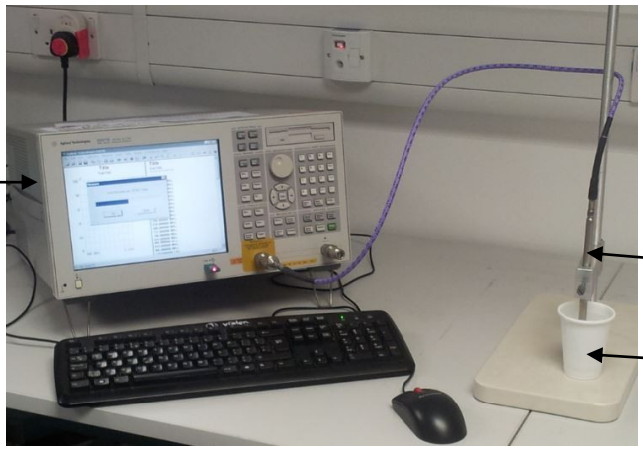

(b)

Figure 6.2: Dielectric properties measurements setup (a) Formula integrants (b) Calibration setup

6.4 Capsule antenna size and gain issues

Implanted ingestible systems have benefited from recent advanced microelectronics and sensor technology of miniaturized wireless communication systems, while the challenge still remains with the antenna. Depending on the operational frequency, designing miniaturised antennas with an attempt to maintain high gain is extremely challenging especially for ingestible capsule systems. The space allowed to design the

antenna for a capsule system is very limited taking into account that all passive (antenna) and active (such as batteries, sensors, etc) parts of the communication system are embedded within the capsule. Researchers have investigated various types of compact antennas that can be used for such systems [15-17]. One of the presented antennas has an overall dimension of 5 mm x 29.2 mm operating at 700 MHz and 1.4 GHz with a maximum gain of – 29 dBi [15]. A dual band antenna operating at 405 MHz and 2.45 GHz with an overall dimension of 13 mm x 8 mm x 5.2 mm (multilayer) and a maximum gain of -30 dBi is presented in [16]. Another capsule antenna has been presented to be working at 434 MHz with dimensions of 5.5 mm x 18 mm with – 33 dBi gain [17].

All gains for published capsule antenna designs are the maximum gain. However, most of these antennas have a drawback in the large difference between the maximum and minimum value of the far-field radiation.

Table 6.2 is a comparison between different types of capsule antennas from published work and shows the maximum and minimum gains. The difference between the maximum and minimum gain varies from 16 dB and up to 32 dB. For this reason, current capsule systems suffer from discontinuous communication when the minimum gain side is in line-of-sight with the receiver system.

Due to the random orientation of the capsule, one of the main disadvantages of the current systems is they may not be able to maintain a continuous communication link between the capsule and the external receiver [18]. Therefore, an efficient

communication link between the capsule (in body) and the external receiver unit (out of body) is highly important for the applicability of wireless capsule endoscopy [4, 18].

Table 6.2: Minimum and maximum capsule antennas gain for some published work

Reference	**Antenna type**	**Frequency**	**Maximum Gain (dB)**	**Minimum Gain (dB)**
[15]	conformal meandered dipole antenna	700 MHz	– 29	- 55 *
[16]	Loop antenna	403 MHz	-32	-50 *
[17]	Flexible microstrip patch	403 MHz	- 33	-65
[19]	Loop antenna	403 MHz	-28.4	-48 *
[20]	Planner antenna	403 MHz	Normalised to 0	- 14 dB from highest gain
[21]	Multilayer spiral antenna	402.8 MHz	-30.2	-55
[22]	Flexible meandered inverted-F Antenna	1.4 GHz	- 25.2	-56

* The number is estimated from the colours chart of the presented antenna

6.5 Antenna Design

To design a proper antenna for capsule endoscopy, the antenna characteristics are discussed in the following subsections:

6.5.1 Frequency

In a relatively recent study, the total loss between transmitter and receiver antennas was calculated. It was founded that the minimum total loss is achieved when the

operation frequency is between 400 and 600 MHz [23]. Moreover, the European Commission identified frequencies 402-405MHz for the Medical Implant Communications Service (MICS) band [24]. Therefore, the operation frequency of the proposed antenna for capsule endoscopy is 403 MHz.

6.5.2 Antenna type

Choosing the proper type of antenna is extremely important particularly when the application is as challenging as implantable systems. Researchers have discussed which antenna has better performance when the radiator is implanted in the human tissues. In [21] a number of studies were reviewed and compared for best solution for antennas surrounded by a lossy media. Loops and miniature spirals antennas are suggested in [25-28]. In particular, a loop is compared over several frequency bands in [26] and this antenna is also used in [25] to characterize the RF transmission for an implantable system in the MedRadio range (Medical Radio Communication Band (401 - 406 MHz)). In [27], a loop is investigated for endoscopy applications at 1 GHz and a multi-turn spiral structure is discussed in [28]. Moreover, the human body tissues are non-magnetic and, therefore, magnetic sources have better performance [29]. It is concluded that magnetic sources have better performance when the antennas are surrounded by lossy tissues. Therefore, the antenna designs investigated in this chapter is a loop antenna.

6.5.3 Antenna Size and materials consideration

To maintain a large space for the electronics components of the capsule, the antenna is designed to be on the shell of the capsule. Therefore, the design has been carried out

on a flexible substrate in order to bend the antenna on the capsule case. The material of the substrate is 25 μm thick flexible polyimide (Kapton), which has a relative dielectric constant ε_r of 3.4 and this substrate is turned 4 times around a plastic capsule case. Thus, the antenna is covered by a flexible, biocompatible material of 4 turns Polyimide film with total thickness of 100 μm.

6.5.4 Antenna structure

This antenna is a wavelength loop antenna with a total length of 122 mm and 1 mm line width. Figure 6.3 (a) shows the structure of the antenna before it is bent around the capsule case and (b) when the antenna is bent. The antenna structure is 31 mm long and 18 mm wide when it is flat. However, when the antenna is bent, the dimensions will be 18 mm long x 10 mm diameter.

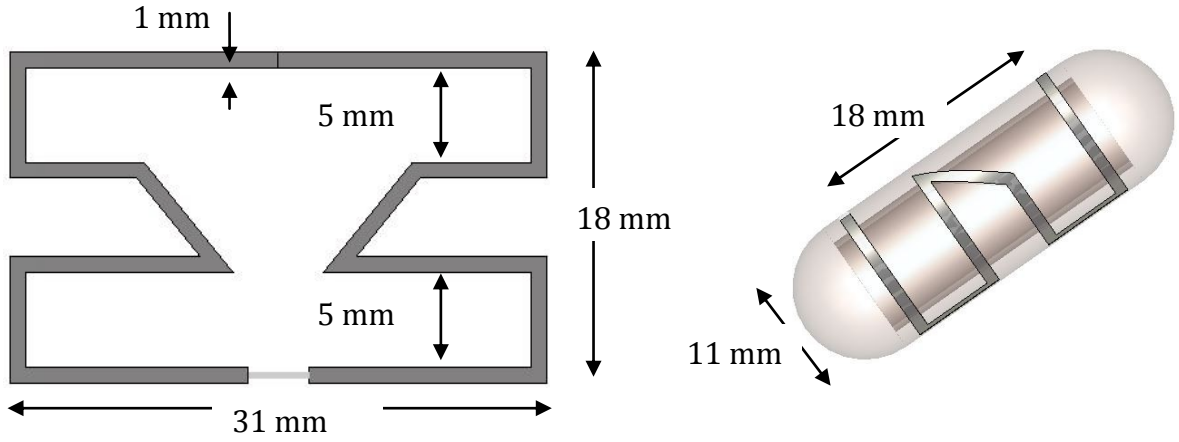

(a) (b)

Figure 6.3: The antenna structure (a) before bending and (b) after bending

6.5.5 Antenna simulation results

Figure 6.4 shows the simulated S11 of the antenna. It shows that the antenna bandwidth is 310 MHz calculated at – 10 dB. This wide bandwidth is important to insure that the antenna is still working where the surrounding media permittivity is changing which can shift the resonant frequency up or down. Figure 6.5 (a) shows the 3D and the two plane simulated far-field of the antenna. They show that the antenna calculated maximum gain is -29.2 dBi in the z- direction. However, the gain is very low in the (–z) direction at nearly – 60 dBi. Therefore, this antenna has the similar problem of most published work which is the high difference between the maximum and minimum gain as discussed in section 6.4 and Table 6.2. Thus, a method to improve the radiation pattern is required.

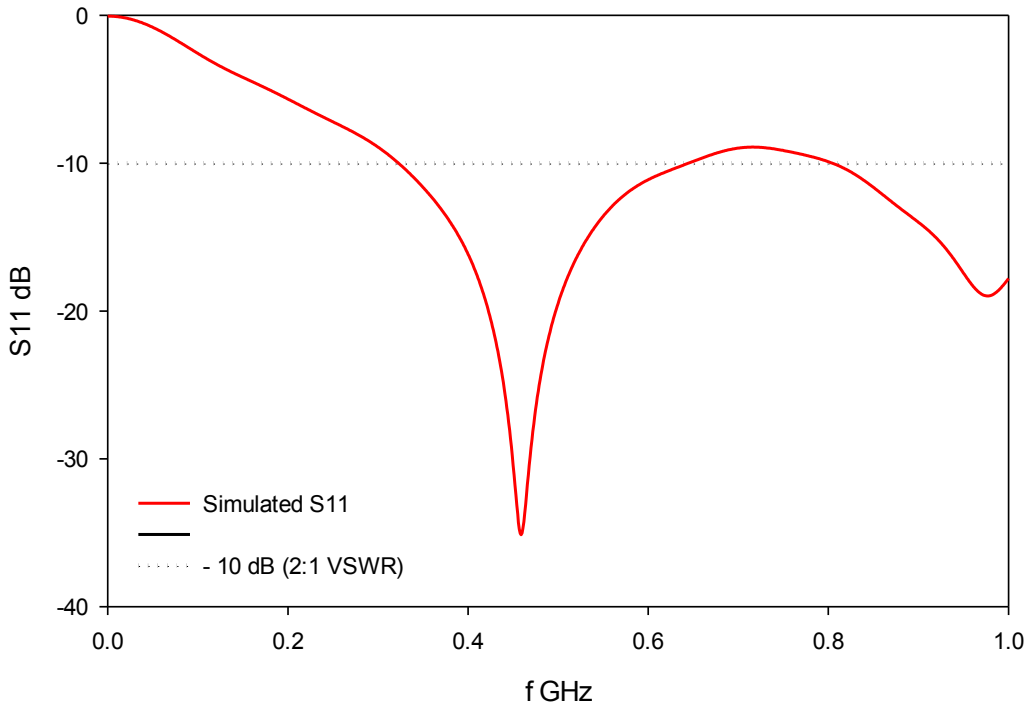

Figure 6.4: Simulated S11 of the capsule loop antenna

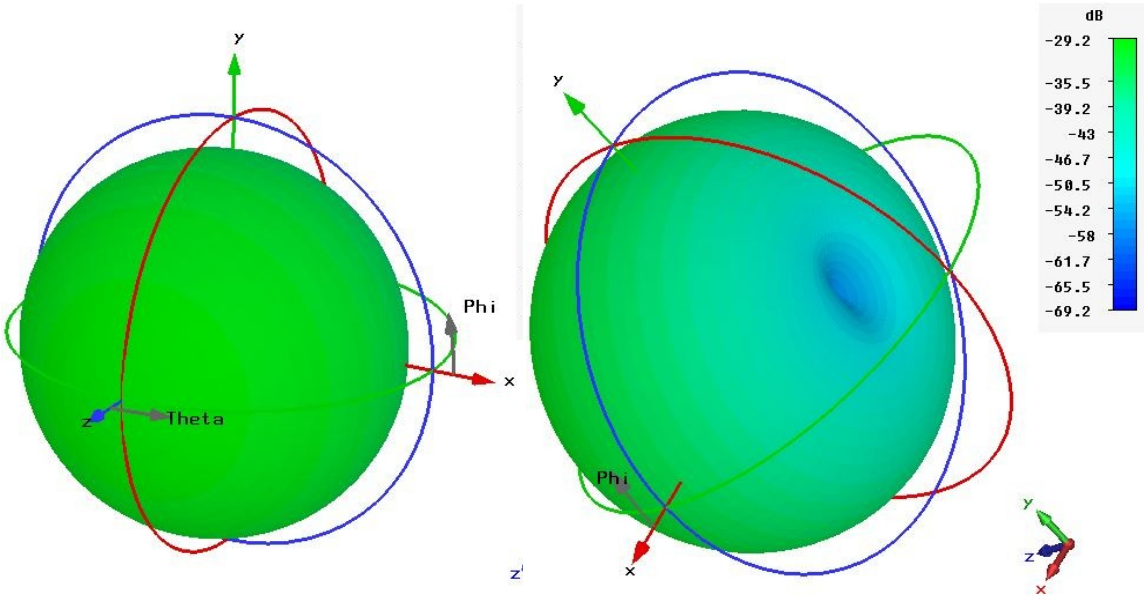

(a) (b)

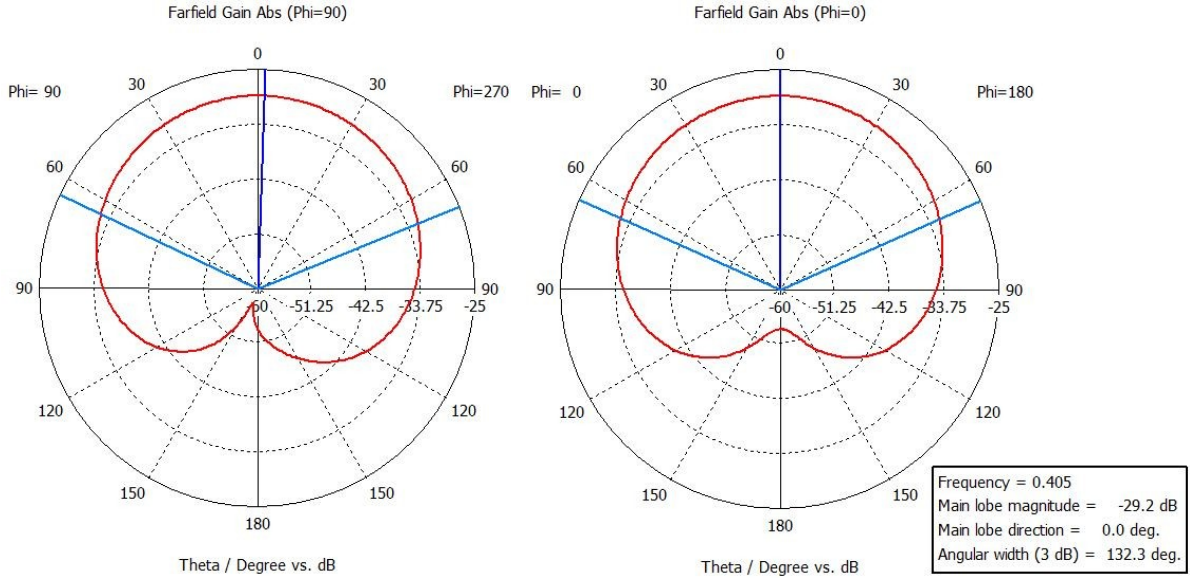

(c) (d)

Figure 6.5: Simulated far-field of the antenna (a) and (b) 3D far-field pattern, (c) xz plane and (d) yz plane

6.6 Radiation pattern improvement

As mentioned in last two sections, the main drawback of current capsule systems is they are not able to maintain a continuous communication link between the capsule and the external receiver. The reason for that is the low (minimum) gain – not the maximum - for most of the antennas that suffer from communication discontinuity. It is noted that most of presented antennas throughout the literature have tried to increase the maximum gain of the capsule antennas. However, this section is presenting a technique to improve the loop antenna minimum gain in order to maintain omni-directional propagation.

The technique is based on how the antenna surface current is distributed around the capsule. Figure 6.6 shows the loop antenna design and its surface current before and after bending. It shows that the maximum current is in dashed areas (1) and (2) in the middle of the antenna. When the antenna is bent on the capsule, both areas that have the strongest current will be in the same side of the capsule. This affects the radiation pattern and produces a higher gain in the side of the stronger current and much lower gain in the other side.

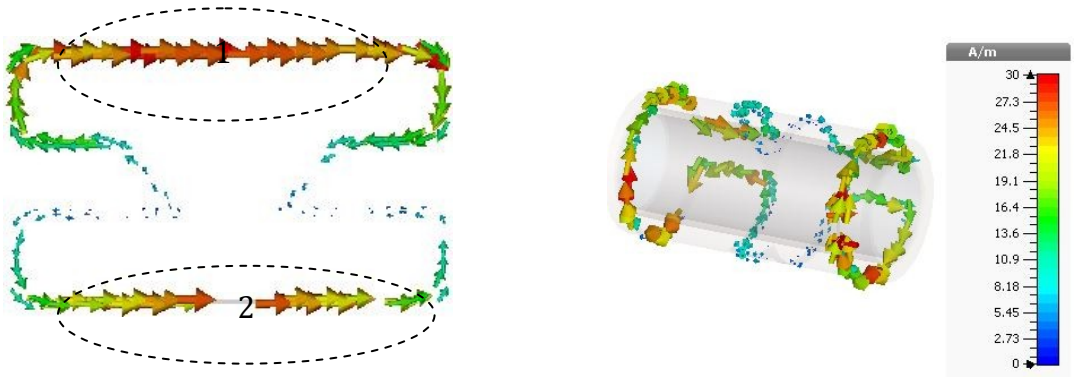

(a) (b)

Figure 6.6: Loop antenna design and its surface current (a) before bending (b) after bending

To improve the minimum gain and to provide an omni-directional propagation, the surface current of the antenna should be distributed around the capsule equally. Thus, to distribute the antenna surface current around the capsule equally, antenna branches should be overlapped. This can be obtained by bending the maximum current areas in antitheses of each other as seen in Figure 6.7 where area (1) is antitheses of area (2). Therefore, the maximum current surface can be obtained in both directions. Figure 6.8 shows the steps of bending the antenna and the final design of the overlapped antenna using this technique.

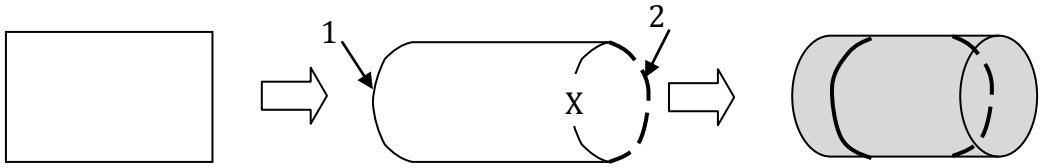

Antenna to be bent on a capsule

Antenna bending

When the Antenna is bent, strong current areas are on different sides

Figure 6.7: Overlapped flexible loop antenna bending process

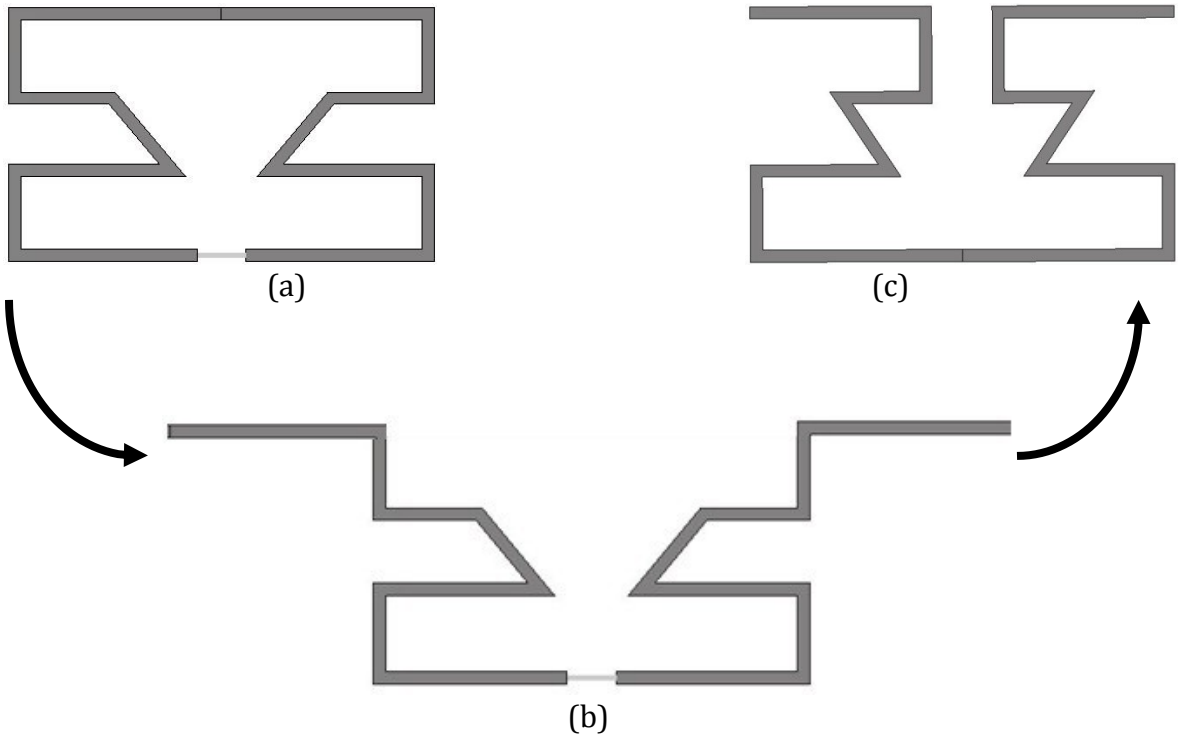

Figure 6.8: Steps to convert the original to overlapped flexible loop antenna

6.7 Antenna Radiation Improvements Simulation Results

Figure 6.9 and Figure 6.10 shows the simulated improved antenna far-field versus the original antenna far-field. It is clear that the minimum gain is improved significantly by almost 20 dB. The difference between the maximum and minimum gain is less than 10 dB. This is due to the equally distributed current around the capsule and, thus, the far-field can be considered as nearly omni-directional.

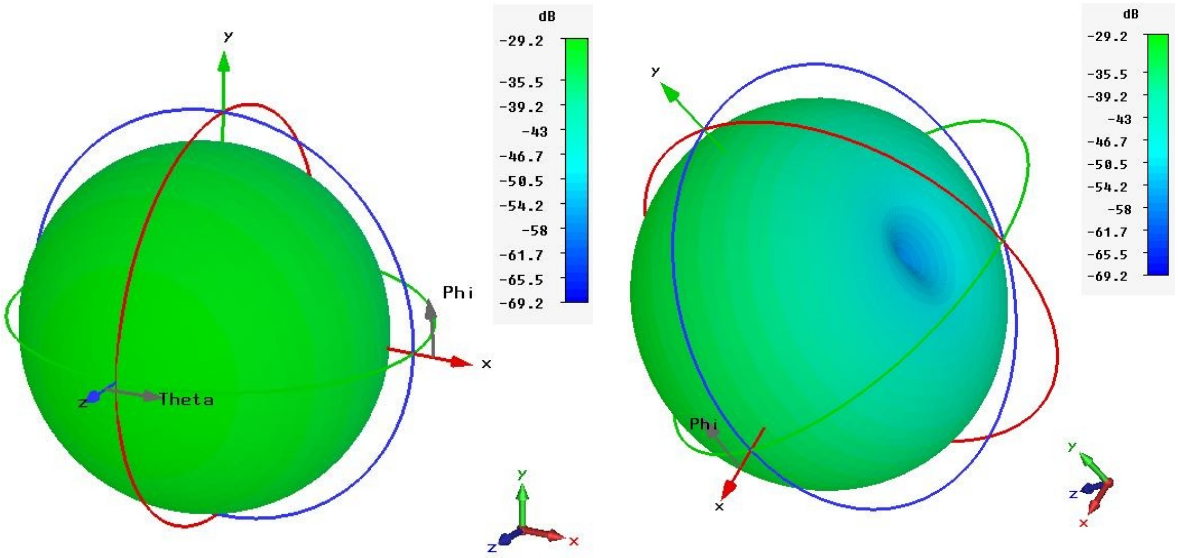

(a)

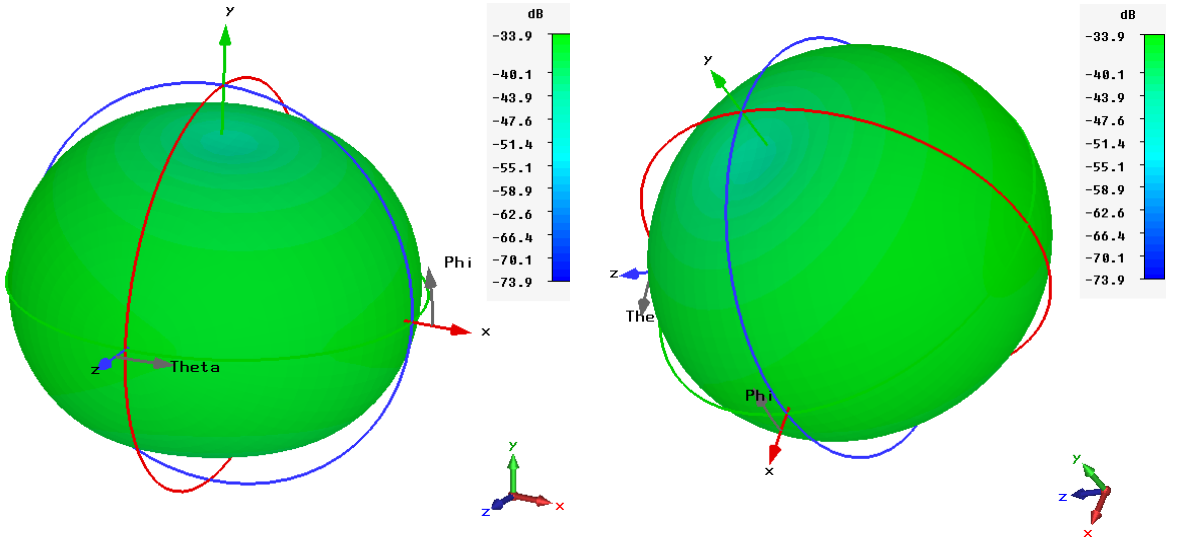

(b)

Figure 6.9: Simulated 3D farfield of the antenna (a) before and (b) after improvement

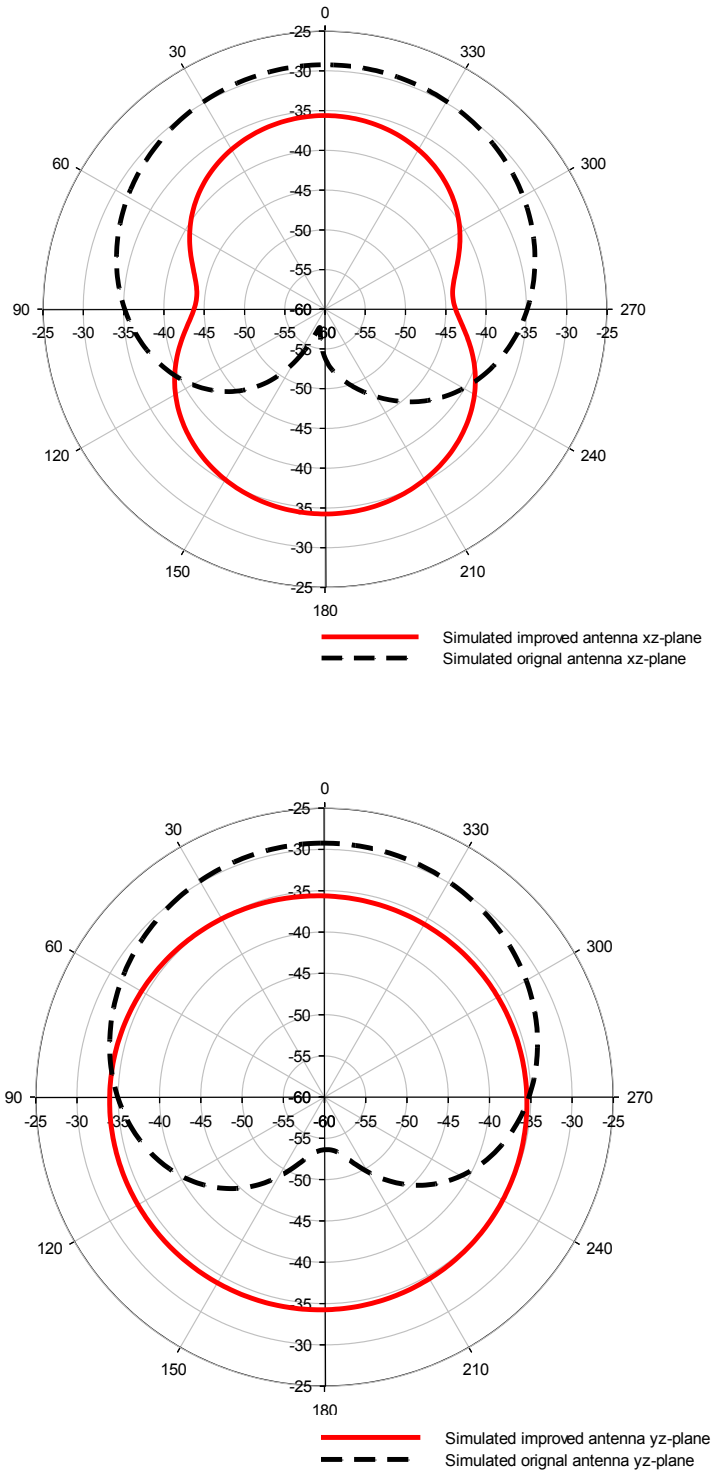

Figure 6.10: Simulated improved vs. original antennas farfield (a) xz plane and (b) yz plane

6.8 Measurements Setup

The simulated results are experimentally validated and measurements were carried out in an anechoic chamber. Figure 6.11 shows the fabricated antenna and the measurements setup in the anechoic chamber. The antennas were inserted in the homogeneous body liquid phantom that was prepared as described in section 6.3.1. The phantom is cylindrical shape and its dimensions are 130 mm height and 110 mm diameter. The S11 and Far-field for the original and improved antennas are measured in the liquid phantom and, in addition, the S11 is measured in free space. It should be noted that this phantom is only to demonstrate the measurements and not represent the body or application.

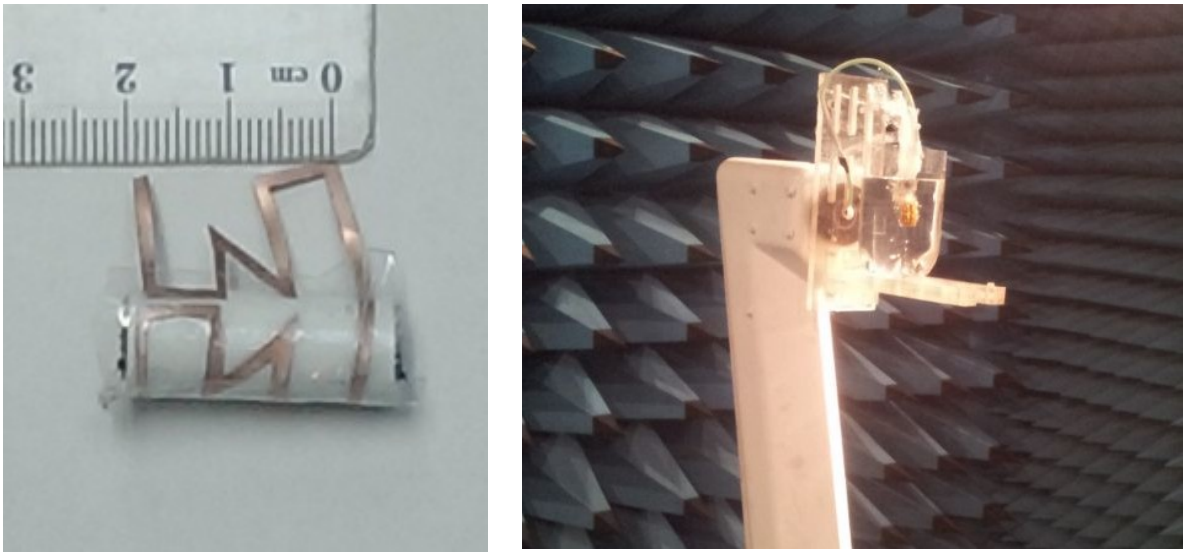

(a) (b)

Figure 6.11: (a) Fabricated antenna (b) Farfield measurements in the anechoic chamber

6.9 Analysis of Measured Results

Figure 6.12 shows the measured compared to the simulated S11 of the capsule loop antenna. It shows that the S11 measurement results are in good agreement with simulations. A wide bandwidth is achieved of 147 MHz measured at -10 dB.

Figure 6.13 shows the measured far field radiation pattern for the improved antenna in the two principal planes compared to the simulated far field radiation pattern. Figure 6.14 shows the measured normalised farfield of the improved antenna compared to the original antenna in the two principal planes. It clearly shows that the minimum gain is improved significantly by almost 20 dB. Moreover, the difference between the maximum and minimum gain is less than 10 dB. This is due to the equally distributed surface current around the capsule and, thus, the farfield can be considered as omni-directional.

This proves that by distributing the surface current around the capsule, the minimum gain of the implanted antenna can be significantly increased and the omni-directional radiation is enhanced. Therefore, the communication link between the capsule and the external receiver can be continually obtained.

To compare these results with those of some other works, Table 6.3 shows results of some referenced literature, published in [12-18]. Moreover, the antenna minimum and maximum gain towards the transceiver are compared to the presented antenna in this chapter. It is clear that this antenna has a high (minimum) gain compared to others with lowest difference between the maximum and minimum gain.

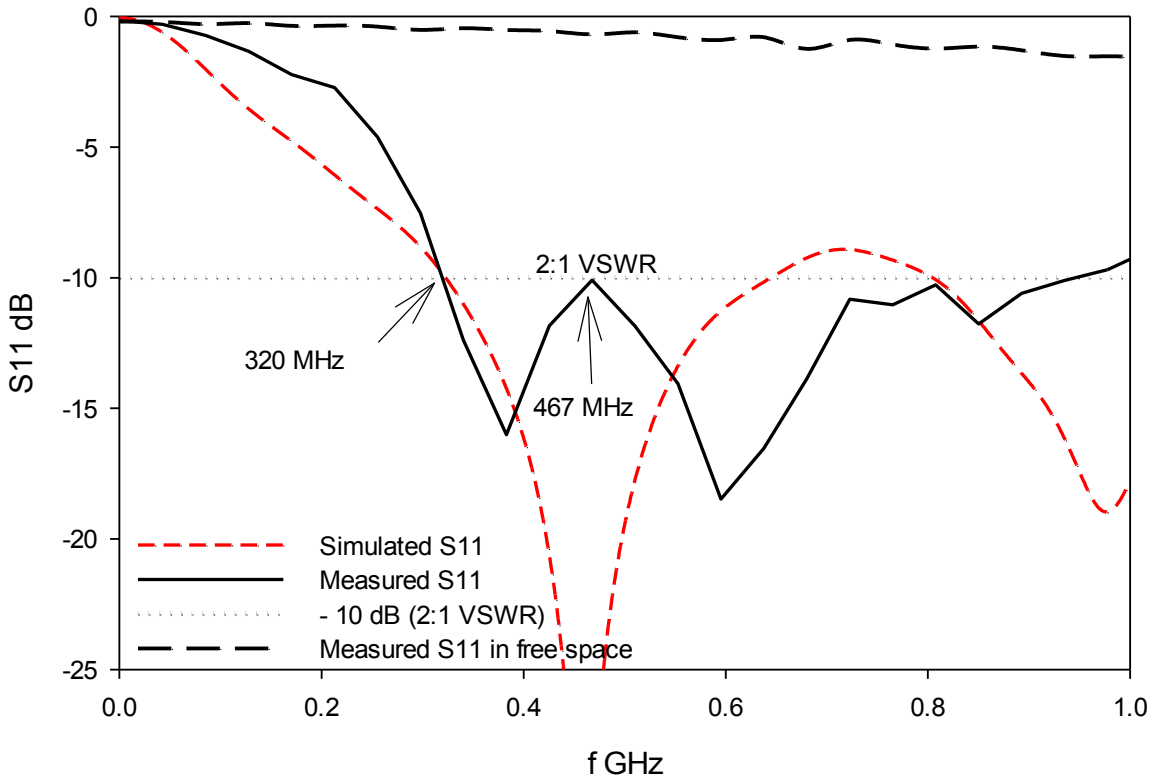

Figure 6.12: Measured vs. Simulated S11 of the capsule loop antenna

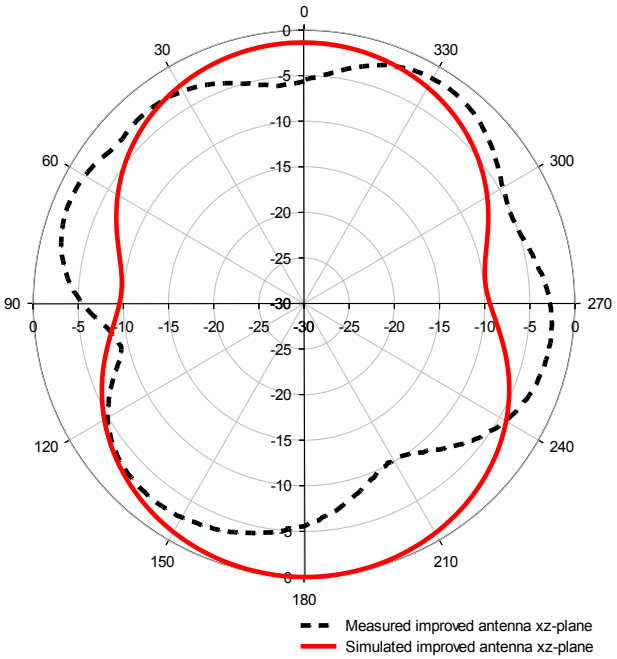

(a)

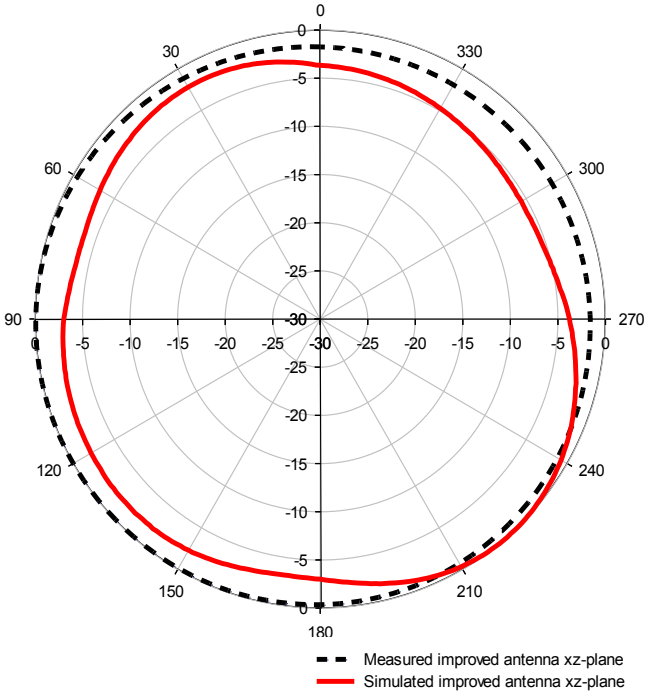

(b)

Figure 6.13: Simulated vs. measured normalised farfield of the improved antennas (a) xz plane and (b) yz plane

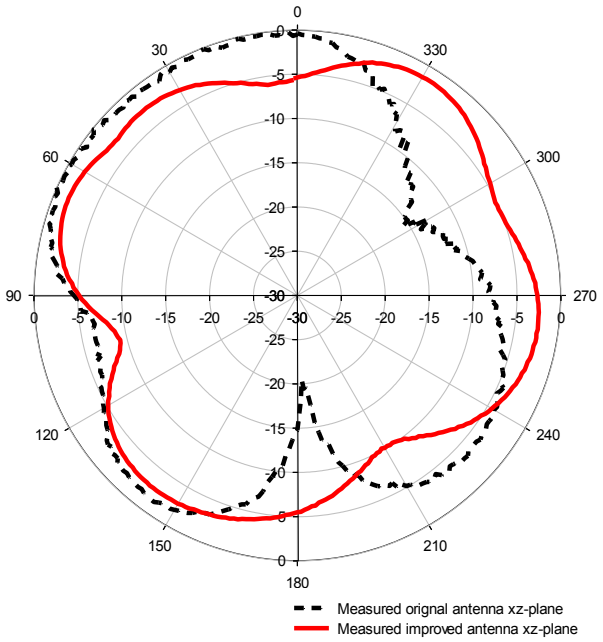

(a)

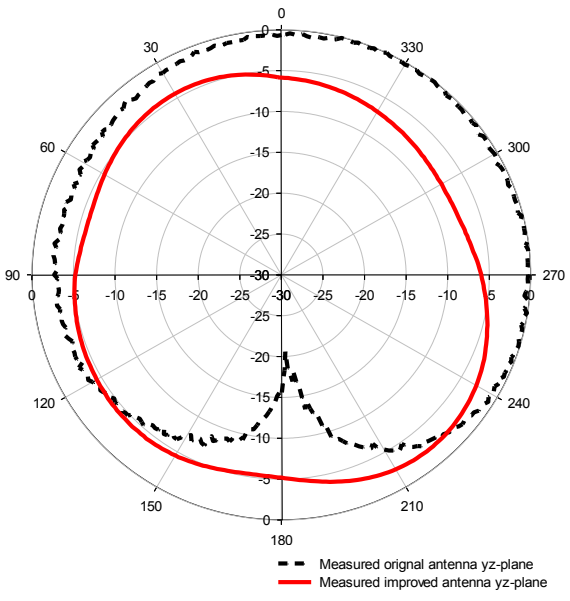

(b)

Figure 6.14: Measured improved vs. original antennas normalised farfield (a) xz plane and (b) yz plane

Table 6.3: Minimum and maximum capsule antennas gain for some published work and this work

Reference	**Antenna type**	**Frequency**	**Maximum Gain (dBi)**	**Minimum Gain (dBi)**
[30]	conformal meandered dipole antenna	700 MHz	– 29	- 55 *
[16]	Loop antenna	403 MHz	-32	-50 *
[17]	Flexible microstrip patch	403 MHz	- 33	-65
[19]	Loop antenna	403 MHz	-28.4	-48 *
[20]	Planner antenna	403 MHz	Normalised to 0	- 14 dB from highest gain
[21]	Multilayer spiral antenna	402.8 MHz	-30.2	-55
[22]	Flexible meandered inverted-F Antenna	1.4 GHz	- 25.2	-56
This work before the improvement	Loop antenna	403 MHz	-29.2	-59
This work after the improvement	Loop antenna	403 MHz	-34	-43

* The number is estimated from the colours chart of the presented antenna

6.10 Summary

In this chapter, an investigation has been conducted on the performance of loop implantable antennas for capsules. In addition, this chapter investigated the current systems discontinuous communication link between the capsule and the external receiver from the literature. A method to improve the gain of this antenna is numerically and experimentally investigated. A new formula to prepare a liquid phantom to be used for measurements is presented and investigated. A number of phantom mixtures were tried and a dielectric Probe Kit was used with a network analyser in order to measure the dielectric properties of the liquid phantom.

This antenna is a loop antenna with a flexible substrate in order to be bent on the capsule case to maintain a large space for the electronics components. The antenna dimensions are 18 mm long and 10 mm diameter.

The antenna and it improvement are investigated numerically and experimentally and both results are in a good agreement. The antenna has a wide bandwidth of 147 MHz measured at -10 dB to insure that the antenna is still working where the surrounding media permittivity is changing which can shift the resonant frequency. When the improvement method is applied, results shows that the minimum gain is improved significantly by almost 20 dB and the difference between the maximum and minimum gain is less than 10 dB. Unlike current antennas, this omni-direction antenna can maintain a continuous communication link between the capsule and the external receiver which improve the early detection of the Gastroenterology disease.

6.11 References

[1] G. Pan and L. Wang, "Swallowable wireless capsule endoscopy: Progress and technical challenges," *Gastroenterology research and practice,* vol. 2012, 2011.

[2] G. Ciuti, A. Menciassi, and P. Dario, "Capsule endoscopy: from current achievements to open challenges," *Biomedical Engineering, IEEE Reviews in,* vol. 4, pp. 59-72, 2011.

[3] M. Simi, P. Valdastri, C. Quaglia, A. Menciassi, and P. Dario, "Design, fabrication, and testing of a capsule with hybrid locomotion for gastrointestinal tract exploration," *Mechatronics, IEEE/ASME Transactions on,* vol. 15, pp. 170-180, 2010.

[4] Z. Fireman and Y. Kopelman, "New frontiers in capsule endoscopy," *Journal of gastroenterology and hepatology,* vol. 22, pp. 1174-1177, 2007.

[5] G. Iddan, G. Meron, A. Glukhovsky, and P. Swain, "Wireless capsule endoscopy," *Nature,* vol. 405, p. 417, 2000.

[6] R. Sidhu, D. Sanders, A. Morris, and M. McAlindon, "Guidelines on small bowel enteroscopy and capsule endoscopy in adults," *Gut,* vol. 57, pp. 125-136, 2008.

[7] T. Houzen, M. Takahashi, K. Saito, and K. Ito, "Implanted planar inverted F-antenna for cardiac pacemaker system," in *Antenna Technology: Small Antennas and Novel Metamaterials, 2008. iWAT 2008. International Workshop on*, 2008, pp. 346-349.

[8] J. Rigelsford and C. Davenport, "A passive RFID implant for soft tissue trauma monitoring," in *Antennas and Propagation Conference (LAPC), 2013 Loughborough*, 2013, pp. 127-130.

[9] Y. Rahmat-Samii and J. Kim, "Implanted antennas in medical wireless communications," *Synthesis Lectures on Antennas,* vol. 1, pp. 1-82, 2005.

[10] C. Gabriel, "Compilation of the Dielectric Properties of Body Tissues at RF and Microwave Frequencies," DTIC Document1996.

[11] K. Ito, K. Furuya, Y. Okano, and L. Hamada, "Development and characteristics of a biological tissue-equivalent phantom for microwaves," *Electronics and Communications in Japan (Part I: Communications),* vol. 84, pp. 67-77, 2001.

[12] T. Karacolak, A. Z. Hood, and E. Topsakal, "Design of a Dual-Band Implantable Antenna and Development of Skin Mimicking Gels for Continuous Glucose Monitoring," *Microwave Theory and Techniques, IEEE Transactions on,* vol. 56, pp. 1001-1008, 2008.

[13] A. Sani, "Modelling and characterisation of antennas and propagation for body-centric wireless communication," faculty of the University of London in partial fulfillment of the requirements for the degree of Doctor of Philosophy Electronic Engineering, Queen Mary, University of London London, 2010.

[14] P. Dimbylow, "FDTD calculations of the whole-body averaged SAR in an anatomically realistic voxel model of the human body from 1 MHz to 1 GHz," *Physics in medicine and biology,* vol. 42, p. 479, 1997.

[15] F. B. Gross, *Frontiers in antennas: next generation design & engineering*: McGraw-Hill New York, NY, 2011.

[16] F. Merli, L. Bolomey, E. Meurville, and A. Skrivervik, "Implanted Antenna for Biomedical Applications F. Merli*, L. Bolomey2, E. Meurville2, and AK Skrivervik1 Laboratory of Electromagnetics and Acoustics 2 Laboratory of Microengineering for Manufacturing 2 Ecole Polytechnique Fédérale de Lausanne, Switzerland," 2008.

[17] Y. Mahe, A. Chousseaud, M. Brunet, and B. Froppier, "New flexible medical compact antenna: Design and analysis," *International Journal of Antennas and Propagation,* vol. 2012, 2012.

[18] E. G. Lim, C. Wang, Z. Wang, G. Juans, T. Tillo, K. L. Man*, et al.*, "Wireless Capsule Antennas," *University of Linköping, Department of Science and Technology-ITN, LiU Norrköping-International Association of Engineer,* 2013.

[19] R. Alrawashdeh, Y.-P. Huang, and P. Cao, "Flexible meandered loop antenna for implants in MedRadio and ISM bands," *Electronics Letters,* vol. 49, pp. 1515-1517, 2013.

[20] J. C. Wang, E. G. Lim, Z. Wang, Y. Huang, T. Tillo, M. Zhang*, et al.*, "UWB planar antennas for wireless capsule endoscopy," in *Antenna Technology (iWAT), 2013 International Workshop on*, 2013, pp. 340-343.

[21] F. Merli, "Implantable antennas for biomedical applications," 2011.

[22] W. Seo, U. Kim, S. Lee, K. Kwon, and J. Choi, "A meandered inverted-f capsule antenna for an ingestible medical communication system," *Microwave and Optical Technology Letters,* vol. 54, pp. 1761-1765, 2012.

[23] J. Lee and S. Nam, "Q evaluation of small insulated antennas in a lossy medium and practical radiation efficiency estimation," in *Microwave Conference, 2007. KJMW 2007. Korea-Japan*, 2007, pp. 65-68.

[24] C. Buratti, R. D'Errico, M. Maman, F. Martelli, R. Rosini, and R. Verdone, "Design of a body area network for medical applications: the WiserBAN project," in *Proceedings of the 4th International Symposium on Applied Sciences in Biomedical and Communication Technologies*, 2011, p. 164.

[25] Z. N. Chen, G. C. Liu, and T. S. See, "Transmission of RF signals between MICS loop antennas in free space and implanted in the human head," *Antennas and Propagation, IEEE Transactions on,* vol. 57, pp. 1850-1854, 2009.

[26] C. Roopnariane, M.-R. Tofighi, and C. M. Collins, "Radiation performance of small implanted antennas in head at MICS, ISM, and GPS bands," in *Bioengineering Conference, Proceedings of the 2010 IEEE 36th Annual Northeast*, 2010, pp. 1-2.

[27] M. Norris, J.-D. Richerd, and D. Raynes, "Sub miniature antenna design for wireless implants," 2007.

[28] V. Shirvante, F. Todeschini, X. Cheng, and Y.-K. Yoon, "Compact spiral antennas for MICS band wireless endoscope toward pediatric applications," in *Antennas and Propagation Society International Symposium (APSURSI), 2010 IEEE*, 2010, pp. 1-4.

[29] J. A. Von Arx, M. D. Amundson, W. R. Mass, R. Balczewski, and W. J. Linder, "Telemetry apparatus and method for an implantable medical device," ed: Google Patents, 2003.

[30] P. M. Izdebski, H. Rajagopalan, and Y. Rahmat-Samii, "Conformal ingestible capsule antenna: A novel chandelier meandered design," *Antennas and Propagation, IEEE Transactions on,* vol. 57, pp. 900-909, 2009.

Chapter 7

Conclusion

7.1 Summary:

This thesis presented significant advancements in characterisation and design of implantable antennas for biomedical applications. In particular, it was highlighted a new and powerful ways to produce high performance implanted antennas. A comprehensive survey for implantable antennas design, challenges and performance were presented. It was founded that one of the most challenging issue for implantable antennas is the gain. Therefore, this study set out to determine novel approaches to improve implantable antennas gain and to achieve overall higher performance for implanted antennas. In order to achieve this goal, this thesis is presented different external elements as a novel approach to improve subcutaneous implantable antennas performance. Moreover, a technique to equally distribute antenna surface current was used to improve the capsule antenna performance.

Designs of four effective communication miniaturised implanted antennas to achieve reliable medical implant communication were presented. Moreover, a comprehensive investigation of seventeen different designs and scenarios were investigated also in order to improve the antenna gain and overall performance.

A probe antenna was designed to be implanted under the skin for biomedical wireless communication and working at ISM band. Moreover, a mictrostrip patch implanted antenna was designed to be implanted under the skin for biomedical wireless communication.

In order to improve subcutaneous implantable antennas performance, an external parasitic grid structure was used for the first time. Both, probe antenna and microstrip antenna gain improved by minimum of 4 dBi. Moreover, an external stripline was used for the first time to improve subcutaneous implantable antennas performance. Both, probe antenna and microstrip antenna gain improved by minimum of 3 dBi. For further performance improvement, both external parasitic elements, grid structure and stripline, were used together. As result of this secinario, the gain for both antennas was improved by minimum of 6 dBi.

In a different technique, an external hemispherical lens was used for the first time to improve the performance of subcutaneous implantable antennas. By using this technique, the microstrip antenna gain was improved by 6 dBi and almost 20% minimum SAR reduction. Furthermore, an external parasitic ring was used for the first time to improve the performance of subcutaneous implantable antennas. Thus, microstrip patch antenna gain was improved by 3 dBi. For additional improvement, a combination of external hemispherical lens and parasitic ring were used together for extra performance improvement of the implantable microstrip antenna. Consequently, gain was improved by 7 dBi.

A new efficient miniaturised and high performance dual-band implantable antenna for biomedical applications was designed to be implanted under the skin and the size

achieved is 1/25 of the wavelength. An External hemispherical lens and parasitic ring were used separately and together to improve the performance of the dual-band implantable antenna and the gain was improved by up to 7 dB.

The Specific Absorption Rate (SAR) affect on the body was numerically studied before and after using performance improvement techniques. It was demonstrated that using these techniques is reducing the SAR affect on the body and helping to satisfy the peak 1-g SAR standard value of ANSI (1.6 W/kg).

A new miniaturised flexible multiband omni-directional implantable antenna for capsule endoscopy was designed and the size achieved is 10 mm diameter and 18 mm length. The performance of this capsule antenna was improved and the minimum gain improved by almost 15 dB.

All antennas were realised by fabrication and all scenarios were comprehensively verified numerically and by measurements. In addition, these results have been compared with these of some other published works from referenced literature.

In this study, the Finite integration technique (FIT) was used for numerical modelling which is built in the CST software. In order to design subcutaneous implantable antennas, the numerical modelling of the human body was conducted by using a simplified biological model consists of three layers of human tissue: skin, fat and muscle. In the case of capsule antenna, a homogenise body phantom was used in order to representing the human body. In order to realise the 3-layers simplified biological model for measurements, a fresh pork meat cut was used. In addition, the

homogenised body phantom was realised by preparing a liquid consisting of deionised water, sugar, salt and ager.

Generally, it is found that using these approaches yields a significant improvement in the implanted antennas gain and overall performance and, thus, increase the implanted antenna battery's life. Such external elements are quit cheap, easy to implement and have a good impact on the medical applications by enhancing the communication of the implanted antenna with the nearest hotspot. Moreover, it can help to reduce SAR values to satisfy the safety standards for medical implant applications.

7.2 Challenges and Limitations:

During the work on the thesis, there were some challenges that have had a limited impact on results. For example, the measurements of the dual-band antenna in Chapter 4 showed an improvement of 2dB in the power radiated out of the body by the matched antenna whereas the simulations predicted a higher figure of 4.5 dB. However the use of pork meat did not give an exact match to the model. Moreover, some radiation patterns are not symmetrical as simulated one due to dissimilarity of the pork samples. In most cases it is very difficult to find a similar pork sample to the used simulated sample.

The capsule antenna was fabricated manually and, thus, the dimensions of the antenna may not be accurate and this, therefore, affected the measurements results. However, the capsule antenna measurements results have reflected high agreement with simulations.

7.3 Future Work:

Presented Techniques in this thesis are effective to improve the implanted antennas power. Therefore, a step forward for apply them on implanted antennas in living organisms should be considered as future work. Research on different lens techniques that can enhance implanted antennas gain such as flat lenses is another possible future work. Moreover, Patients can benefit from the recent technologies of smart watches to continually monitor some of biological information. However, due the fact that these watches use a wearable sensors, the limitation of current smart watches is the limited number of biological information that can be detected. Information such as blood glucose levels can be detected only by invasive test or implanted sensors. Therefore, to extend the abilities of these watches to help patients who need such information; an implantable antenna can be used to work in compatible current watches. Furthermore. Figure 3.25 shows external grid structure, stripline or ring that can be attached to the watch to work in combination with both systems, the watch and the implant, and it can improve the implanted antenna gain and, thus, increase the battery's life.

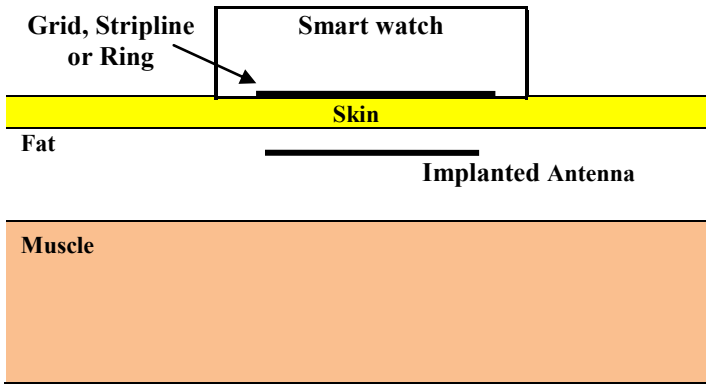

Figure 7.1: Implanted antenna and external improvement element work in compatible with a Smart watch

Appendix A

Dielectric Properties of Body Tissues at RF and Microwave Frequencies

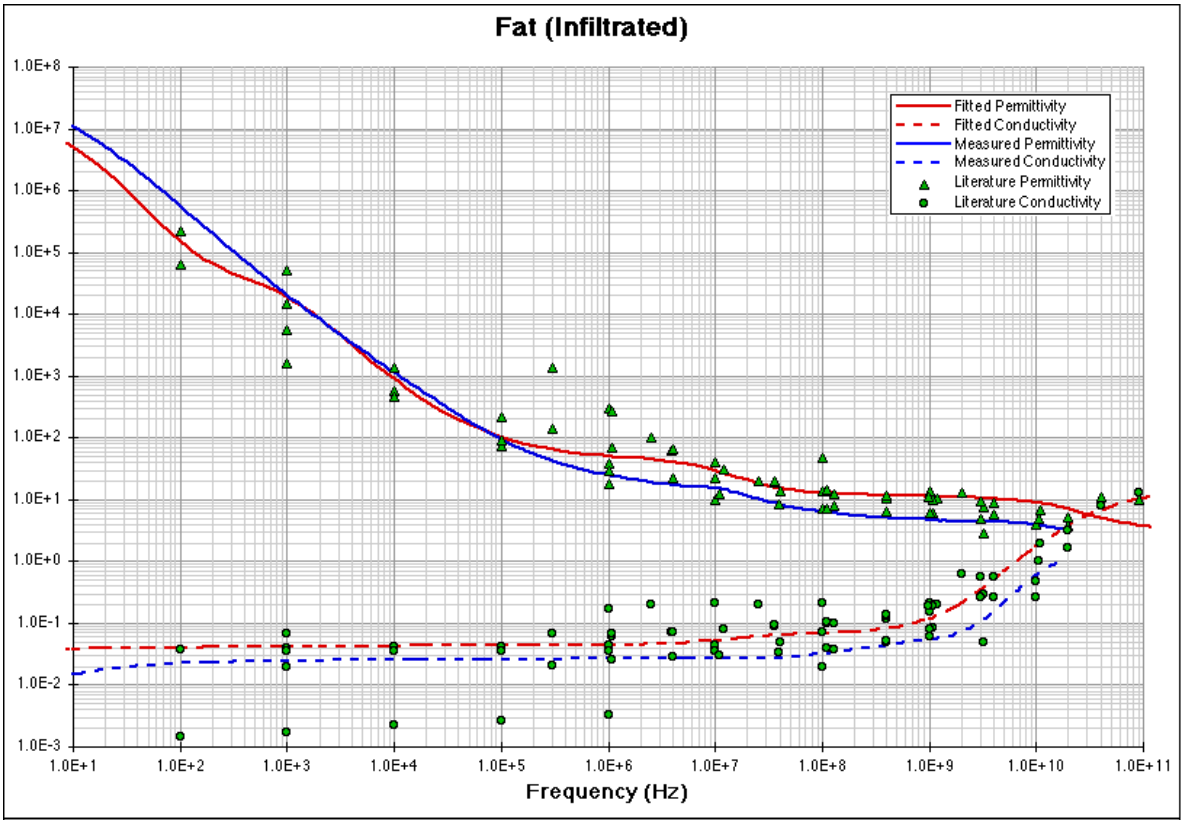
Fat (Infiltrated)
Fitted Permittivity
Fitted Conductivity
Measured Permittivity
Measured Conductivity
Literature Permittivity
Literature Conductivity
1.0E+8
1.0E+7
1.0E+6
1.0E+5
1.0E+4
1.0E+3
1.0E+2
1.0E+1
1.0E+0
1.0E-1
1.0E-2
1.0E-3
1.0E+1
1.0E+2
1.0E+3
1.0E+4
1.0E+5
1.0E+6
1.0E+7
1.0E+8
1.0E+9
1.0E+10
1.0E+11
Frequency (Hz)

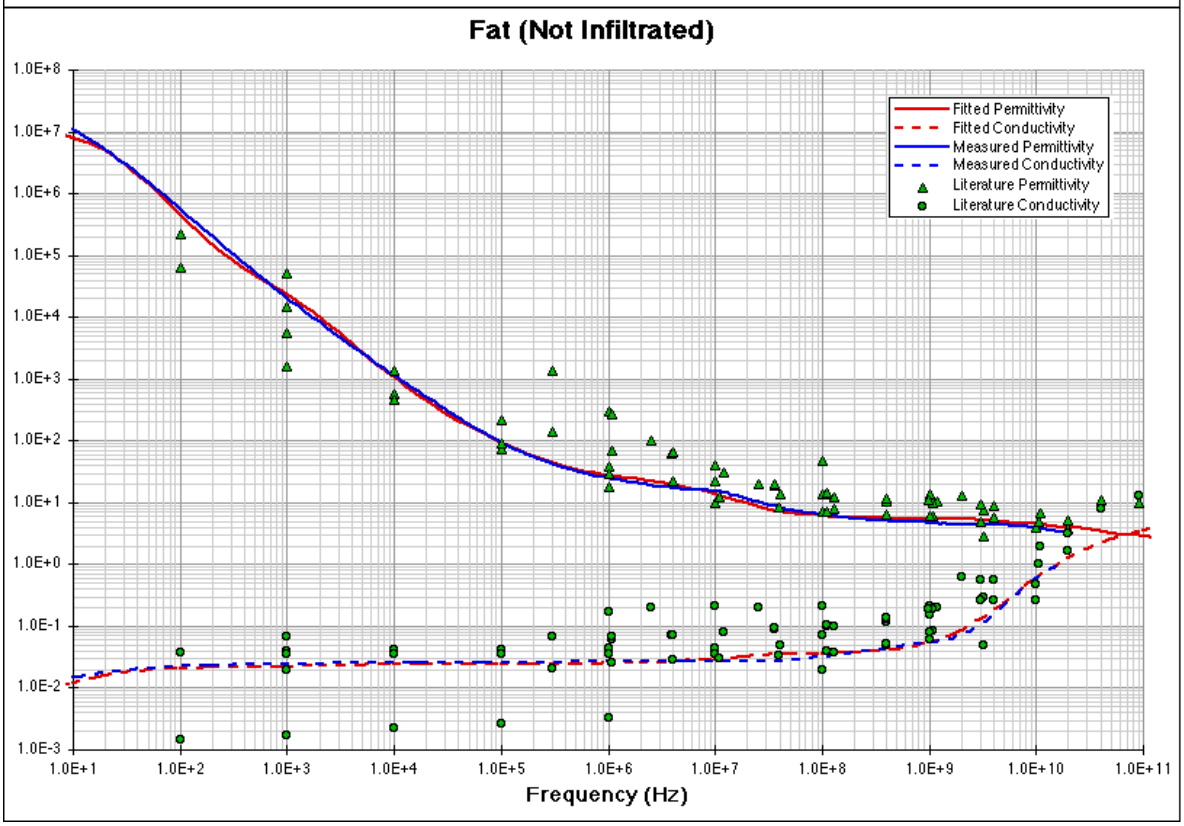
Fat (Not Infiltrated)
Fitted Permittivity
Fitted Conductivity
Measured Permittivity
Measured Conductivity
Literature Permittivity
Literature Conductivity
1.0E+8
1.0E+7
1.0E+6
1.0E+5
1.0E+4
1.0E+3
1.0E+2
1.0E+1
1.0E+0
1.0E-1
1.0E-2
1.0E-3
1.0E+1
1.0E+2
1.0E+3
1.0E+4
1.0E+5
1.0E+6
1.0E+7
1.0E+8
1.0E+9
1.0E+10
1.0E+11
Frequency (Hz)

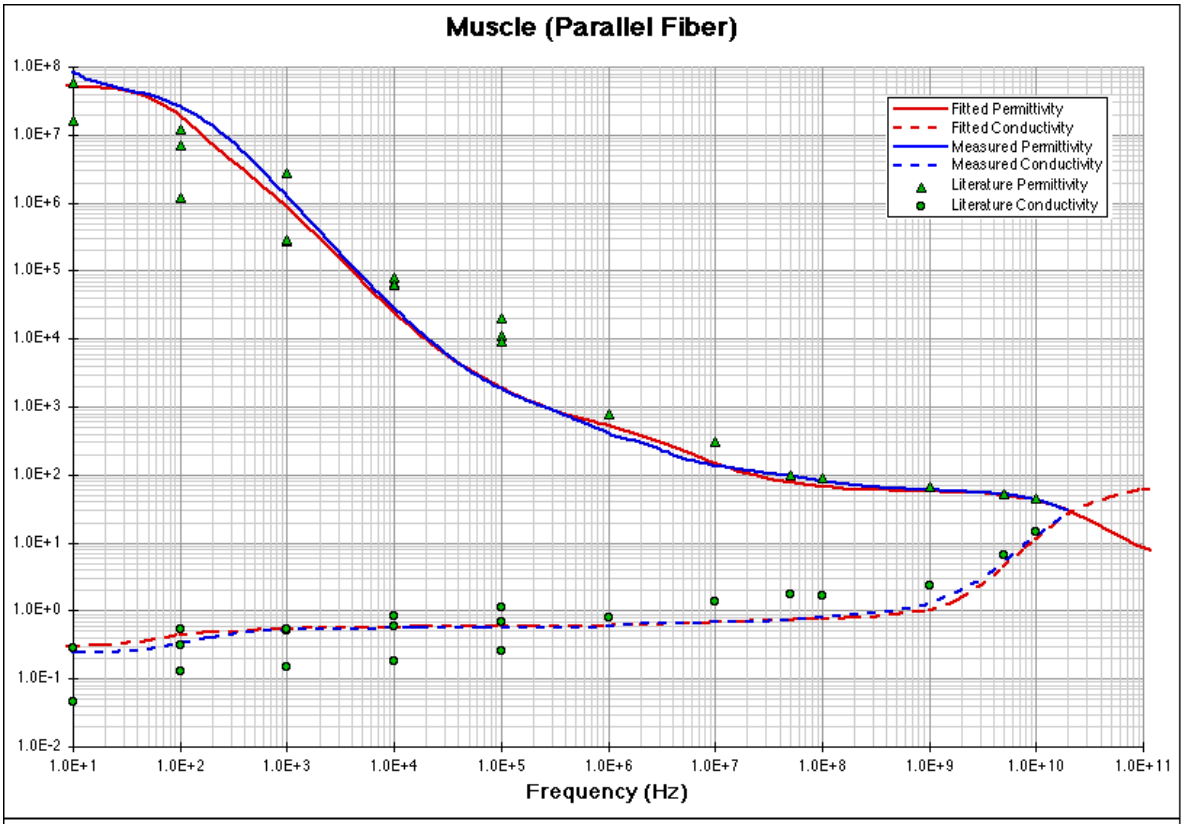
Muscle (Parallel Fiber)
Fitted Permittivity
Fitted Conductivity
Measured Permittivity
Measured Conductivity
Literature Permittivity
Literature Conductivity
1.0E+8
1.0E+7
1.0E+6
1.0E+5
1.0E+4
1.0E+3
1.0E+2
1.0E+1
1.0E+0
1.0E-1
1.0E-2
1.0E+1
1.0E+2
1.0E+3
1.0E+4
1.0E+5
1.0E+6
1.0E+7
1.0E+8
1.0E+9
1.0E+10
1.0E+11
Frequency (Hz)

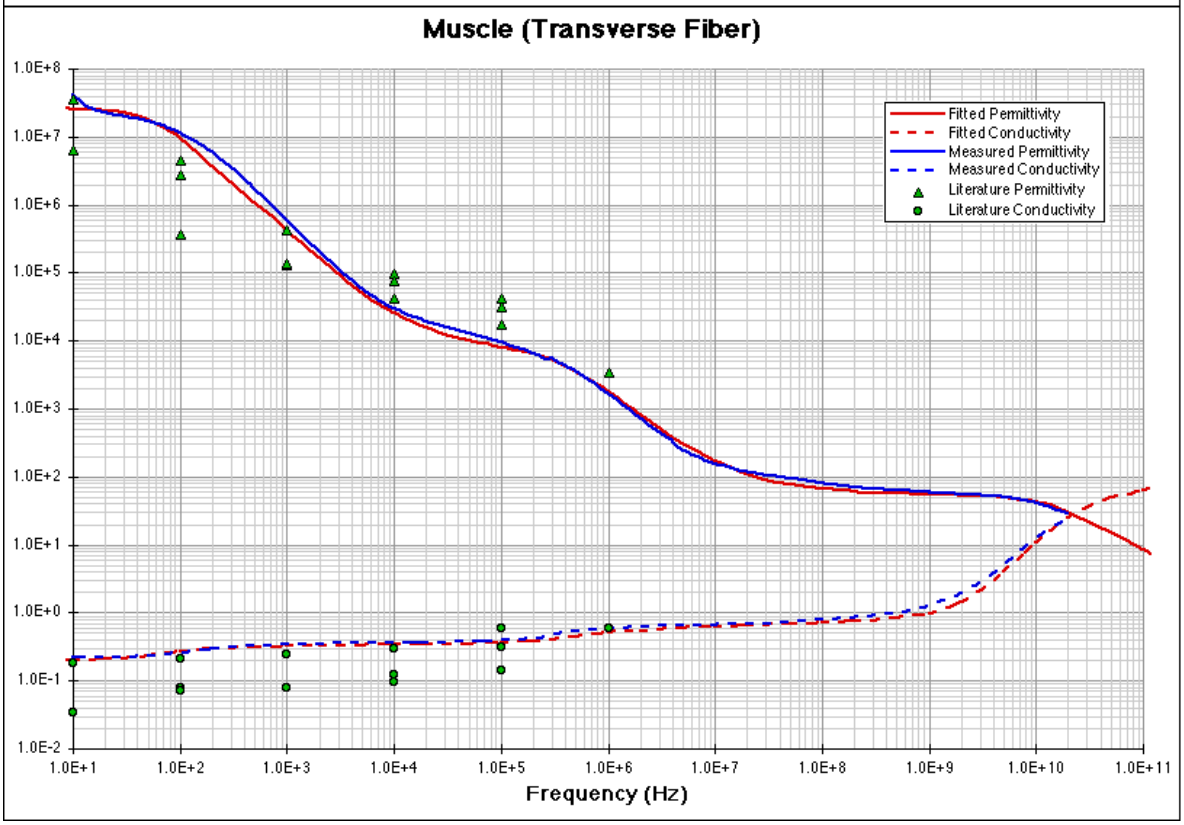
Muscle (Transverse Fiber)
Fitted Permittivity
Fitted Conductivity
Measured Permittivity
Measured Conductivity
Literature Permittivity
Literature Conductivity
1.0E+8
1.0E+7
1.0E+6
1.0E+5
1.0E+4
1.0E+3
1.0E+2
1.0E+1
1.0E+0
1.0E-1
1.0E-2
1.0E+1
1.0E+2
1.0E+3
1.0E+4
1.0E+5
1.0E+6
1.0E+7
1.0E+8
1.0E+9
1.0E+10
1.0E+11
Frequency (Hz)

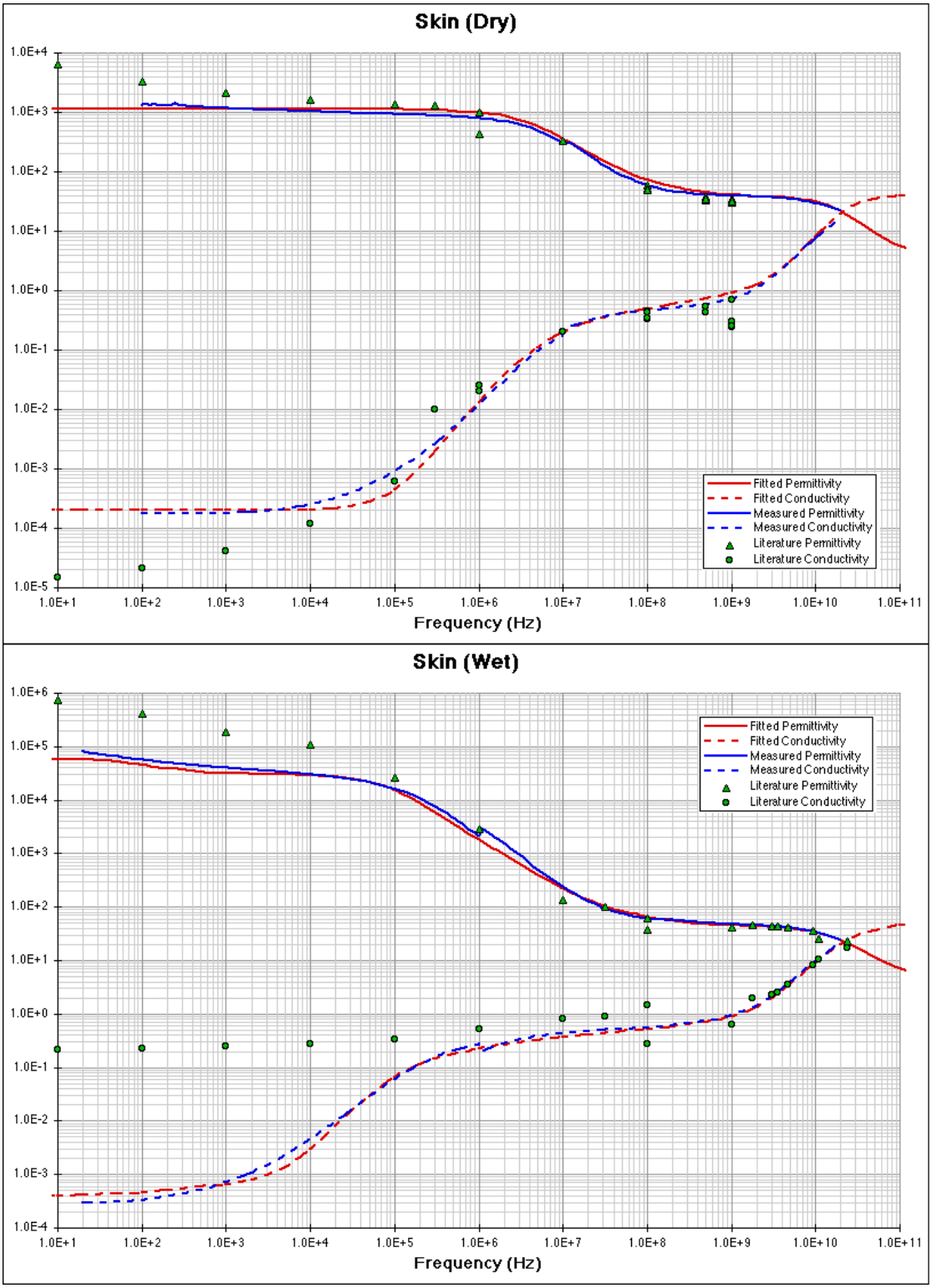

Figure 8A.1: Dielectric Properties of human Skin, muscle and fat at RF and Microwave Frequencies [1]

Table 8A.1: Electrical data of biological tissues used from Human body model at 402 MHz [2]

	2.4 GHz		
Tissue	σ (S/m)	ϵ_r	δ **(mm)**
Aorta	1.40	42.59	24.86
Bladder	0.67	18.03	33.83
Blood	2.50	58.35	16.41
Body Fluid	2.44	68.24	18.14
Bone	0.79	18.61	29.43
Grey Matter	1.77	48.99	21.15
White Matter	1.19	36.23	27.05
Breast Fat	0.13	5.16	90.76
Fat	0.10	5.29	119.56
Gall Bladder	2.02	57.68	20.10
Gland	1.93	57.27	21.00
Heart	2.22	54.92	17.95
Kidney	2.39	52.86	16.37
Liver	1.65	43.12	21.30
Lung Deflated	1.65	48.45	22.59
Lung Inflated	0.79	20.51	30.73
Muscle	1.71	52.79	22.79
Pancreas	1.93	57.27	21.00
Prostate	2.13	57.63	19.12
Skin Dry	1.44	38.06	22.96
Skin Wet	1.56	42.92	22.47
Spleen	2.20	52.55	17.70
Stomach	2.17	62.24	19.49
Tendon	1.64	43.21	21.44
Testis	2.13	57.63	19.12

Appendix B

Permittivity and Loss tangent of some materials

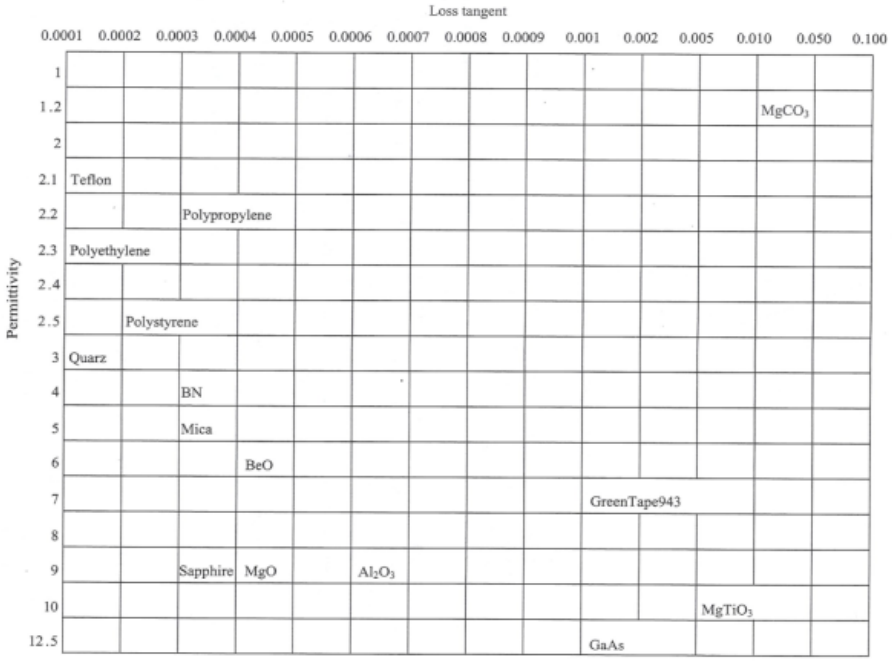

Figure 9A.1: The permittivity and loss tangent of some well know materials [3].

Appendix C

CST Validations for human body and implanted antennas modelling

In order to validate our work using CST, the work in [4] was implemented using CST. The objective of this is to verify that the used simulation package, CST, is working correctly by comparing its results with other work results.

This paper presented an implanted spiral microstrip antenna for biomedical applications. The antenna was measured in a human tissue-simulating fluid as a simplified one layer as shown in Figure 4.13. The electrical characteristics of the fluid (Er = 49.6, σ = 0.51 S/m at 402 MHz) are very similar to the skin tissue (Er = 46.7, σ = 0.96 S/m at 402 MHz).

Figure B.2 and FigureB.3 shows the S11 and the far-field pattern, respectively, for both works. Figures shows very similar results of this simulation to the results published in the original work. This is indicating that results presented in 4.2 to 4.5 are accurate.

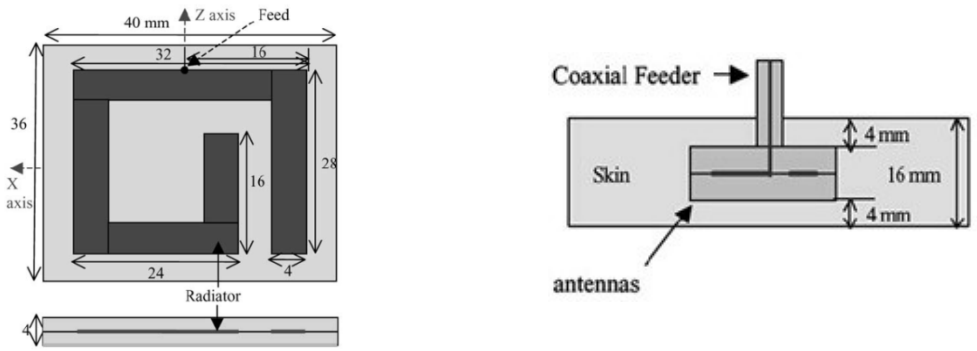

(a) (b)

Figure B.1: The implanted antenna (a) antenna design (b) The antenna inside the simplified one layer [4]

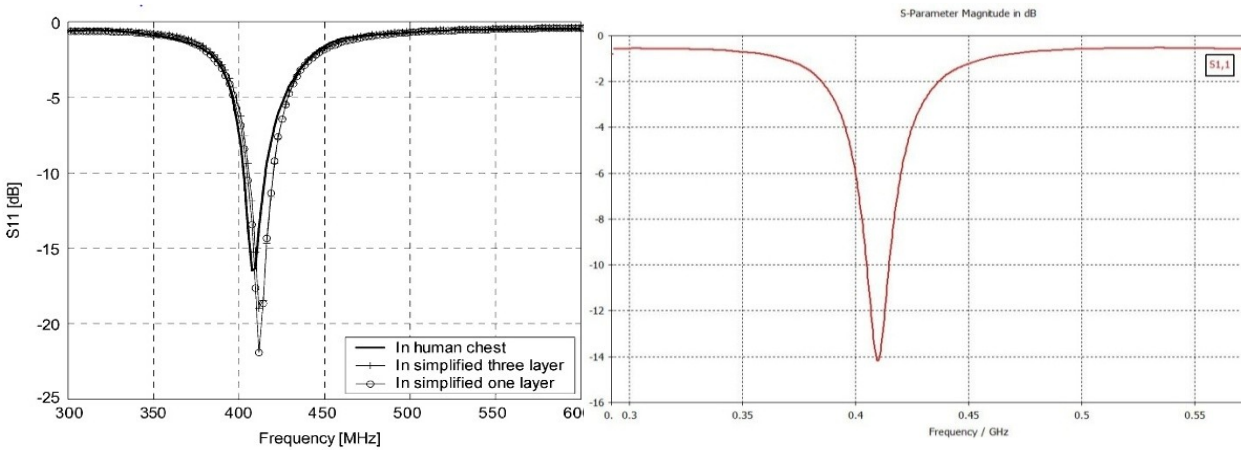

(a) (b)

Figure B.2: S11 of the implanted antenna (a) Original work (b) This simulation

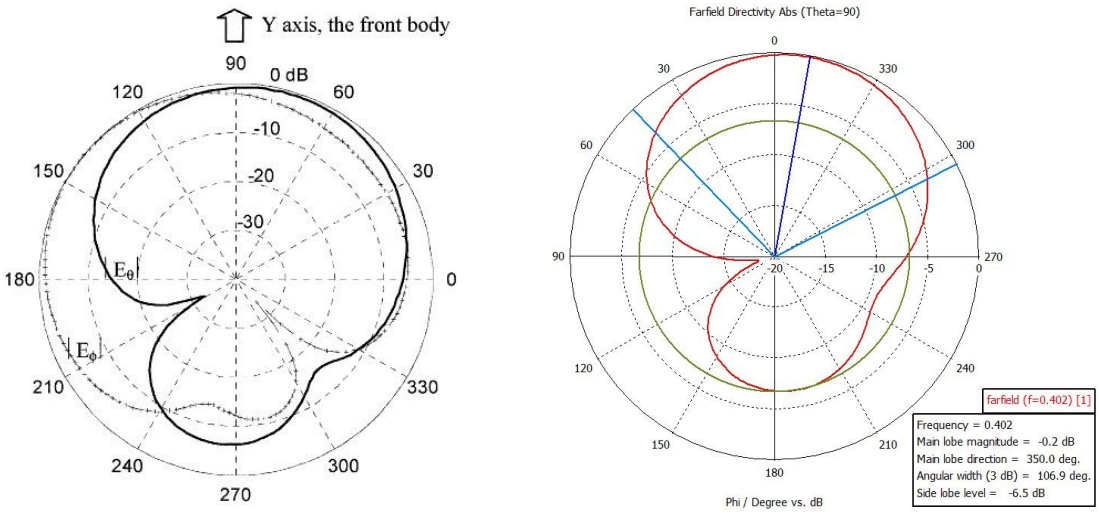

(a) (b)

FigureB.3: Far-Field of the implanted antenna (a) Original work [4] (b) This simulation

References for Appendices:

[1] C. Gabriel, "Compilation of the Dielectric Properties of Body Tissues at RF and Microwave Frequencies," DTIC Document1996.

[2] Y. Rahmat-Samii and J. Kim, "Implanted antennas in medical wireless communications," *Synthesis Lectures on Antennas,* vol. 1, pp. 1-82, 2005.

[3] J. Kim and Y. Rahmat-Samii, "Implanted antennas inside a human body: Simulations, designs, and characterizations," *Microwave Theory and Techniques, IEEE Transactions on,* vol. 52, pp. 1934-1943, 2004.

[4] J. Kim and Y. Rahmat-Samii, "Implanted antennas inside a human body: Simulations, designs, and characterizations," *Microwave Theory and Techniques, IEEE Transactions on,* vol. 52, pp. 1934-1943, 2004.